AD-A117 665 NATIONAL AERONAUTICS AND SPACE ADMINISTRATION MOFFET--ETC F/G 1/3
ESTABLISHMENT OF A ROTOR MODEL BASIS.(U)
JUN 82 R E MCFARLAND
UNCLASSIFIED NASA-A-8605 NASA-TP-2026 NL

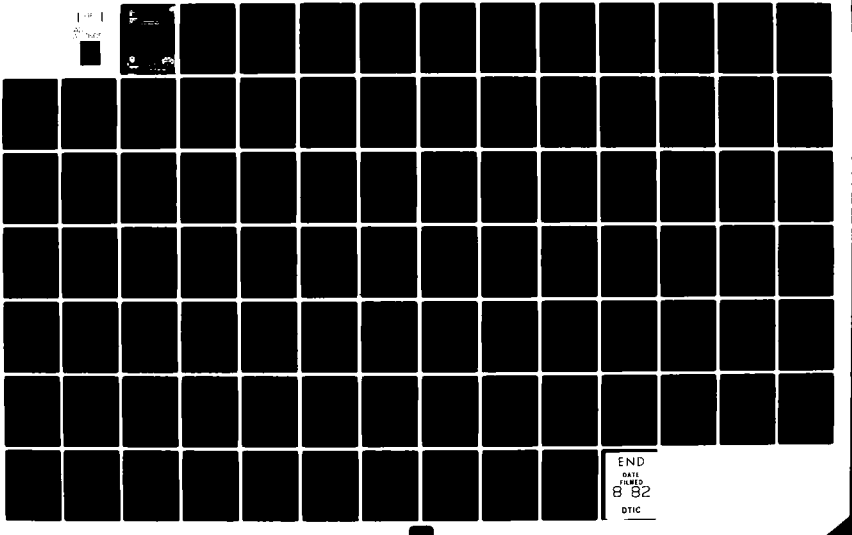

END
DATE FILMED
8 82
DTIC

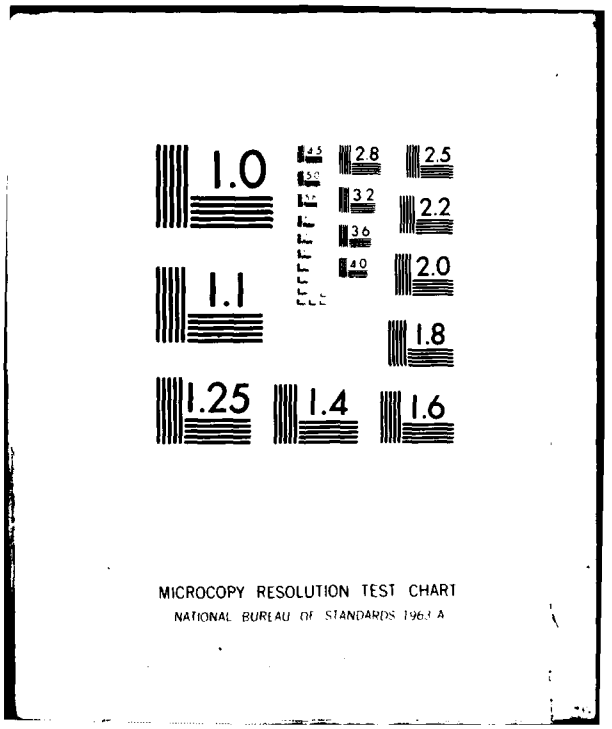
1.0
1.1
1.25
1.4
1.6
2.8
3.2
3.6
4.0
2.5
2.2
2.0
1.8
MICROCOPY RESOLUTION TEST CHART
NATIONAL BUREAU OF STANDARDS 1963 A

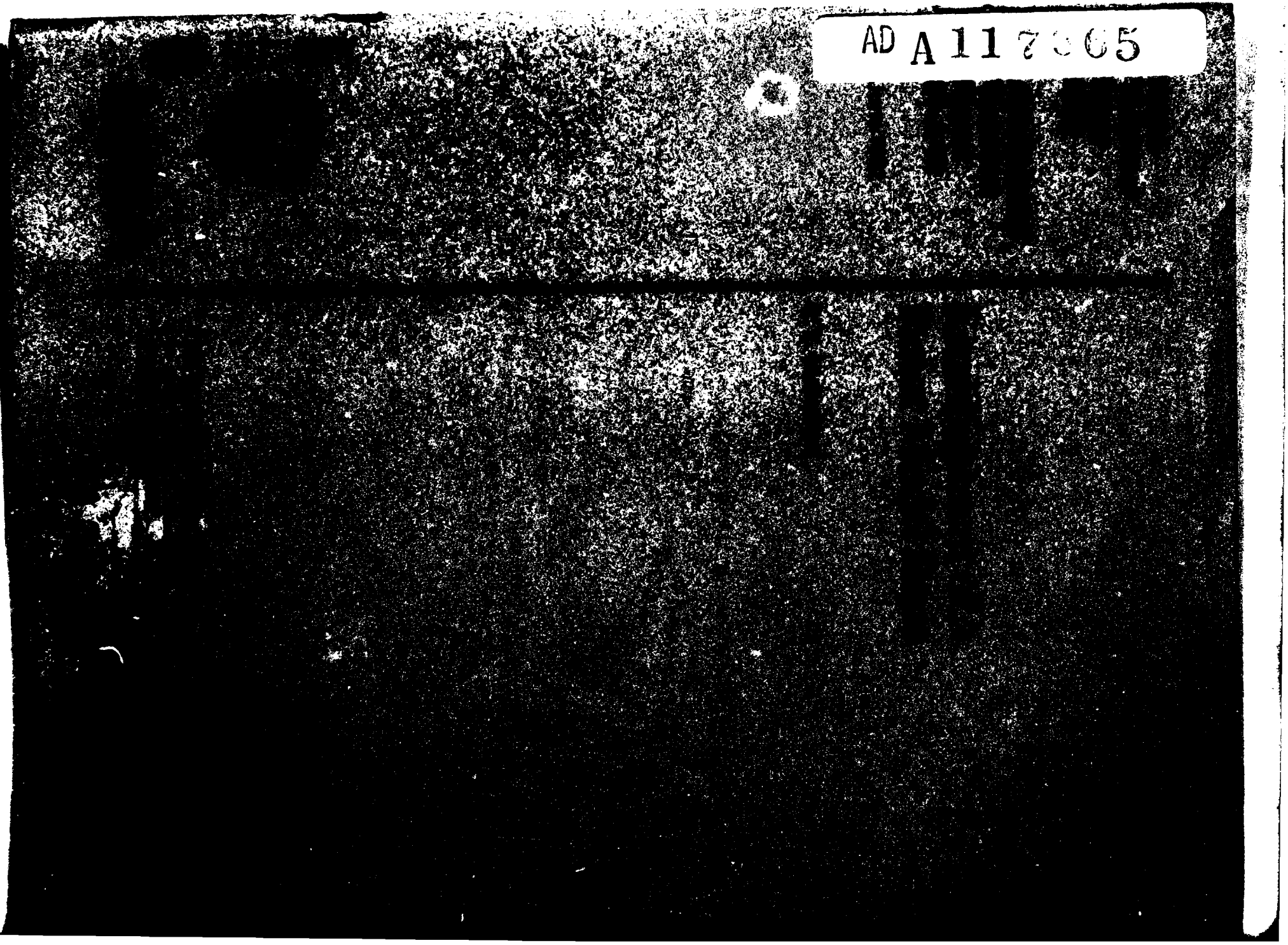
AD A11

NASA Technical Paper 2026

AVRADCOM Technical Report 81-A-14

1982

Establishment of a Rotor Model Basis

R. E. McFarland
Aeromechanics Laboratory
AVRADCOM Research and Technology Laboratories
NASA Ames Research Center
Moffett Field, California

National Aeronautics and Space Administration

Scientific and Technical Information Branch

TABLE OF CONTENTS

LIST OF FIGURES

LIST OF TABLES

SYMBOLS

Pertinent symbols are reproduced here from Houck et al., 1977. The equations and data in this reference were derived in the U.S. Customary Units to expedite development of the flight vehicles by Sikorsky Aircraft Company.

A	generalized area, ft^2
A_{1S}	total lateral cyclic input, deg
a_{0L}	principal lagging Fourier series coefficient, deg
a_n	suggested force summation coefficients, ft
B	number of blades
B_{1S}	total longitudinal cyclic input, deg
b_n	suggested moment summation coefficients, ft^2
B_{MR}	main rotor blade-tip loss factor
C	operational constant, lb/ft^2
C_{DY}	blade-segment drag coefficient
C_{LY}	blade-segment lift coefficient
c	main rotor blade chord, ft
d	differential operator
e	main rotor hinge offset from center of rotation, ft
e'	distance from hinge to start of blade, ft
F	generalized aerodynamic blade force, lb
F_P, F_T, F_R	blade-segment forces — perpendicular, tangential, radial, lb
f_P, f_T, f_R	radial derivatives of F_P, F_T, F_R, lb/ft
F_{XI}, F_{YI}, F_{ZI}	blade inertial-shear forces, rotating shaft axes, lb
F_{XT}, F_{YT}, F_{ZT}	blade total-shear forces, rotating shaft axes, lb
h	vehicle altitude, ft
L_{MR}	main rotor body axes rolling moment, ft-lb
M	generalized blade aerodynamic moment, ft-lb
M_{FA}	aerodynamic moment about flapping hinge, ft-lb

M_{LA}	aerodynamic moment about lagging hinge, ft-lb
M_{LD}	lag damper moment, ft-lb
M_{MR}	main rotor body axes pitching moment, ft-lb
M_b	blade first mass moment about hinge, slugs-ft
N	total number of radial evaluations per blade
N_{MR}	main rotor body axes yawing moment, ft-lb
n	blade index (n = 1,2,...,N)
Q	total rotor torque, ft-lb
R_{MN}	total body axes rotor yaw moment, ft-lb
r	radial distance from main rotor hub, ft
r_A	radius from main rotor hub to cuff, ft
r_{MR}	radius from hub to tip of main rotor blade, ft
r_n	discrete radial evaluation point, ft
$r_{n(-)}$	interior segment extremity, ft
$r_{n(+)}$	exterior segment extremity, ft
r_T	effective blade tip for lifting purposes, ft
r_x	generalized lower limit of integration, ft
r_y	generalized upper limit of integration, ft
S	generalized linear distance, ft
v_P	blade-segment perpendicular velocity, ft/sec
v_R	blade-segment radial velocity, ft/sec
v_T	blade-segment tangential velocity, ft/sec
v_Y	total blade-segment velocity magnitude, ft/sec
X_{MR}	main rotor body axes longitudinal force, lb
Y_{MR}	main rotor body axes lateral force, lb
y_n	normalized radial evaluation point
Z_{MR}	main rotor body axes vertical force, lb

α_{TRANS}	blade function angle-of-attack map entry, rad
α_Y	blade-segment angle of attack, rad
β	blade flapping angle, rad
$\Delta F_{P(TL)}$, $\Delta F_{R(TL)}$, $\Delta F_{T(TL)}$, $\Delta M_{FA(TL)}$, $\Delta M_{LA(TL)}$	superimposed aerodynamic force and moment terms accounting for tip loss by using the suggested interval definitions, ft and ft-lb
Δr_n	length of a blade segment, ft
Δy_n	Δr_n normalized by r_{MR}
δ	blade lagging angle, rad
θ_A	blade-segment pitch angle, rad
θ_{CUFF}	impressed main rotor collective pitch angle, deg
ψ	vehicle yaw angle, deg
γ	blade-segment flow skew angle, rad
ρ	air density, slugs/ft^3
Ω	main rotor rotational velocity, rad/sec
ξ	hinge offset e normalized by r_{MR}
ξ'	hinge distance e' normalized by r_{MR}

ESTABLISHMENT OF A ROTOR MODEL BASIS

R. E. McFarland

Ames Research Center
Aeromechanics Laboratory
and
AVRADCOM Research and Technology Laboratories

I. SUMMARY

Rotating blade-element mathematical models for use in discrete, man-in-the-loop rotorcraft simulation have considerable engineering value, but they are computationally expensive. A comprehensive blade-element model of the RSRA rotor system is examined here to provide accurate baseline data for the analysis of modifications to the present model. It is important that models be developed for real-time simulation which retain the important features of the original, while significantly reducing the computational expense.

Lift and drag data are presented for each of five blades at aircraft speeds up to 300 knots. Total main rotor forces and moments are also provided over this speed range. This body of data is the basis for comparison with data from alternate rotor models.

Obtaining these data required developments in both rotorcraft modeling and computer sciences. In the first discipline it was determined that the model for the blade element angle of attack should be modified. This modification was used in the generation of the basis data. Also, the tip-loss model was found to require modification when a large number of segmental elements is used, as in the case of a basis generation. An exploration of this phenomenon leads to an inverted tip-loss definition.

The computer-science impact is evaluated in the discussion of elemental spacing criteria; this evaluation influences the method of integrating the elemental forces and moments along the radius of a rotor blade. It is shown that locations within segments at which the lift and drag evaluations are made are critical to accuracy when the quadrature technique is used, and that inconsistent forces and moments may result. This aspect is examined, and independent of the spacing algorithm, consistent summation coefficients are developed using the assumption of linear force profiles between observation points. Another computer-science-related idea which is developed involves the technique of performing the force and moment evaluations at fixed azimuthal positions for ease in data comparison. Coupled with this idea is the observation that the aerodynamic and kinematic portions of the dynamics of a blade may then be independently analyzed. The idea of "constrained" dynamics allows aerodynamic parametric changes to be evaluated by essentially holding the kinematic portions to a prescribed condition. The result is a considerable reduction in computation required for data collection, and a clear establishment of cause and effect for analysis.

A very accurate basis for model comparison, which is appropriate for explorations into real-time model efficiencies, has emerged from this study. Many of the corrections and improvements developed are recommended for immediate applicability to a simulation model already being used. Although the spacing characteristics of

the equal annuli algorithm are preserved, alternate techniques are recommended for the use of summation coefficients, and the computation of the tip-loss phenomenon.

II. INTRODUCTION

The RSRA simulation mathematical model was developed by Sikorsky Aircraft for performance and handling qualities evaluations; it is also intended "for pilot training, preflight of test programs, and the evaluation of promising concepts before their implementation on the flight vehicle" (Houck et al., 1977). The author is indebted to Houck et al., for the extensive use of their data in this study. It is assumed that the reader has some familiarity with blade-element mathematical modeling, and in particular with the main rotor model described by Houck et al., which is herein referred to as the "extant model." As supplied to the Langley and Ames Research Centers, the model represents a computational requirement that can only be synchronized with real time by the use of rather sophisticated computers. Because of the applicability of the blade-element model, NASA has an interest in its wider utility (Mackie and Alderete, 1977), for instance, on such modest computers as the Xerox Sigma 8. The equations and data contained in the real-time model represent a proprietary derivation from Sikorsky Aircraft's General Helicopter (GENHEL) simulation model. Only the radial dimension is investigated here.

The objective of this study is to establish a rotor-system data base of high fidelity, using relatively arbitrary inputs that may be used in establishing the accuracy of alternate mathematical models. It is assumed that these alternate mathematical models will use the same physical principles as the extant rotating, blade-element model, but they will contain various modifications in order to accrue real-time computational benefits. Because of the magnitude of the computational problem for blade-element rotor models, their accuracy is highly correlated with their execution speed. It is maintained that an approximate model may be developed that will compare favorably with the complete model by capitalizing upon speed advantages. If these advantages approach the factor of two, the model will then be capable of real-time synchronization using a modest digital computer such as the Xerox Sigma 8. Hence, real-time constraints are the motivation for this study, although only accuracy is addressed here.

In order to establish a basis, or data base of high fidelity for comparison purposes, it must be assumed that the selected discretized model collapses to the proper continuum when the number of discrete elements is large (but considering computer word length, not too large). Unfortunately, the extant RSRA simulation model (Houck et al., 1977) converges very slowly with segment count, and this behavior prompted an investigation of the radial spacing convergence properties. Both a low- and high-speed flight condition were selected, and are presented in figures 1 and 2. Curves tagged "extant" reveal the convergence difficulties. The rotor-system thrust differences as functions of the total number of evaluation points are slowly convergent for a large number of points, and radically divergent for a small number of points. Hence, in this document we shall go somewhat beyond the mere creation of a data base and develop certain corrections and improvements that are applicable to the extant real-time simulation model.

A basis is created which meets the test of invariancy with perturbations in the number of radial evaluations. This corrected and improved model is not for real-time use, but for establishing a standard, for comparison purposes, with 20 radial evaluation points. This "basis" produces the rotor-system thrust differences tagged "basis"

in figures 1 and 2. The use of 20 evaluation points clearly eliminates discretization phenomena and algorithmic distortion from this model.

In contrast to the extant real-time model (Houck et al., 1977), an alternate model is developed which has better convergence features. This model is also appropriate for real-time simulation, and delivers the thrust differences tagged "alternate" in figures 1 and 2. Since real-time constraints usually dictate a small number of evaluation points, this alternate model is recommended for simulation work.

In the process of creating a data-acquisition algorithm for this analysis, a technique was discovered for literally taking a snapshot of dynamic variables; this technique is useful in isolating the small differences normally associated with various discrete algorithms. This feature has considerably reduced the computational expense of this and other studies; and it is also useful for the problem of rotorcraft trimming.

A technique is developed for handling the tip-loss phenomenon by introducing the concept of a pseudotip for lifting purposes. This technique reduces computational errors and simplifies the generalization of the integration process to a summation process.

With respect to a force profile along a blade, the combination of summation and spacing algorithms are investigated and found to be less than optimum. Improvement to the summation algorithm motivates the development of a slightly different spacing algorithm, used primarily for illustrative purposes; it is identified as equal-annuli midpoint spacing and is shown to better accommodate the quadrature technique. Without influencing computational expense, summation coefficients are developed for improvements in accuracy, and for consistency between forces and moments, regardless of the spacing algorithm. These coefficients feature a linear assumption for elemental forces between evaluation radii and extrapolation at endpoints.

A five-point model that uses the corrections and improvements developed here becomes so accurate that it is difficult to justify the use of more segments in real-time simulation work.

III. DATA ACQUISITION

An extensive mathematical model of the RSRA (Houck et al., 1977) has been programmed at NASA/Ames Research Center in both a single and a dual computer configuration (Mackie and Alderete, 1977). Although satisfactory real-time synchronization with this software has not been achieved using modest digital computers, the single computer formulation is nonetheless readily available for analyses using data generated in a batch (nonreal-time) mode. When an appropriate driving routine is used, the subroutine identified as ROTOR may be exercised as a separate entity for investigations into rotor modeling techniques.

In order to create a basis with which to compare alternate model structures, extensive data were obtained from ROTOR. Using 20 segments per blade, and with modifications that will be developed herein, ROTOR was run with an azimuth advance angle of 9°; the (pseudo) cycle time was varied from 7.094 to 9.851 msec in order to accommodate the scheduled rpm constraints (Mach 1 avoidance) as shown in table 1.

Data acquisition occurred at multiples of eight times the 9° azimuth advance increment, that is, every 72°, in order to avoid data interpolation.

For an arbitrary input control configuration within the capacity of a rotor system, after blade transients vanish after a few revolutions, the tracking blade phenomenon is observed in this model such that at any selected azimuth station the dynamics of a given blade are replicated by the other blades as they arrive at that station. In this condition of equilibrium, blade-element rotational kinematics at these orientations may be described with Fourier coefficients. For the RSRA model at all flight regimes this phenomenon has been observed to occur in something less than ten complete rotor revolutions, or 400 cycles through the 9°-increment logic. The orientation given in figure 3 has been selected as a standard for observation purposes, where the "master blade" is pointing aft.

The problem of obtaining a control profile that is within the capacity of the rotor system was treated with some seriousness, although it is not necessarily germain to this study. All that is actually required in this analysis is that all the degrees of freedom be exercised, and this requirement turns out to be a foregone conclusion with an arbitrary control profile. Nonetheless, a voluminous, unpublished document[1] was consulted for data over the entire flight envelope, and a control profile was selected that produced a reasonably smooth transition from point to point in velocity space (10-knot increments). This profile, shown in figure 4, is sufficient to acquire a large data base from the ROTOR routine, as modified. Since the rotor as a system has been isolated in this study, it is not necessary to consider the viability of the selected control profile with respect to body-loop closure. These controls certainly do not constitute trim positions, and the probability or even possibility that they will actually occur "in flight" is questionable.

It is shown herein how tip-loss effects may be independently considered by utilization of the concept of a pseudotip for lifting purposes, and how this concept eliminates discontinuous end effects from the force profiles as a function of radius. The integration (summation) of these smoother "force profiles,"

$$\left.\begin{aligned} f_P &= dF_P/dr \\ f_T &= dF_T/dr \\ f_R &= dF_R/dr \end{aligned}\right\} \qquad (1)$$

is shown still to present an array of discretization problems, which are compounded when the aerodynamic moments are also considered.

With two fixed locations along the blade, one being the cuff (beginning of the effective blade) and the other being the pseudotip (which is shown to be the effective tip for lifting purposes), the blade-force profiles are presented by using 20 evaluations per blade, and these data are given every 10 knots from 0 to 300 knots; lift profiles are presented in figure 5, and drag profiles are presented in figure 6. The quantity f_R is a minor term and is not displayed here.

All the data in this document have been created after the implementation of the angle-of-attack correction given in the next section.

[1]Robert A. Monteleone, Systems Requirements Handbook for the Rotor Systems Research Aircraft, Sikorsky Report SER-72039, March 1977. Also available from NASA management, Contract NAS1-13000.

Angle-of-Attack Error

In the reference formulation (Houck et al., 1977) α_Y is a four-quadrant angle ($180° < \alpha \leq 180°$) that may be given in terms of the dimensional velocity variables (v_P, v_T, v_R) by

$$\alpha_Y = \tan^{-1} \frac{(v_T \tan \theta_A + v_P)|\cos \gamma|}{v_T - v_P \tan \theta_A \cos^2 \gamma} \tag{2}$$

When the denominator of this expression is positive, $|\alpha_Y| \leq 90°$ and the positive table lookup argument (α_{TRANS} for lift) is obtained by determining whether or not the inplane angle of attack given by $|\alpha_Y \cos \gamma|$ is within a small band about the positive abscissa:

$$\alpha_{TRANS} = \begin{cases} |\alpha_Y \cos \gamma| & (|\alpha_Y \cos \gamma| \leq 13.5°,\ |\alpha_Y| \leq 90°) \\ |\alpha_Y| & (|\alpha_Y \cos \gamma| > 13.5°,\ |\alpha_Y| \leq 90°) \end{cases} \tag{3}$$

When the denominator of equation (2) is negative, $|\alpha_Y| > 90°$ and reverse flow occurs. The value of α_{TRANS} for lift is then determined by examining a similar small band about the negative abscissa:

$$\alpha_{TRANS} = \begin{cases} 180° - (180° - |\alpha_Y|)|\cos \gamma| & [(180° - |\alpha_Y|)|\cos \gamma| \leq 8°,\ |\alpha_Y| > 90°] \\ |\alpha_Y| & [(180° - |\alpha_Y|)|\cos \gamma| > 8°,\ |\alpha_Y| > 90°] \end{cases} \tag{4}$$

Section A-20(c) of the paper by Houck et al., 1977 (the first line of eq. (9) below) is therefore assumed to be in error, and should appear as

$$\alpha_{TRANS} = \left| |\alpha_Y| \cos \gamma | + \frac{\alpha_Y}{|\alpha_Y|} 180°(1 - |\cos \gamma|) \right|$$

$$= 180° - (180° - |\alpha_Y|)|\cos \gamma| \tag{5}$$

which is the same as the first line of equation (4). Since the angle of attack is also used to compute the switch point between univariant and multivariant lift and drag functions, this section of the function-generation logic is clarified in figure 7.

This angle-of-attack error in reverse flow probably has little effect on previous simulation results, although it has caused considerable delay in this analysis. Its influence is examined below.

If the equal-annuli spacing algorithm of the extant model is used, the initial evaluation (inboard) radius is given by (see section VII)

$$r_1 = \sqrt{\frac{r_{MR}^2 - r_A^2}{2N} + r_A^2} \tag{6}$$

which for five segments is equal to 11.56 ft. The interior portion of the effective aerodynamic blade, which is therefore treated as lacking in any important functionality, is given by the proportion

$$P = \frac{r_1 - r_A}{B_{MR}r_{MR} - r_A} \tag{7}$$

or 21.6% for a five-segment simulation. For the simplified relationship of tangential velocity,

$$v_T = \Omega r + 1.69(v_{knots})\sin \psi \tag{8}$$

at the worst-case azimuth of 270°, and setting the tangential velocity equal to zero permits the calculation of the radius at which stall occurs; this calculation is presented in figure 8. If the computed values of rpm of table 1 are used, it is seen that the stall phenomenon begins to occur on the effective aerodynamic surface at about 85 knots of vehicle velocity. It is also seen that until about 155 knots this phenomenon is ignored in the extant model since it occurs interior to the initial evaluation radius (five segments). Hence, even without the angle-of-attack correction given here, the extant simulation model performs as it was intended in velocity regions less than 155 knots. Beyond this velocity, or *if more than five segments are used at lower velocities*, the errors are dramatic.

As an example of the effect of this error, let us consider the extant (erroneous) formulation, which is independent of the sign of α_Y whenever the absolute value of α_Y is greater than 90°:

$$\begin{aligned}
\alpha_{TRANS} &= \left|\alpha_Y \cos\gamma + \frac{\alpha_Y}{|\alpha_Y|} 180°(1 - |\cos\gamma|)\right| \\
&= \left|\cos\gamma|\alpha_Y| + 180°(1 - |\cos\gamma|)\right| \\
&= \left|-|\alpha_Y \cos\gamma| + 180°(1 - |\cos\gamma|)\right|
\end{aligned} \tag{9}$$

The latter step is performed when $|\alpha_Y| > 90°$ because $\cos\gamma$ is negative when $v_T < 0$.

If $\alpha_Y = 179°$, which is well within the 8° band about the negative abscissa, then α_{TRANS} should be even closer to 180°. Also, for $\cos\gamma = 0.9$, where its sign is immaterial, one would anticipate a value for α_{TRANS} somewhere within 1° of the negative abscissa (180°), but what actually occurs from equation (9) is:

$$\alpha_{TRANS} = \left|-|(179°)(0.9)| + 180°(1 - |0.9|)\right| = 143.1° \tag{10}$$

The correct value from equation (5) is 179.1° (closer to coincidence with the airstream), which produces a relatively small lift coefficient (about -0.09). The value 143.1° produces a huge lift coefficient (about -1.1) and has been observed to cause spectacular N-per-revolution force and moment variations.

Data Density

The blade orientation of figure 3 and the control profile of figure 4 were used in order to obtain a reasonable output history; figures 5 and 6 show the diverse albeit piecewise continuous-curve shapes of the individual-blade lift- and drag-force profiles. Twenty observations of each lift- and drag-profile curve, as shown in these figures, appear to be more than heuristically sufficient for continuum emulation, and this fact is reinforced by invariancy under summation, as is shown by the curves tagged "basis" in figures 1 and 2. (The actual summation algorithm, which produces invariant answers for a reasonable number of segments N, will be seen to be different if a minimal value of N is required.) However, with the luxury of 20 observations, the summation algorithm becomes relatively inconsequential.

The data displayed in figures 5 and 6 contain the angle-of-attack correction discussed previously. The observation radii that have been selected for this data display are uniformly spaced, and although the inboard observation is placed at the beginning of the aerodynamic surface of the blade, the outboard observation radius will be seen to have a unique definition in a subsequent section of this report.

It has previously been ascertained that "reducing blade segments does not appear to influence the solution to any great extent (Houck and Bowles, 1976). Thus, one might question the necessity for such a fine mesh of points in this analysis. In order to answer this question, let us consider the following:

In this study, under all conditions, only a very small azimuth advance angle of 9° is used, thereby effectively eliminating this degree of freedom as an error source. It has indeed been our experience that "the worst single effect is that of increasing integration [azimuth] interval" (Houck and Bowles, 1976). It is also a very complex problem, which is under investigation but not addressed here. Only improvements to the radial dimension are addressed here, and in this dimension, which is displayed in figures 5 and 6, the "frequency content" is quite low, provided that the tip-loss technique of section IV is used (discontinuities are avoided). Hence, the standard technique of reducing element size until invariant answers ensue is quite proper, and figures 1 and 2 indicate that the value of 20 evaluation points is also quite proper.

Balanced and Constrained Dynamics

The two conditions, "balanced dynamics" and "constrained dynamics," are convenient for analysis. In the balance condition the flap/lag moments are allowed to operate as forcing functions for the flap/lag differential equations (normal operations), and hence produce new flapping and lagging states. In this condition, however, the slight modification of any parameter or algorithm generally produces myriad state changes and masks any causal relationship under investigation. For this reason, once the tracking-blade phenomenon is observed, the applicable Fourier coefficients are captured for use in the constrained condition. Thus, the condition of "constrained dynamics" means that blade trajectories are constrained to follow those previously determined (by the 20-segment model) so that force and moment differences may be isolated to differences in algorithms and segmentation. This process yields for both the balanced and constrained cases identical dynamics at the specific azimuth stations selected for observation. (The standard orientation of figure 3 is always used here.) In this orientation, where the master blade is aft and others

follow sequentially every $2\pi/B$ rad in the direction of positive rpm (B is the number of blades), flap/lag states are the same in both the balanced and constrained conditions.

It is interesting to note that in the constrained condition only one computational pass through the rotor equations is necessary in order to determine control variation responses. Responses to collective (θ_{CUFF}) and cyclic controls (A_{1S}, B_{1S}) may be approximated by use of partial derivatives with respect to low-order Fourier coefficients. As a subject for future research the static feature of the "constrained-dynamics" condition suggests an efficient, general trimming algorithm for rotorcraft since control-variation responses may then be isolated from the sensitive balance process. When such a two-pass trimming algorithm is performed the relatively long transients induced by control variations (due to the low damping in blade responses) are constrained until approximately correct control signals for trim are determined; the blades are then released until a balance is obtained. This process is then repeated until the constrained results become quiescent. It is believed that this sequence is more efficient than the alternate process of determining total responses to each control variation since long-period rotor transients interfere with cause and effect.

IV. TIP LOSS

The tip-loss technique is discussed and arguments are presented for its modification based upon consistency, applicability, accuracy, and ability to remain relatively invariant with changes in the number of segments N. Tip loss is presented early in this discussion because it results in a complete redefinition of integral limits, which influences other parameters. The resultant concept permits the implementation of tip loss as a superimposed quantity that may then be ignored throughout the remainder of this paper.

Where $r_{MR} = 31$ ft is the total blade length, the radius to the cuff from the hub ($r_A = 6.45$ ft) is given as the sum of the hinge offset ($e = 1.05$ ft) and spar ($e' = 5.4$ ft):

$$r_A = e + e' = r_{MR}(\xi + \xi') \tag{11}$$

In terms of dimensional segments Δr_n or nondimensional segments Δy_n, the sum over all N segments totals the effective blade distance, that is,

$$\sum_{n=1}^{N} \Delta r_n = r_{MR} \sum_{n=1}^{N} \Delta y_n = r_{MR}(1 - \xi - \xi') = r_{MR} - r_A \tag{12}$$

or 24.55 ft. Houck et al. state that for the outboard segment the lift coefficient is modified for tip loss by use of the relationship

$$C_{LY} = \left(\frac{\alpha_Y}{|\alpha_Y|}\right)\left(1 - \frac{1 - B_{MR}}{\Delta y_N}\right) f(\alpha_{TRANS}, \text{Mach}) \tag{13}$$

which is equivalent to an Nth segment radial-distance scale, or interpolation in the Nth segment via the proportion

$$P = 1 - \frac{1 - B_{MR}}{\Delta y_N} = 1 - (1 - B_{MR}) \frac{r_{MR}}{\Delta r_N} \tag{14}$$

where $B_{MR} = 0.97$. Therefore, the contribution of the Nth (outboard) segment to the force summation process for all terms that contain the quantity C_{LY} (lift terms) is scaled, and from the associative law this scaling is shown below to be identical to a radial-distance scale.

Let us consider the discretized lift-force-profile definition (Houck et al., 1977) with its radial increment multiplier Δr_n,

$$\Delta F_{Pn} = \frac{1}{2} \rho c v_{Yn} [(C_{LYn} v_{Tn}) / |\cos \gamma_n| + C_{DYn} v_{Pn}] \Delta r_n \tag{15}$$

$$C_{LYn} = \begin{cases} \mathrm{Sgn}(\alpha_{Yn}) f_n & (1 \le n < N) \\ P\,\mathrm{Sgn}(\alpha_{Yn}) f_n & (n = N) \end{cases} \tag{16}$$

where f_n is a tabled function, and Sgn( ) is plus or minus unity. For the purpose of simplification, we may define

$$\left.\begin{aligned} g_n &= \frac{1}{2} \rho c v_{Yn} \mathrm{Sgn}(\alpha_{Yn}) f_n v_{Tn} / |\cos \gamma_n| \\ h_n &= \frac{1}{2} \rho c v_{Yn} C_{DYn} v_{Pn} \end{aligned}\right\} \tag{17}$$

so that equations (15) and (16) may be written

$$\Delta F_{Pn} = g_n \Delta r_n + h_n \Delta r_n \qquad (1 \le n < N) \tag{18}$$

and, including the scale factor P in the applicable term,

$$\Delta F_{PN} = g_N (P \Delta r_N) + h_N \Delta r_N \qquad (n = N) \tag{19}$$

The blade lift force is obtained by the summation over all segments,

$$F_P = \sum_{n=1}^{N} h_n \Delta r_n + \sum_{n=1}^{N-1} g_n \Delta r_n + g_N (P \Delta r_N) \tag{20}$$

which is the discrete form of the continuous integration process

$$F_P = \int_{r_A}^{r_{MR}} h(r)dr + \int_{r_A}^{B_{MR} r_{MR}} g(r)dr \tag{21}$$

Hence, C_{LY} scaling is equivalent to scaling the upper radial limit for terms involving C_{LY} in the force-profile-integration process. Even if a more complex tip-loss formulation is assumed, such as linearly decreasing C_{LY} in some radial interval within the Nth segment, the discrete force summation (with B_{MR} adjustment) is identical. One cannot, therefore, ascertain the motivation for C_{LY} scaling from

the provided information (eq. (13)), but the effect is clearly the abrupt vanishing of C_{LY}-related terms at $B_{MR}r_{MR}$ as in equation (21). The availability of the continuum formulation (eq. (21)) is important when a large number of segments are considered, as will be seen. The upper radial limit $B_{MR}r_{MR}$ will be exploited in this section, but it is important to keep in mind that both C_{LYN} scaling and Δr_N scaling are identical techniques for the force summation problem, with the exceptions that are developed below.

When the number of segments N is allowed to become large, inconsistencies in the mathematical algorithms become apparent. One such inconsistency in the extant model involves the summation of moments, where the moment arm to the proportioned segment is not adjusted. It is not aerodynamically sound to consider C_{LY} as absolutely constant in the outboard segment all the way to the tip r_{MR}, even if it has been conceived as properly scaled (although its actual characteristic is an open question), so such an adjustment to the moment arm is always necessary. Thus, no physical assumption exists where the moment-summation element in the Nth segment reduces to the product $f_N \Delta r_N r_N$ of the extant model.

In this paper the discontinuous cutoff of lifting potential at $B_{MR}r_{MR}$ is generalized and assumed to be the motivation for the formulation (13). This assumption permits the development of a moment-summation algorithm that is consistent with the force-summation algorithm without added computational expense. Also, this assumption will lead to a more general treatment of the force profiles themselves, which will become quite important when the asymmetrical distribution properties of the equal-annuli spacing algorithm are considered. Unless the lift coefficient is constant in the outboard segment, the proportion operation (14) takes liberties with the mean-value theorem for integrals, and it actually contributes to force as well as moment errors.

Let us consider the spacing algorithm for the extant model developed in section VII. Using the outboard-segment increment Δr_N,

$$\Delta r_N = r_{MR} - \sqrt{\frac{N-1}{N}(r_{MR}^2 - r_A^2) + r_A^2} \tag{22}$$

the proportion (14) goes negative when $N > 16$. This operation is equivalent to subtracting more than the entire force contribution of the outboard segment, and in moment space such a subtraction cannot be justified even if the force increments are constants. Indeed, figure 5 demonstrates that there is considerable variation in the lift-force profiles in this region, and comparison with figure 6 shows that typical lift values are an order of magnitude larger than drag values. Since this unusual subtraction feature occurs just when the quantity N is getting large enough in an accuracy analysis to replicate continuum results, a large number of segments N and this technique for tip-loss compensation are inconsistent. Hence, at least for the establishment of a basis, this technique begs modification. It should be noticed that the outboard-segment size Δr_N in equation (22) is approximately hyperbolic with N (Taylor series),

$$\Delta r_N \approx [1 - (r_A/r_{MR})^2]r_{MR}/(2N) \approx \frac{14.83}{N} \tag{23}$$

so that P in equation (14) is nearly linear with N.

$$P \approx 1 - 0.0627N \tag{24}$$

For comparison purposes, we shall consider uniform spacing where the increment size is independent of n. In this case,

$$\Delta r_{(N)} = (r_{MR} - r_A)/N \tag{25}$$

so that the proportion (14) does not go negative until $N > 26$. However, it still goes negative with N, and this fact raises questions about a discrete formulation of continuous phenomena that deteriorates as the number of elements becomes heuristically sufficient to replicate the continuum. It should be noted that when $N > 26$, or with the equal-annuli algorithm when $N > 16$, the $(N - 1)^{st}$ segment and possibly other segments should actually enter into the computation, and the Nth segment should be virtually ignored.

The blade terminus for lifting purposes may be computed from the summation of the cuff, $N - 1$ elements, and the scaled outboard element:

$$r_T = r_A + \sum_{n=1}^{N-1} \Delta r_n + P\,\Delta r_N = r_{MR} B_{MR} \tag{26}$$

This formulation is independent of the spacing algorithm. The radius r_T constitutes the terminus of integration for terms involving the lift coefficient C_{LY}, and the suggested tip-loss technique follows:

$$\left.\begin{aligned} \text{Lift} &= \int_{r_A}^{r_T} f(r)dr && \text{(suggested)} \\ &\approx \int_{r_A}^{r_{N(-)}} f(r)dr + P \int_{r_{N(-)}}^{r_{MR}} f(r_N)dr && \text{(extant)} \end{aligned}\right\} \tag{27}$$

$$\left.\begin{aligned} \text{Drag} &= \int_{r_A}^{r_{MR}} g(r)dr && \text{(extant)} \\ &\approx \int_{r_A}^{r_T} g(r)dr + \int_{r_T}^{r_{MR}} g(r_N, r_{N-1})dr && \text{(suggested)} \end{aligned}\right\} \tag{28}$$

With the suggested formulation the interval of numerical integration becomes independent of the size of the Nth segment, which begins at $r_{N(-)}$ and ends at $r_{N(+)}$, so that previous objections are invalidated.

The concept of a pseudoblade is such that it encompasses just the constant-lifting-surface interval (r_A, r_T). This concept will be seen to benefit not only this analysis and the establishment of a basis, but will also benefit the extant simulation model. The technique uses linear extrapolation on the drag coefficient beyond r_T rather than interpolation (assuming a constant segment value) on the lift coefficient, and the number N may be as large or small as is desired without mathematical inconsistency.

Advantages are gained with the suggested technique. Figure 5 shows that lift-force gradients are generally large near the tip, and the suggested technique does not approximate in this region. The *linear extrapolation of drag* over the small interval (r_T, r_{MR}) will be shown to be equivalent to superimposing a perturbation; the magnitude of the lift profile in the region of the outboard segment is generally an order of magnitude larger than that of the drag profile. Hence, lift space is inferior to drag space as an approximation medium. A final argument for the rejection of the extant technique concerns the distortion of continuity, which is reserved until the end of this section.

In order to appreciate the tip-loss phenomenon in the context of a pseudoblade, we shall consider the aerodynamic-force differentials in terms of the dimensional velocities in the nth segment (Houck et al., 1977),

$$\left.\begin{aligned} dF_{Pn} &= \frac{1}{2}\rho c v_{Yn}[(C_{LYn}v_{Tn})/|\cos\gamma_n| + C_{DYn}v_{Pn}]dr_n \\ dF_{Tn} &= \frac{1}{2}\rho c v_{Yn}(C_{DYn}v_{Tn} - C_{LYn}v_{Pn}|\cos\gamma_n|)dr_n \\ dF_{Rn} &= (v_{Rn}/v_{Tn})dF_{Tn} \end{aligned}\right\} \tag{29}$$

which must be integrated over appropriate radial limits to obtain the blade aerodynamic forces and moments. For terms involving C_{LY} these limits are the pseudoblade interval (r_A, r_T), whereas for terms involving C_{DY} these limits are the total effective blade interval (r_A, r_{MR}), which is identical to the combination (r_A, r_T) and (r_T, r_{MR}). This latter interval, defined as the drag extrapolation distance, is given by

$$r_{MR} - r_T = (1 - B_{MR})r_{MR} = 0.93 \text{ ft} \tag{30}$$

which is less than 4% of the total effective blade. This region is always beyond the outboard evaluation point even if N approaches infinity. During this small interval (r_T, r_{MR}), the lift coefficient C_{LY} is zero and the drag coefficient C_{DY} along with its appropriate kinematic functionality may be extrapolated in both force and moment space. This procedure is outlined below in terms of superimposed increments:

$$\left.\begin{aligned} \Delta F_{P(TL)} &= \frac{1}{2}\rho c \int_{r_T}^{r_{MR}} v_Y v_P C_{DY}\, dr \\ \Delta F_{T(TL)} &= \frac{1}{2}\rho c \int_{r_T}^{r_{MR}} v_Y v_T C_{DY}\, dr \\ \Delta F_{R(TL)} &= \frac{1}{2}\rho c \int_{r_T}^{r_{MR}} v_Y v_R C_{DY}\, dr \end{aligned}\right\} \tag{31}$$

Also, the moment differentials about the hinge are defined (Houck et al., 1977) as

$$\left.\begin{aligned} dM_{FA} &= (r - e)dF_P \\ dM_{LA} &= (r - e)dF_T \end{aligned}\right\} \tag{32}$$

so that the extrapolated moment increments are given by

$$\left.\begin{aligned} \Delta M_{FA(TL)} &= \frac{1}{2}\rho c \int_{r_T}^{r_{MR}} v_Y v_P (r - e) C_{DY}\, dr \\ \Delta M_{LA(TL)} &= \frac{1}{2}\rho c \int_{r_T}^{r_{MR}} v_Y v_T (r - e) C_{DY}\, dr \end{aligned}\right\} \tag{33}$$

By assuming linearity between the available *combinations of terms* $v_{Yn}v_{Pn}C_{DYn}$, $v_{Yn}v_{Tn}C_{DYn}$, and $v_{Yn}v_{Rn}C_{DYn}$ at the two outboard evaluation radii r_{N-1} and r_N, we can define four constant coefficients:

$$\left.\begin{aligned} A_{F(N-1)} &= \frac{r_{MR} - r_T}{r_N - r_{N-1}}\left[r_N - \frac{1}{2}(r_{MR} + r_T)\right] \\ A_{F(N)} &= \frac{r_{MR} - r_T}{r_N - r_{N-1}}\left[\frac{1}{2}(r_{MR} + r_T) - r_{N-1}\right] \\ A_{M(N-1)} &= \frac{r_{MR} - r_T}{r_N - r_{N-1}}\left[\frac{1}{2} r_N (r_{MR} + r_T) - (r_{MR}^2 + r_{MR}r_T + r_T^2)/3\right] - eA_{F(N-1)} \\ A_{M(N)} &= \frac{r_{MR} - r_T}{r_N - r_{N-1}}\left[(r_{MR}^2 + r_{MR}r_T + r_T^2)/3 - \frac{1}{2} r_{N-1}(r_{MR} + r_T)\right] - eA_{F(N)} \end{aligned}\right\} \tag{34}$$

so that by using the coefficients

$$\left.\begin{aligned} K_{N-1} &= \frac{1}{2}\rho c v_{Y(N-1)} C_{DY(N-1)} A_{F(N-1)} \\ K_N &= \frac{1}{2}\rho c v_{Y(N)} C_{DY(N)} A_{F(N)} \\ L_{N-1} &= \frac{1}{2}\rho c v_{Y(N-1)} C_{DY(N-1)} A_{M(N-1)} \\ L_N &= \frac{1}{2}\rho c v_{Y(N)} C_{DY(N)} A_{M(N)} \end{aligned}\right\} \tag{35}$$

the indicated integrations of equations (31) and (33) are approximated by:

$$\left.\begin{aligned}
\Delta F_{P(TL)} &= K_{N-1} v_{P(N-1)} + K_N v_{P(N)} \\
\Delta F_{T(TL)} &= K_{N-1} v_{T(N-1)} + K_N v_{T(N)} \\
\Delta F_{R(TL)} &= K_{N-1} v_{R(N-1)} + K_N v_{R(N)} \\
\Delta M_{FA(TL)} &= L_{N-1} v_{P(N-1)} + L_N v_{P(N)} \\
\Delta M_{LA(TL)} &= L_{N-1} v_{T(N-1)} + L_N v_{T(N)}
\end{aligned}\right\} \tag{36}$$

The total aerodynamic forces and moments are thus generated by integrals of equations (29) over the constant interval (r_A, r_T) plus the superimposed tip-loss compensation terms, that is,

$$\left.\begin{aligned}
F_P &= \int_{r_A}^{r_T} dF_P + \Delta F_{P(TL)} \\
F_T &= \int_{r_A}^{r_T} dF_T + \Delta F_{T(TL)} \\
F_R &= \int_{r_A}^{r_T} dF_R + \Delta F_{R(TL)} \\
M_{FA} &= \int_{r_A}^{r_T} (r - e) dF_P + \Delta M_{FA(TL)} \\
M_{LA} &= \int_{r_A}^{r_T} (r - e) dF_T + \Delta M_{LA(TL)}
\end{aligned}\right\} \tag{37}$$

It should be noticed that these "superimposed tip-loss terms" are not related to the usual definition for tip-loss effects, and their magnitudes are considerably less than usual values because they utilize drag rather than lift space as an approximation medium. Also, the linear-extrapolation process to obtain these terms does not influence the computational workload.

In the form of equations (37) any continuity in the force profiles of equations (1) may be exploited by both the spacing and summation algorithms. Since these force profiles are exactly the content of figures 5 and 6, reference to these curves shows that the physics of a rotor blade contribute enough discrete modeling problems without the arbitrary introduction of the tip-loss discontinuity into the outboard evaluation value. When equation (13) is applied to these curves as in the extant model, the outboard evaluation value *on both the lift and drag profiles* usually is distorted to a position that bears no recognizable relationship to the other points, easily being less than half the magnitude of its adjacent (N - 1) value, thereby creating a computer-science problem where none should exist. This discontinuous phenomenon is observed in all flight regimes and with various values of N. When N = 5, for instance, Δr_N = 3.12 ft with equal-annuli spacing and the

Nth segment lift evaluation is distorted to approximately 70% of its "true" or continuous value. Drag distortion depends upon the relative contribution of the terms comprising F_T.

In the general form of equations (37) the tip-loss phenomenon is superimposed after the exacting tasks of the spacing and summation algorithms have been accomplished. The suppression of distortion in the continuous-derivative information is extremely important when the integration of equations (37) is approximated by a summation process. Distortion of derivatives should be avoided when using discrete integration schemes; if any correlation is assumed between points, which is certainly an objective of discrete modeling of continuous phenomena and is the primary basis for more sophisticated integration schemes, this distortion becomes computationally destructive.

For the 20-segments-per-blade case the summed aerodynamic lift, drag, and radial forces on each blade (*excluding the superimposed tip-loss terms developed here*) are presented in figures 9(a) through 9(c), and the flapping and lagging moments are given in figures 9(d) and 9(e). These forces, shown for every 10 knots of vehicle velocity, represent an accurate summation process operating on the specific content of figures 5 and 6.

When the tip-loss effects are superimposed, the curve shapes of figures 9(a) through 9(e) are modified to become those of figures 10(a) through 10(e). It is seen that lift-related terms vary negligibly when this tip-loss technique is used because of the unique summation limits. Drag variations are small because the extrapolation distance (eq. (30)) is small.

The quantities involving the multiplier v_P (perpendicular velocity) are negligible, as can be seen by comparing the curves of figures 9(a) and 9(d) with those of figures 10(a) and 10(d), respectively. However, the quantities involving the multiplier v_T (tangential velocity) can become significant, as can be seen for the advancing blades by comparing the drag curves of figures 9(b) and 10(b). These results have been numerically investigated and the quantities $\Delta F_{P(TL)}$ and $\Delta M_{FA(TL)}$ may be arbitrarily set equal to zero.

Since drag as a numerical quantity is usually smaller than lift and the extrapolation distance is a small and constant portion (0.03) of the total radius, C_{LY} is integrated to a good approximation in this formulation from the cuff to the aerodynamic terminus for lifting purposes (r_T) with a significant gain in accuracy (as compared with the extant technique), and C_{DY} is integrated to the blade tip (r_{MR}) with a slight degradation of accuracy.

Equations (34) through (37) constitute the superimposed tip-loss correction terms that are assumed throughout the remainder of this paper.

V. SIMPLIFIED SPACING AND SUMMATION

Three spacing/summation algorithms are here examined in order to reveal their relative-error convergence properties and to investigate their efficiency in the rotorcraft environment. A simplified model for force profiles is used to demonstrate that the moment-summation algorithm of the extant model, for example, has slow convergence properties. This algorithm is later expanded to the full model and accountable error sources are identified in both forces and moments.

In the extant model the increment distribution is asymmetrical about the individual radial evaluation points because of equal-annuli spacing, and the summation processes are given by the quadrature technique

$$\left.\begin{aligned} F &= r_{MR} \sum_{n=1}^{N} f(y_n)\Delta y_n = \sum_{n=1}^{N} f(r_n)\Delta r_n \\ M &= r_{MR}^2 \sum_{n=1}^{N} y_n f(y_n)\Delta y_n = \sum_{n=1}^{N} (r_n - e) f(r_n)\Delta r_n \end{aligned}\right\} \tag{38}$$

where y_n is designated as the center of lift of the segment. Although the limits are proper in these expressions as N approaches infinity, it will be shown that they are first approximations with relatively poor convergence rates when asymmetrical spacing is used.

In order to demonstrate convergence features of summation processes, a simplified blade-force profile is used; it is developed as follows:

Let us consider a constant, unitary force where y is the nondimensional radial variable, and neglect spar and offset, which complicate (and modify somewhat) this analysis. Under these conditions the force-summation problem is to find an efficient, discrete algorithm that closely approximates the closed-form solutions for the force and moment:

$$F = \int_0^1 dy = 1$$

$$M = \int_0^1 y\, dy = \frac{1}{2}$$

If this simplified model is generalized to a force of order k in the independent variable, the continuous solutions are given by

$$F(y^k) = \int_0^1 y^k\, dy = \frac{1}{k+1}$$

$$M(y^k) = \int_0^1 y^{k+1}\, dy = \frac{1}{k+2}$$

and the direct summations (38) operating on this simplified force profile produce relative force and moment errors given by

$$\left.\begin{aligned} E[F(y^k)] &= (k+1)\sum_{n=1}^{N} y_n^k\,\Delta y_n - 1 \\ E[M(y^k)] &= (k+2)\sum_{n=1}^{N} y_n^{k+1}\,\Delta y_n - 1 \end{aligned}\right\} \tag{39}$$

Since $E[F(y^k)] = E[M(y^{k-1})]$, the force errors are subsets of the moment errors in this simplified model (using the summation process given), and they need not be included in this discussion. For this reason the "*relative moment error due to a force profile of order k*" will be used to demonstrate the slow-convergence feature of the extant moment summation algorithm for equal-annuli spacing. First, however, a very simple spacing scheme is examined for comparison purposes.

Uniform-Segment Algorithm

We shall consider the summation of moments for uniform spacing of segments, where the force-profile evaluations are made at the midpoints of the segments. The simplified, nondimensional radial parameters are given by

$$\left.\begin{aligned} \Delta y_{(n)} &= 1/N \\ y_n &= \left(n - \tfrac{1}{2}\right)\Delta y_{(n)} = \left(n - \tfrac{1}{2}\right)/N \end{aligned}\right\} \tag{40}$$

This algorithm will be useful in isolating the error source in the extant model. The evaluation radii for various numbers of segments are presented in table 2. (Coincidence of the observation radii for all lift and drag forces and moments is an assumed feature of a real time model.)

For this algorithm, as the number of evaluation points is decreased, the end-point evaluation radius moves away from the tip and the density of evaluations near the tip drops off in equal proportion to the density elsewhere.

For regular polynomial forms, let us consider the relative moment error from equations (39):

$$E[M(y^k)]_{Un} = \frac{k+2}{N^{k+2}}\sum_{n=1}^{N}\left(n - \tfrac{1}{2}\right)^{k+1} - 1 \tag{41}$$

For a force characteristic that is either constant, linear, or quadratic, these sums are

$$E[M(y^0)]_{Un} = 0$$

$$E[M(y^1)]_{Un} = -1/4N^2$$

$$E[M(y^2)]_{Un} = -1/2N^2$$

and they are presented in table 3 for up to 10 evaluation radii.

For polynomial forms this table shows the general underprediction of moments when the uniform-segment algorithm is used. *A priori* information is necessary to use the simplied correction factors. Factors such as these, which imply an assumption about the behavior of the force profiles between observation radii y_n, are later described in terms of modifying the summation algorithm (38). When observation spacing is nonuniform, the effect under summation of products such as $f(y_n)\Delta y_n$ is equivalent to a weighting algorithm capable of accommodating an assumed curve profile. When physical information is available that indicates a tendency under certain conditions for some curves (such as an advancing-blade drag profile) to assume a particular polynomial form, this motivates the selection of a nonuniform-spacing algorithm, but does not release the spacing/summation algorithm from the responsibility for accommodation of either simple or arbitrary curve shapes, which may in fact be the dominant characteristics.

Equal-Annuli Algorithm

In contrast to the uniform-segment algorithm, the simplified nondimensional radial parameters for the equal-annuli algorithm (Houck et al., 1977), which are developed in section VII, are given by

$$\left.\begin{aligned} \Delta y_n &= (\sqrt{n} - \sqrt{n-1})/\sqrt{N} \\ y_n &= \sqrt{n - \tfrac{1}{2}}\Big/\sqrt{N} \end{aligned}\right\} \tag{42}$$

The asymmetrical property of these relationships is due to the fact that y_n, the evaluation radius, is not the midpoint of Δy_n, which is variable. For various numbers of segments the evaluation radii are presented in table 4, which may be compared with table 2.

Unlike the uniform-segment algorithm of the last section, this spacing algorithm shifts the observation radii toward the blade tip. However, it is also true that the endpoint retreats from the tip with a decreasing number of segments, which is pertinent to the tip-loss discussion of section IV.

For regular-polynomial forms using the equal-annuli algorithm and the direct summation (38), the relative moment error for a force profile of order k is:

$$E[M(y^k)]_{Eq} = \frac{k+2}{N^{(k+2)/2}} \sum_{n=1}^{N} \left(n - \tfrac{1}{2}\right)^{(k+1)/2} (\sqrt{n} - \sqrt{n-1}) - 1 \tag{43}$$

By using the Euler-McLaurin Sum-Formula (Selby, 1970), that is, the series expansion

$$\sum_{n=1}^{N-1} \sqrt{n} = \sqrt{N}\left(\frac{2}{3}N - \frac{1}{2} + \frac{1}{24N} - \frac{1}{1920N^3} + \frac{1}{9216N^5} - \frac{11}{163840N^7} + \ldots\right) - 0.207886225 \ldots \tag{44}$$

the relative moment error for a linear-force profile may be evaluated,

$$E[M(y^1)]_{Eq} = \frac{3}{N^{3/2}} \sum_{n=1}^{N} \left(n - \frac{1}{2}\right)(\sqrt{n} - \sqrt{n-1}) - 1$$

$$= 0.623658675 \ldots - \frac{1}{8N^2} + \frac{1}{640N^3} - \frac{1}{3072N^5} + \ldots \qquad (45)$$

By performing an absolute ratio of the relative moment errors the performance of this algorithm relative to the uniform-segment algorithm with $k = 1$ is then found

$$\left|\frac{E[M(y^1)]_{Eq}}{E[M(y^1)]_{Un}}\right| = 2.494634\ \sqrt{N} - \frac{1}{2} + \frac{1}{160N} - \frac{1}{768N^3} + \ldots \qquad (46)$$

which reveals that, for a *linear* force and five segments, the relative convergence rate of the moment sum using the equal-annuli algorithm is over five times slower than the moment sum using the uniform-segment algorithm. For comparison with the uniform-segment algorithm of table 3, the relative moment errors are presented in table 5 for the equal-annuli algorithm. Moment errors produced by using the equal-annuli algorithm thus compare poorly with those produced by using the uniform-segment algorithm of table 3 when the force profile is relatively simple. The large error present when the force profile is very simple (e.g., constant) is disturbing because it indicates that the extant simulation model produces avoidable errors at low vehicle velocity. This problem is isolated in section VII to an inconsistency between the selection of the interval Δy_n and its observation radius y_n, and this problem is compounded when the moment arm y_n is used for moment calculations, as above.

Equal-Annuli Midpoints

If equal-annuli segment spacing is specified from other considerations, the midpoint of the interval may optionally be selected as the observation radius, that is,

$$y_n = \frac{1}{2}\ (\sqrt{n} + \sqrt{n-1})/\sqrt{N} \qquad (47)$$

which preserves the spacing features of pure equal-annuli spacing as shown in table 6, although it gives slightly more weight to inboard segments.

For regular polynomial forms using this spacing algorithm and the direct summation algorithm (38), the relative moment error for a force profile of order k is given from equations (39),

$$E[M(y^k)]_{EM} = \frac{k+2}{2^{k+1}N^{(k+2)/2}} \sum_{n=1}^{N} (\sqrt{n} + \sqrt{n-1})^k - 1 \qquad (48)$$

Compared with the pure equal-annuli algorithm shown in table 5, this algorithm tends to eliminate the large moment errors that are observed for simple force profiles, as shown in table 7. The constant column is noteworthy. This table indicates, however, that when the force profile becomes quadratic or higher order, the gain in accuracy is lost. This loss of accuracy will be shown in section VI to be a consequence of the summation algorithm rather than the spacing algorithm.

The use of the simplified spacing and summation models for illustrative purposes has been examined, and the following observations may be made about the summation scheme (38), or quadrature technique:

1. It works well for uniform spacing and produces errors compatible with the difference between linearity and the actual order of the force profile; that is, table 3 is quite elementary.

2. It does not work well at all for equal-annuli spacing, although some improvement is noticed if the force profile is high order.

3. It works better for equal-annuli midpoint spacing but seems to deteriorate too rapidly as the curve order increases.

Momentum or statistical-sampling theories indicate that equal-annuli spacing should deliver equivalent or less error than uniform spacing, even if the actual force profiles are simple polynomial forms, and these approaches should all deliver zero error when the force profile is constant. The discrepancy in the extant model is explored in section VI.

VI. SUMMATION PROCESSES

The summation processes of Houck et al. (1977), where $r_{n(+)}$ and $r_{n(-)}$ are the upper and lower nth segment boundaries, are equivalent in dimensional space to

$$F = \sum_{n=1}^{N} f(r_n)[r_{n(+)} - r_{n(-)}] \tag{49}$$

$$M = \sum_{n=1}^{N} (r_n - e)f(r_n)[r_{n(+)} - r_{n(-)}] \tag{50}$$

and have been shown (sec. V) to be consistent with midpoint spacing of the evaluation radii, that is,

$$r_n = \frac{1}{2}[r_{n(+)} + r_{n(-)}] \tag{51}$$

for elementary forms of the force profile $f(r)$. However, they are inconsistent with an asymmetrical-spacing algorithm such as equal annuli, in which the evaluation radii will be shown to reduce to

$$r_n = \sqrt{\frac{1}{2}[r_{n(+)}^2 + r_{n(-)}^2]} \tag{52}$$

in that they cause errors in both the force and moment summations when the force profiles are elementary (e.g., linear). This point is important since the very nature of equal-annuli spacing permits the acquisition of a limited amount of data over significant intervals, that is, reduces the individual segment contributions to what appears to be elementary forms under summation.

When the force profile is composed of N perfectly distributed (segment boundaries coincident with discontinuities) constant steps over each $(r_{n(-)}, r_{n(+)})$, the summation processes may be examined at the elemental level. For the force-summation process, the force $f(r_n)$ could be evaluated anywhere in the interval $(r_{n(-)} \leq r_n \leq r_{n(+)})$ because it is constant:

$$\int_{r_{n(-)}}^{r_{n(+)}} f(r)dr = f(r_n)[r_{n(+)} - r_{n(-)}] \tag{53}$$

However, the moment-summation process (50) then requires r_n to be the midpoint of the interval,

$$\int_{r_{n(-)}}^{r_{n(+)}} (r - e)f(r)dr = [r_{n(+)} - r_{n(-)}]\left\{\frac{1}{2}[r_{n(+)} + r_{n(-)}] - e\right\}f(r_n) \tag{54}$$

because each element of equation (54) is equal to each element of equation (50) if and only if equation (51) holds. This fact explains the large errors observed in column one of table 5.

When the force profile is composed of N perfectly distributed (coincident boundaries and piecewise discontinuities) linear elements, the summation process may again be examined at the elemental level. In this case the force summation process itself defines r_n as the midpoint. By fitting a linear curve between the segment extremities,

$$\int_{r_{n(-)}}^{r_{n(+)}} f(r)dr = \int_{r_{n(-)}}^{r_{n(+)}} \left\{f[r_{n(-)}] + \{f[r_{n(+)}] - f[r_{n(-)}]\}\left[\frac{r - r_{n(-)}}{r_{n(+)} - r_{n(-)}}\right]\right\}dr$$

$$= \frac{1}{2}[r_{n(+)} - r_{n(-)}]\{f[r_{n(+)}] + f[r_{n(-)}]\} \tag{55}$$

it is shown that for the force to be linear its midpoint value must be the average in the interval,

$$f(r_n) = \frac{1}{2}\{f[r_{n(+)}] + f[r_{n(-)}]\} \tag{56}$$

so that equation (51) is again dictated. Errors begin creeping into the midpoint algorithm beyond this point of complexity, and this very fact is the motivation for the selection of a spacing algorithm that tends to concentrate observations in regions of high gradient activity.

The inconsistency in the equal-annuli algorithm of the extant model will be shown to be due to the failure of the summation processes (49) and (50) to accommodate the spacing of equation (52). It should be noted that equation (51) is consistent with these summation processes and appears to be a viable substitute. For this substitute spacing algorithm the segment boundaries themselves will be shown in section VII to have an independent derivation based upon equal-annuli arguments. However, objections still exist to using equations (49) and (50) even if the midpoint spacing of equation (51) is used. For instance, since the initial evaluation

radius r_1 is quite distant from the cuff r_A for both pure equal-annuli and midpoint spacing, and since high gradient activity near the tip is obvious, then equations (49) and (50) produce errors even for piecewise linear curves because they fail to extrapolate exterior to r_N (by using $f(r_{N-1})$) or interior to r_1 (by using $f(r_2)$). (The interior slopes have a canceling action when piecewise linear curves are used.) In addition, again assuming this linear form, the moment summation (50) produces rather large errors because the midpoint radial arm is a gross approximation to the actual integrated functionality; that is,

$$\int_{r_{n(-)}}^{r_{n(+)}} (r - e)f(r)dr \neq (r_n - e)f(r_n)[r_{n(+)} - r_{n(-)}] \tag{57}$$

An integration scheme that incorporates both the extrapolation feature and piecewise linear functionality is developed in the next section.

Integration of linear segments

In this section a consistent summation algorithm is developed. The force profiles are assumed to be linear between observation radii, which are arbitrary,

$$f_n(r) = f_n + \left(\frac{r - r_n}{r_{n+1} - r_n}\right)(f_{n+1} - f_n) \qquad (1 \leq n < N) \tag{58}$$

and (if necessary) linearly extrapolated beyond the evaluation extrema. With these assumptions, the integrations for the forces and moments over the entire pseudoblade interval (r_A, r_T) may be given by

$$F = \int_{r_A}^{r_2} f_1(r)dr + \int_{r_{N-1}}^{r_T} f_{N-1}(r)dr + \sum_{n=2}^{N-2} \int_{r_n}^{r_{n+1}} f_n(r)dr \tag{59}$$

$$M = \int_{r_A}^{r_2} rf_1(r)dr + \int_{r_{N-1}}^{r_T} rf_{N-1}(r)dr + \sum_{n=2}^{N-2} \int_{r_n}^{r_{n+1}} f_n(r)dr - eF \tag{60}$$

(excluding the superimposed tip-loss effects). The discrete solutions are given by linear combinations of the force observations f_n,

$$\left.\begin{aligned} F &= \sum_{n=1}^{N} a_n f_n \\ M &= \sum_{n=1}^{N} b_n f_n \end{aligned}\right\} \tag{61}$$

when the precomputed coefficients are as follows for $N > 3$:

$$
\left.
\begin{aligned}
a_1 &= \frac{1}{2}\,(r_2 - r_A)^2/(r_2 - r_1) \\
a_2 &= \frac{1}{2}\,[r_3 - r_1 - (r_1 - r_A)^2/(r_2 - r_1)] \\
a_{N-1} &= \frac{1}{2}\,[r_N - r_{N-2} - (r_T - r_N)^2/(r_N - r_{N-1})] \\
a_N &= \frac{1}{2}\,(r_T - r_{N-1})^2/(r_N - r_{N-1}) \\
a_n &= \frac{1}{2}\,(r_{n+1} - r_{n-1}) \qquad (2 < n < N - 1)
\end{aligned}
\right\} \tag{62}
$$

and

$$
\left.
\begin{aligned}
b_1 &= \frac{1}{6}\,(r_2 - r_A)^2(r_2 + 2r_A)/(r_2 - r_1) - ea_1 \\
b_2 &= \frac{1}{6}\,[(r_3 - r_2)(r_3 + 2r_2)(r_2 - r_1) + 2(r_2^3 - r_A^3) \\
&\quad - 3r_1(r_2^2 - r_A^2)]/(r_2 - r_1) - ea_2 \\
b_{N-1} &= \frac{1}{6}\,[(r_{N-1} - r_{N-2})(r_{N-2} + 2r_{N-1})(r_N - r_{N-1}) + 3r_N(r_T^2 - r_{N-1}^2) \\
&\quad - 2(r_T^3 - r_{N-1}^3)]/(r_N - r_{N-1}) - ea_{N-1} \\
b_N &= \frac{1}{6}\,(r_T - r_{N-1})^2(r_{N-1} + 2r_T)/(r_N - r_{N-1}) - ea_N \\
b_n &= \frac{1}{6}\,(r_{n+1} - r_{n-1})(r_{n+1} + r_n + r_{n-1}) - ea_n \qquad (2 < n < N - 1)
\end{aligned}
\right\} \tag{63}
$$

Hence, by merely assuming a linear transition of the observed force profiles from point to point, a consistent set of coefficients are made available for general summation application by using equations (61); they accommodate any monotonic spacing algorithm $r_A \le r_k < r_{k+1} \le r_T$ $(1 \le k < N)$, and they extrapolate internal to the inboard and external to the outboard observation radii. In addition, for moment summation a linear force profile is error free.

These general summation coefficients are independent of the spacing algorithm, and they will be applied to the basis in the next section. Later, they will also be applied to the "equal-annuli midpoint algorithm" with accuracy improvement over the extant model.

When $N = 3$, the summations in equation (59) vanish, so that:

$$a_2 = \frac{1}{2}\left[r_3 - r_1 - (r_1 - r_A)^2/(r_2 - r_1) - (r_T - r_3)^2/(r_3 - r_2)\right]$$

$$b_2 = \frac{1}{6}\left(\frac{r_2 - r_A}{r_2 - r_1}\right)\left[-3r_1(r_2 + r_A) + 2(r_2^2 + r_2 r_A + r_A^2)\right]$$

$$+ \frac{1}{6}\left(\frac{r_T - r_2}{r_3 - r_2}\right)\left[3r_3(r_T + r_2) - 2(r_T^2 + r_T r_2 + r_2^2)\right] - ea_2$$

Algorithm for the Basis

The basis always utilizes 20 equally spaced observation radii. The initial evaluation radius is at the cuff $r_1 = r_A$, and the final evaluation radius is at the tip for lifting purposes $r_N = r_T$. This selection obviates extrapolation except for the tip-loss correction, and it assures that the best available parameters are used for the tip-loss extrapolation process. The basis also uses the piecewise linear summation process of the previous section. The summation coefficients reduce to

$$a_n = \begin{cases} \frac{1}{2}\Delta r & (n = 1) \\ \Delta r & (1 < n < N) \\ \frac{1}{2}\Delta r & (n = N) \end{cases} \tag{64}$$

$$b_n = \begin{cases} \frac{1}{2}\Delta r(r_A + \Delta r/3 - e) & (n = 1) \\ \Delta r(r_n - e) & (1 < n < N) \\ \frac{1}{2}\Delta r(r_T - \Delta r/3 - e) & (n = N) \end{cases} \tag{65}$$

where

$$\left.\begin{aligned} \Delta r &= (r_T - r_A)/(N - 1) \\ r_n &= r_A + (n - 1)\Delta r \end{aligned}\right\} \tag{66}$$

The reduction of the coefficients to these simple forms, which appear similar to those of the extant model, is due to the selection of r_1 to correspond to the cuff, r_N to correspond to the tip for lifting purposes, and uniform segments. When a nonuniform-spacing algorithm is used this simple form does not occur.

Because of the occasional high rate of curvature change in the outboard portion of the drag profiles, if it is required that the number of segments be minimal (~5), this particular subset of the linear-integration algorithm is not recommended. However, as shown in figures 5 and 6, since the plotting software has conveniently drawn straight lines through each of the inclusive observation points, it is easily seen that by using 20 observations (standard for the basis) this linear-integration algorithm produces negligible differences from the continuum.

Figure 10 has been created by using this 20-segment algorithm and including the superimposed tip-loss terms as given in section IV. When resolutions of the

aerodynamic forces and moments are performed and inertial terms are included, the rotor system delivers body-axes forces and moments as given in figure 11. Figures 10 and 11 thus constitute the standard for comparison that may be used to establish the efficiency of alternate models.

Integration of Quadratics

It is maintained that if the spacing algorithm accounts for curvature in the force profiles via the use of unequal observation "windows," then the summation algorithm may be proportionally simplified. In particular, for the RSRA data the linear-segment-integration technique discussed previously is sufficient provided only that the observation radii are appropriately placed within each window. In order to demonstrate this fact a higher-order integration process was also examined.

As in the linear-segment-integration case, a set of coefficients may be developed that give a consistent summation process when the behavior between points is assumed to be quadratic. Of course, at least three observations are required. If the observation radii are assumed to be r_n, r_{n+1}, and r_{n+2}, the pertinent integrals of an assumed quadratic function $f(r)$ over the interval (r_x, r_y) are given by combinations of the observed f_n, where $k = 0$ or $k = 1$:

$$\begin{aligned}\int_{r_x}^{r_y} r^k f(r)dr = {} & \frac{f_n}{(r_{n+2} - r_n)(r_{n+1} - r_n)}\left[\frac{1}{k+1} r_{n+2}r_{n+1}(r_y^{k+1} - r_x^{k+1})\right. \\ & \left. - \frac{1}{k+2}(r_{n+2} + r_{n+1})(r_y^{k+2} - r_x^{k+2}) + \frac{1}{k+3}(r_y^{k+3} - r_x^{k+3})\right] \\ & - \frac{f_{n+1}}{(r_{n+2} - r_{n+1})(r_{n+1} - r_n)}\left[\frac{1}{k+1} r_{n+2}r_n(r_y^{k+1} - r_x^{k+1})\right. \\ & \left. - \frac{1}{k+2}(r_{n+2} + r_n)(r_y^{k+2} - r_x^{k+2}) + \frac{1}{k+3}(r_y^{k+3} - r_x^{k+3})\right] \\ & + \frac{f_{n+2}}{(r_{n+2} - r_n)(r_{n+2} - r_{n+1})}\left[\frac{1}{k+1} r_{n+1}r_n(r_y^{k+1} - r_x^{k+1})\right. \\ & \left. - \frac{1}{k+2}(r_{n+1} + r_n)(r_y^{k+2} - r_x^{k+2}) + \frac{1}{k+3}(r_y^{k+3} - r_x^{k+3})\right] \end{aligned} \tag{67}$$

The range of integration or applicability of equation (67) must be decided, and this process becomes somewhat complicated when N is general. However, for $n = 5$, a fairly natural selection seems to be to pivot two quadratics about the observation at r_3. In this case the range of (r_x, r_y) would be (r_A, r_3) for the first quadratic and (r_3, r_T) for the second. In this case the summation coefficients for use in equation (61) are:

$$
\left.
\begin{aligned}
a_1 &= \left[r_3 r_2 (r_3 - r_A) - \tfrac{1}{2}(r_3 + r_2)(r_3^2 - r_A^2) + (r_3^3 - r_A^3)/3\right]/[(r_3 - r_1)(r_2 - r_1)] \\
a_2 &= -\left[r_3 r_1 (r_3 - r_A) - \tfrac{1}{2}(r_3 + r_1)(r_3^2 - r_A^2) + (r_3^3 - r_A^3)/3\right]/[(r_3 - r_2)(r_2 - r_1)] \\
a_3 &= \left[r_2 r_1 (r_3 - r_A) - \tfrac{1}{2}(r_2 + r_1)(r_3^2 - r_A^2) + (r_3^3 - r_A^3)/3\right]/[(r_3 - r_1)(r_3 - r_2)] \\
&\quad + \left[r_5 r_4 (r_T - r_3) - \tfrac{1}{2}(r_5 + r_4)(r_T^2 - r_3^2) + (r_T^3 - r_3^3)/3\right./[(r_5 - r_3)(r_4 - r_3)] \\
a_4 &= -\left[r_5 r_3 (r_T - r_3) - \tfrac{1}{2}(r_5 + r_3)(r_T^2 - r_3^2) + (r_T^3 - r_3^3)/3\right]/[(r_5 - r_4)(r_4 - r_3)] \\
a_5 &= \left[r_4 r_3 (r_T - r_3) - \tfrac{1}{2}(r_4 + r_3)(r_T^2 - r_3^2) + (r_T^3 - r_3^3)/3\right]/[(r_5 - r_3)(r_5 - r_4)]
\end{aligned}
\right\} \tag{68}
$$

and

$$
\left.
\begin{aligned}
b_1 &= \left[\tfrac{1}{2} r_3 r_2 (r_3^2 - r_A^2) - \tfrac{1}{3}(r_3 + r_2)(r_3^3 - r_A^3) + \tfrac{1}{4}(r_3^4 - r_A^4)\right]/[(r_3 - r_1)(r_2 - r_1)] \\
&\quad - ea_1 \\
b_2 &= -\left[\tfrac{1}{2} r_3 r_1 (r_3^2 - r_A^2) - \tfrac{1}{3}(r_3 + r_1)(r_3^3 - r_A^3) + \tfrac{1}{4}(r_3^4 - r_A^4)\right]/[(r_3 - r_2)(r_2 - r_1)] \\
&\quad - ea_2 \\
b_3 &= \left[\tfrac{1}{2} r_2 r_1 (r_3^2 - r_A^2) - \tfrac{1}{3}(r_2 + r_1)(r_3^3 - r_A^3) + \tfrac{1}{4}(r_3^4 - r_A^4)\right]/[(r_3 - r_1)(r_3 - r_2)] \\
&\quad + \left[\tfrac{1}{2} r_5 r_4 (r_T^2 - r_3^2) - \tfrac{1}{3}(r_5 + r_4)(r_T^3 - r_3^3) + \tfrac{1}{4}(r_T^4 - r_3^4)\right./[(r_5 - r_3)(r_4 - r_3)] \\
&\quad - ea_3 \\
b_4 &= -\left[\tfrac{1}{2} r_5 r_3 (r_T^2 - r_3^2) - \tfrac{1}{3}(r_5 + r_3)(r_T^3 - r_3^3) + \tfrac{1}{4}(r_T^4 - r_3^4)\right]/[(r_5 - r_4)(r_4 - r_3)] \\
&\quad - ea_4 \\
b_5 &= \left[\tfrac{1}{2} r_4 r_3 (r_T^2 - r_3^2) - \tfrac{1}{3}(r_4 + r_3)(r_T^3 - r_3^3) + \tfrac{1}{4}(r_T^4 - r_3^4)\right]/[(r_5 - r_3)(r_5 - r_4)] \\
&\quad - ea_5
\end{aligned}
\right\} \tag{69}
$$

Interestingly enough, the use of these coefficients produces negligible improvement over the use of the linear coefficients given in equations (62) and (63) when

the "equal-annuli midpoints" algorithm (developed in sec. VII) is used to select the observation radii. Hence, higher-order summation approximations such as this are superfluous when the spacing algorithm itself accounts for the curvature of the force profiles.

VII. EQUAL-ANNULI DERIVATION

Since a more general and accurate summation process has been developed, we now turn our attention to the spacing algorithm. We shall consider the azimuth advance angle $d\psi$ that occurs during some time interval such that the distance that a point on the blade at the observation radius r_n travels is

$$dS_n = r_n \, d\psi$$

and the area swept out from the hub to this point is

$$dA_n = \frac{1}{2} r_n \, dS_n = \frac{1}{2} r_n^2 \, d\psi$$

The equal-annuli concept is that the area swept out by an adjacent observation radius

$$dA_{n+1} = \frac{1}{2} r_{n+1} \, dS_{n+1} = \frac{1}{2} r_{n+1}^2 \, d\psi$$

is used to define the differential area

$$\Delta A = dA_{n+1} - dA_n = \frac{1}{2} (r_{n+1}^2 - r_n^2) d\psi \tag{70}$$

which is independent of n. Hence, the difference in the squares of radii is constant,

$$K = r_{n+1}^2 - r_n^2 \tag{71}$$

which is another way of saying that the density of observations increases hyperbolically with the midpoints between observations, that is,

$$r_{n+1} - r_n = \frac{\frac{1}{2} K}{\frac{1}{2} (r_{n+1} + r_n)} \tag{72}$$

By induction, equation (71) may be written in terms of the initial radius r_1.

$$r_n^2 = (n - 1)K + r_1^2 \tag{73}$$

The constant K is determined by dividing the total area swept out by the effective blade (r_T used here rather than r_{MR}) into N equal areas,

$$(r_T^2 - r_A^2) d\psi = NK \, d\psi \tag{74}$$

so that

$$r_n^2 = \frac{n-1}{N}(r_T^2 - r_A^2) + r_1^2 \tag{75}$$

The initial observation radius is obtained by noting that the area from r_A to r_1 is half the area from r_1 to r_2, which is equivalent to

$$r_1^2 - r_A^2 = \frac{1}{2}(r_2^2 - r_1^2) \tag{76}$$

and substituting this into equation (75) with $n = 2$ yields

$$r_1^2 = r_A^2 + (r_T^2 - r_A^2)/(2N) \tag{77}$$

so that (when r_{MR} is substituted for r_T) the blade observation radii are given by the reference result (Houck et al., 1977),

$$\left.\begin{aligned} r_1 &= [r_A^2 + (r_T^2 - r_A^2)/(2N)]^{1/2} \\ r_n &= [r_{n-1}^2 + (r_T^2 - r_A^2)/N]^{1/2} \qquad (1 < n \le N) \end{aligned}\right\} \tag{78}$$

which by induction may be written for all n:

$$r_n = \left[r_A^2 + (r_T^2 - r_A^2)\left(n - \frac{1}{2}\right)\Big/N\right]^{1/2} \tag{79}$$

As a spacing algorithm this one appears satisfactory because it tends to appreciate the occasional curvature change in drag forces with radius or at least recognize the linear radial factor required for the computation of aerodynamic moments. A summation algorithm, however, should recognize the convergence problem associated with the approximation processes,

$$\left.\begin{aligned} F &= \int_{r_A}^{r_T} f(r)dr \approx \sum_{n=1}^{N} f(r_n)a_n \\ M &= \int_{r_A}^{r_T} (r - e)f(r)dr \approx \sum_{n=1}^{N} f(r_n)b_n \end{aligned}\right\} \tag{80}$$

and, therefore, the coefficients (a_n, b_n) should be determined from assumptions about the behavior of $f(r)$ between observation radii rather than be averaged over segments that are artifacts in the development of the spacing algorithm. This process is discussed in the next section.

Equal-Annuli and Quadratures

In this section the *segment spacing* for the equal-annuli algorithm is developed. It is noted that the selection of observation radii within these segments involves other considerations when the quadrature technique is used in the derivation.

Let us consider the *segment* bounded by $r_{n(+)}$ on its exterior and $r_{n(-)}$ on its interior. The distances that these extremity positions travel during some azimuth advance angle $d\psi$ are given by

$$dS_{n(+)} = r_{n(+)}d\psi$$

$$dS_{n(-)} = r_{n(-)}d\psi$$

so that the total area swept out by the segment is

$$\Delta A = \frac{1}{2}\,[r^2_{n(+)} - r^2_{n(-)}]d\psi \tag{81}$$

When these segment areas are independent of n we have

$$K = r^2_{n(+)} - r^2_{n(-)} \tag{82}$$

so that by using the contiguous relationships

$$\left.\begin{aligned} r_{n(+)} &= r_{n+1(-)} \\ r_{n(-)} &= r_{n-1(+)} \end{aligned}\right\} \tag{83}$$

the indices may be made compatible:

$$\left.\begin{aligned} K &= r^2_{n(+)} - r^2_{n-1(+)} \\ K &= r^2_{n+1(-)} - r^2_{n(-)} \end{aligned}\right\} \tag{84}$$

The extremities of the segment are then found by induction,

$$\left.\begin{aligned} r^2_{n(+)} &= nK + L \\ r^2_{n(-)} &= (n - 1)K + L \end{aligned}\right\} \tag{85}$$

where the constants are determined from the boundaries

$$\left.\begin{aligned} r_{1(-)} &= r_A \\ r_{N(+)} &= r_T \end{aligned}\right\} \tag{86}$$

and the solutions are given by:

$$\left.\begin{aligned} r_{n(+)} &= [r^2_A + (r^2_T - r^2_A)n/N]^{1/2} \\ r_{n(-)} &= [r^2_A + (r^2_T - r^2_A)(n - 1)/N]^{1/2} \end{aligned}\right\} \tag{87}$$

The segment length may be expressed by

$$\Delta r_n = r_{n(+)} - r_{n(-)}$$

but it has not been relevant to this development since only the differences in the squares of radii have been used. Furthermore, one may define a radius such as in the extant algorithm (eq. (79)), but it has not been relevant to this development either. A possible reason for its inclusion in the algorithm for the extant model is as follows: If the assumption is made that the force between points is quadratic in radius, specifically at the extremities, that is,

$$f_{n(+)} = Cr_{n(+)}^2$$

$$f_{n(-)} = Cr_{n(-)}^2$$

then another assumption is necessary, *which is inconsistent with the first assumption*: that the average of the functional values at the segment extrema is equal to the observation value, that is,

$$f_n = \frac{1}{2}\,[f_{n(+)} + f_{n(-)}] = \frac{1}{2}\,C[r_{n(+)}^2 + r_{n(-)}^2] \tag{88}$$

so that, by applying the original assumption to the evaluation point itself,

$$f_n = Cr_n^2 \tag{89}$$

the simultaneous solution of equations (88) and (89) produces the formulation of the extant model, which is equivalent to equation (79):

$$r_n = \sqrt{\frac{1}{2}\,[r_{n(+)}^2 + r_{n(-)}^2]} \tag{90}$$

But if $f(r)$ is indeed quadratic as in equation (89), then the correct integration process is given by

$$\int_{r_{n(-)}}^{r_{n(+)}} f(r)dr = C\int_{r_{n(-)}}^{r_{n(+)}} r^2\,dr = \frac{1}{3}\,C[r_{n(+)} - r_{n(-)}][r_{n(+)}^2 + r_{n(+)}r_{n(-)} + r_{n(-)}^2] \tag{91}$$

so that the correct quadrature method of integrating the forces within the interval is

$$\begin{aligned} f(r_n)[r_{n(+)} - r_{n(-)}] &= Cr_n^2[r_{n(+)} - r_{n(-)}] \\ &= \frac{1}{3}\,C[r_{n(+)} - r_{n(-)}][r_{n(+)}^2 + r_{n(+)}r_{n(-)} + r_{n(-)}^2] \end{aligned} \tag{92}$$

This expression results in an observation-radius definition in terms of the segment extremities, which is quite different from the reference spacing:

$$r_n = \sqrt{\frac{1}{3}\,[r_{n(+)}^2 + r_{n(+)}r_{n(-)} + r_{n(-)}^2]} \tag{93}$$

Thus, this particular segment-oriented derivation of the equal-annuli algorithm isolates the observed mathematical inconsistency. *Equal-annuli spacing of the observation radii is not compatible with the quadrature technique.* However, as given in equation (79), equal annuli spacing may be used with the summation coefficients of Section VI. Indeed, this combination is recommended for real-time simulation programs, where a minimal number of radial observations are required.

Equal-Annuli Midpoints

The combination of the quadrature technique and equal-annuli spacing tends to improve results when the force profile is a high-order polynomial in radius. However, this feature is rarely of benefit,[2] while its destructive tendencies are much more common. In order to illustrate this process, an alternate spacing algorithm is introduced, which is more compatible with the quadrature technique because it uses the midpoints of the artificial segments, given in equations (87):

$$r_n = \frac{1}{2}\left[\sqrt{\frac{n}{N}\left(r_T^2 - r_A^2\right) + r_A^2} + \sqrt{\frac{n-1}{N}\left(r_T^2 - r_A^2\right) + r_A^2}\right] \tag{94}$$

For a quadratic force profile, this spacing algorithm is shown in appendix A to deliver half as much error as equal-annuli spacing, when the quadrature technique is used.

The spacing algorithm of equation (94) is also of interest when the suggested summation coefficients (62) and (63) are used,

$$\begin{aligned} F &= \sum_{n=1}^{N} a_n f(r_n) \\ M &= \sum_{n=1}^{N} b_n f(r_n) \end{aligned} \tag{95}$$

In appendix B this process is compared to the original combination of equal-annuli spacing and quadrature technique. The use of summation coefficients is shown to have a distinct advantage for arbitrary curve shapes.

In combination with the tip-loss technique of equation (37), the inconsistencies in the radial computations are eliminated for both real-time simulation and for continuum emulation, provided the equal-annuli spacing algorithm of equation (79) or the alternate spacing algorithm of equation (94) is used, along with the summation coefficients. No real-time computational penalty accrues. Of particular importance to real-time simulation (using a minimal number of radial observations) are the features of linearity between observation radii, extrapolation internal to the inboard observation radius and external to the outboard observation radius, superimposed tip loss that does not influence the continuity of the functionals to be summed, a consistent solution for forces and moments, and no extra real-time computational expense.

[2]Only the drag profiles for advancing blades during high-speed flight benefit (e.g., blade 2 in fig. 6(ee)).

VIII. ERROR COMPARISON

The errors from both the extant and alternate algorithms are examined here by using 5-segment models and comparing them with the 20-segment basis. In order to fully appreciate this comparison the "constrained and balanced" operations are necessary.

In exercising the extant model, only the angle-of-attack correction of section III was implemented.

In figure 12 the total-body-axis forces and moments for the extant model are presented in the constrained condition. Thus, the blade trajectories have been constrained to the same trajectories as the 20-segment basis case. The forces and moments of the basis of figure 11 (the basis always uses 20 segments) are also repeated on these graphs for comparison purposes. The differences are due to the decreased number of segments,[3] slow summation convergence, the tip-loss computation technique, and equal-annuli spacing.

Since figure 12 has been created in the constrained condition so that inertial terms are invariant, differences are entirely caused by the computation of aerodynamic terms. These aerodynamic errors are presented in figure 13. Among items that should be noticed are the force and moment standoff differences at low vehicle velocity, the deterioration (see blade 5 in fig. 13(b)) of reverse-flow computation, and error variation when the blade encounters drag divergence (see blade 2 in fig. 13(a)). From the data set this latter phenomenon is identified by variations in the drag coefficient due to Mach number variation without regard to angle-of-attack variation.

When the blade states are allowed to interact with their flap/lag differential equations, the balanced condition is achieved. Figure 14 shows the extant and basis rotor-system total-body-axes forces and moments. The new spatial orientation of the rotor disc produces differences, some of which involve inertial terms. Although the forces of figures 12(a) and 14(a) do not experience much variation, an interesting phenomenon occurs in moment space, especially in yawing moment; it is seen in comparing the value of R_{MN} between figures 12(b) and 14(b). In order to explain this phenomenon figure 15 is presented, which gives the rotor-torque differences. This figure shows that the torque difference under the constrained condition is minimal; however, when the flapping- and lagging-moment variations of figures 13(d) and 13(e) are allowed to interact with the differential equations, new blade states are created that minimally influence the force values but cause a rather large variation in total rotor-system torque. This effect is shown in the following section to be attributable to one specific inertial term.

The alternate simulation model creates errors that are more consistent with its assumptions, and usually much less than those of the extant model. Individual-blade aerodynamic force and moment errors for this five-segment model are given in figure 16 for comparison with figure 13. The total system outputs in the constrained

[3]At low vehicle velocity the unusually large displacement of the initial evaluation radius for the extant algorithm delivers an error in perpendicular force of approximately 100 lb per blade. Increasing the number of segments from 5 to 10 only reduces this error to approximately 70 lb per blade. The extrapolation feature of the alternate model eliminates this error.

condition are given in figure 17 for comparison with the extant-model outputs shown in figure 12. The total system outputs in the balanced condition are given in figure 18 for comparison with the extant-model outputs shown in figure 14. As might be expected, the total torque error is much improved. This error, given in figure 19 for both the balanced and constrained conditions, may be directly compared with the error for the extant model shown in figure 15; a further examination of the torque error is given in the next section.

Figures 1 and 2 have been presented to demonstrate thrust variations with segment number. Only on these two graphs does the "basis" contain less than 20 elements. The improvement in thrust obtained by using the alternate algorithm rather than the extant algorithm is demonstrated in these figures for vehicle velocities of 10 and 250 knots. Specifically, for a small number of segments the alternate algorithm is at least twice as accurate, and for a larger number N the convergence is faster. Invariancy with N is displayed by the basis in the region of $N = 20$. Another feature that is indicated by these graphs is that lift forces are improved with uniform spacing (basis). Because of their nearly arbitrary variations this improvement with uniform spacing is most probably true in general, but this fact is not true for drag forces. These drag forces exhibit distinct polynomial forms, especially at significant velocities for advancing blades, and uniform spacing fails to accommodate this feature when the number of segments is small. Indeed, high-order polynomial drag characteristics are the justification for equal-annuli spacing, and this feature has been preserved in the development of the alternate algorithm. It should be noted that this alternate algorithm is also consistent with lower-order curves, which are dominant in figures 5 and 6.

Error Propagation

The extant model is here used to trace an error from its source in the constrained condition to the balanced condition. It will be shown that the major differences in balanced and constrained conditions are simply due to an inertial term. (This fact supports the contention that a major contribution to rotorcraft trimming will result from the "constrained" concept.) In the previous section the importance of accurate summation along the blade was illustrated by a variation in torque (fig. 15). Although the aerodynamic force outputs during the balanced condition vary only slightly from the outputs during the constrained condition (as can be seen by comparing figs. 12(a) and 14(a)), the slight reorientation of the rotor disc, caused by the inaccurate moment summation process, produces torque errors. These errors are due primarily to the contribution of a single inertial term, as shown below.

The total rotor system yawing moment N_{MR} is nearly identical to the torque Q. Slight differences are attributable to the moment arm and to the shaft-to-body-axis transformation, which is almost an identity matrix. Hence for B blades,

$$N_{MR} \simeq Q \simeq -\sum_{i=1}^{B} (M_{LDi} \cos \beta_i + eF_{XAi} + eF_{XIi}) \tag{96}$$

For the purpose of a perturbation analysis, we consider a portion of the inertial term,

$$N_{MR} \simeq -e \sum_{i=1}^{B} F_{XIi} + \ldots = -e \sum_{i=1}^{B} M_b \cos \beta_i \sin \delta_i (r_s - \Omega)^2 + \ldots$$

$$\simeq -eM_b\Omega^2 \sum_{i=1}^{B} \delta_i + \ldots \simeq -eBM_b\Omega^2 a_{OL}/57.3 + \ldots \tag{97}$$

where the principal lagging Fourier coefficient is defined (in deg) as

$$a_{OL} = \frac{57.3}{B} \sum_{i=1}^{B} \delta_i \tag{98}$$

Thus, if the torque error is due primarily to a reorientation of the lagging angles, it may be reconstructed by considering only the contribution

$$\Delta N_{MR} = -eBM_b\Omega^2 \Delta a_{OL}/57.3 \tag{99}$$

where rpm follows the computed schedule of table 1.

The lagging coefficient a_{OL} is presented in figure 20 from the basis. Also appearing on this graph is the difference in lagging coefficient Δa_{OL} observed from the extant simulation model with balanced conditions for five segments. Using equation (99), with the parameters $e = 1.05$, $M_b = 91$, $B = 5$, and rpm as in table 1, figure 21 is produced, showing very little deviation from the torque-error history of figure 15. Hence, inaccuracies in the computation of the lagging moment during the constrained condition are seen in the balanced condition to contribute directly to the yawing-moment error, as should be expected.

From this comparison an important fact is revealed: In order to obtain accurate rotor system outputs the moment summations are at least as important as the force summations. The amplification due to the radial moment arm means that any effort spent in replicating the true force profiles is effort well spent.

The lagging-moment error, which directly influences the lag states through the forcing functions of the differential equations (Houck et al., 1977), influences a_{OL} via equation (98), and thus contributes to the torque error via equation (99). It has been shown here that this logic path is the one that produces the torque error for the extant simulation, which manifests itself in the total-yawing-moment errors given in figure 14(b).

IX. CONCLUSIONS

An angle-of-attack correction for reverse-flow computation has been developed by using symmetry arguments, and this correction has been demonstrated to influence simulation results at vehicle speeds in excess of 155 knots.

The balanced/constrained dynamics concept has been developed for rotor systems and shown to be a valuable tool for comparing different formulations. It should also lead to the development of a generalized rotorcraft trimming process that promises to be computationally efficient.

An alternate tip-loss model has been developed that simplifies the integration process by using a minor perturbation that is superimposed upon integrals of continuous derivatives. The pseudoblade concept has been demonstrated to exploit the relative magnitudes of lift and drag forces for the approximation process.

The slow convergence properties of the radial summation scheme using quadratures has been noted, and the propagation of errors has been illustrated. The summation scheme has been improved with a set of coefficients that are applicable to various spacing algorithms; they are demonstrated herein by using the alternate algorithm that features equal-annuli midpoints. Equal-annuli spacing is recommended for real-time use with these summation coefficients. Output improvements are shown to be especially noteworthy during low vehicle velocity. A general improvement in the computation of lift-related quantities has been demonstrated, although at higher flight velocities some deterioration has been observed in drag-related quantities. Since lift quantities are usually an order of magnitude greater than drag quantities, the total-rotor-system outputs are improved.

The advancing-blade drag profiles are shown to occasionally exhibit a high-order radial polynomial behavior that is best accommodated by a biased spacing algorithm such as in the extant model, but this advantage is deleterious to the convergence of other quantities, including the retreating-blade drag profiles. Further research is recommended in the area of summation coefficients that recognize both the characteristic differences in lift and drag and the azimuth-dependency problem.

A data base of high fidelity has been created by using 20 uniform segments. This data base has been graphically illustrated and exists as a basis for additional model development activities. This basis exhibits neither standoff errors nor evaluation weighting usually associated with real-time algorithms that require a minimal number of evaluations; it is virtually invariant with the number of segments used. For a large number of segments, the alternate algorithm converges to the basis. When tip loss is reformulated as developed herein, the extant algorithm also converges to the basis, but more slowly.

Ames Research Center
National Aeronautics and Space Administration
and
Aeromechanics Laboratory
AVRADCOM Research and Technology Laboratories
Moffett Field, Calif. 94035, January 27, 1982

APPENDIX A

QUADRATIC COMPARISON

For a force profile that is quadratic in radius, equal-annuli midpoint spacing produces half the error of pure equal-annuli spacing, even when the summation algorithm for the extant model is used. This fact is proved below.

If the force profile is assumed to be quadratic in radius

$$f(r) = r^2 \tag{A1}$$

then the closed-form solution is

$$F_C = \int_{r_A}^{r_T} r^2 \, dr = \frac{1}{3} (r_T^3 - r_A^3) \tag{A2}$$

Defining

$$\left.\begin{aligned} b_1 &= \frac{1}{N} (r_T^2 - r_A^2) \\ b_2 &= r_A^2 \end{aligned}\right\} \tag{A3}$$

the segment extremities are given by equations (87) as

$$\left.\begin{aligned} r_{n(+)} &= (nb_1 + b_2)^{1/2} \\ n_{n(-)} &= [(n - 1)b_1 + b_2]^{1/2} \end{aligned}\right\} \tag{A4}$$

and the force-summation process for the extant model is

$$F = \sum_{n=1}^{N} f(r_n)[r_{n(+)} - r_{n(-)}] \tag{A5}$$

The two candidates for $f(r_n)$ are the pure equal-annuli assumption,

$$f(r_n) = (r_n)^2 = \left\{\sqrt{\frac{1}{2} [r_{n(+)}^2 + r_{n(-)}^2]}\right\}^2 = \frac{1}{2} [r_{n(+)}^2 + r_{n(-)}^2] \tag{A6}$$

and the equal-annuli midpoint assumption,

$$f(r_n) = (r_n)^2 = \left\{\frac{1}{2} [r_{n(+)} + r_{n(-)}]\right\}^2 = \frac{1}{4} [r_{n(+)} + r_{n(-)}]^2 \tag{A7}$$

For the pure equal-annuli algorithm the force error is given by

$$E_{Eq} = \frac{1}{2} \sum_{n=1}^{N} [r_{n(+)}^2 + r_{n(-)}^2][r_{n(+)} - r_{n(-)}] - F_C$$

$$= \frac{1}{2} \sum_{n=1}^{N} [(2n - 1)b_1 + 2b_2][\sqrt{nb_1 + b_2} - \sqrt{(n - 1)b_1 + b_2}] - F_C$$

$$= \frac{1}{2} [(2N - 1)b_1 + 2b_2]r_T - \frac{1}{2} (b_1 + 2b_2)r_A - b_1 \sum_{n=1}^{N-1} \sqrt{nb_1 + b_2} - F_C$$

$$= 2 \left[\frac{1}{3} (r_T^3 - r_A^3) - \frac{(r_T^2 - r_A^2)(r_T + r_A)}{4N} - \frac{1}{2} b_1 \sum_{n=1}^{N-1} \sqrt{nb_1 + b_2} \right] \tag{A8}$$

and for the equal-annuli midpoint algorithm the force error is

$$E_{EM} = \frac{1}{4} \sum_{n=1}^{N} [r_{n(+)} + r_{n(-)}]^2[r_{n(+)} - r_{n(-)}] - F_C$$

$$= \frac{1}{4} \sum_{n=1}^{N} [r_{n(+)}^2 - r_{n(-)}^2][r_{n(+)} + r_{n(-)}] - F_C$$

$$= \frac{1}{4} b_1 \left(\sqrt{Nb_1 + b_2} + \sqrt{b_2} + 2 \sum_{n=1}^{N-1} \sqrt{nb_1 + b_2} \right) - F_C$$

$$= -\frac{1}{3} (r_T^3 - r_A^3) + \frac{(r_T^2 - r_A^2)(r_T + r_A)}{4N} + \frac{1}{2} b_1 \sum_{n=1}^{N-1} \sqrt{nb_1 + b_2} \tag{A9}$$

Hence,

$$|E_{EM}| = \frac{1}{2} |E_{Eq}| \tag{A10}$$

APPENDIX B

NUMERICAL EXAMPLE

With five segments, the resultant forces are here compared by using the suggested, alternate algorithm (equal-annuli midpoints) and the extant algorithm (pure equal-annuli spacing). The applicable summation algorithms are different, as noted in the text.

For five segments the segment extremities (the same for both algorithms) are given from equations (87) as

$$\left.\begin{aligned} r_{1(-)} &= r_A = 6.45 \\ r_{1(+)} &= r_{2(-)} = 14.632942 \\ r_{2(+)} &= r_{3(-)} = 19.663252 \\ r_{3(+)} &= r_{4(-)} = 23.646648 \\ r_{4(+)} &= r_{5(-)} = 27.049666 \\ r_{5(+)} &= r_T = 30.07 \end{aligned}\right\} \tag{B1}$$

From equation (94), for equal-annuli midpoint spacing the observation radii are

$$\left.\begin{aligned} r_1 &= 10.541471 \\ r_2 &= 17.148097 \\ r_3 &= 21.148097 \\ r_4 &= 25.34815 \\ r_5 &= 28.559833 \end{aligned}\right\} \tag{B2}$$

which enable us to compute the force coefficients from equations (62):

$$\left.\begin{aligned} a_1 &= 8.6617041 \\ a_2 &= 4.2898194 \\ a_3 &= 4.10003 \\ a_4 &= 3.0973926 \\ a_5 &= 3.4710539 \end{aligned}\right\} \tag{B3}$$

Thus, for equal-annuli midpoint spacing with five segments the force-summation algorithm is given by:

$$F_{EM} = 8.6617041f(10.541471) + 4.2898194f(17.148097) + 4.10003f(21.65495) + 3.0973926f(25.348157) + 3.4710539f(28.559833) \quad \text{(B4)}$$

For the pure equal-annuli algorithm, as in the extant model, the observation radii are given from equation (79) as

$$\left.\begin{aligned} r_1 &= 11.307641 \\ r_2 &= 17.331567 \\ r_3 &= 21.746349 \\ r_4 &= 25.4052 \\ r_5 &= 28.599732 \end{aligned}\right\} \quad \text{(B5)}$$

so that in accordance with equation (49), using the differences $[r_{n(+)} - r_{n(-)}]$, the extant model with five segments produces the force-summation algorithm:

$$F_{Eq} = 8.182942f(11.307641) + 5.03031f(17.331567) + 3.983396f(21.746349) + 3.4031858f(25.4052) + 3.0203342f(28.599732) \quad \text{(B6)}$$

For a force of order k in radius the correct integration process is

$$F_C = \int_{r_A}^{r_T} r^k \, dr = \frac{1}{k+1} \left(r_T^{k+1} - r_A^{k+1}\right) \quad \text{(B7)}$$

and, therefore, the relative force errors in these two algorithms are given by:

$$\left.\begin{aligned} E_{EM} &= \frac{F_{EM}}{F_C} - 1 \\ E_{Eq} &= \frac{F_{Eq}}{F_C} - 1 \end{aligned}\right\} \quad \text{(B8)}$$

These relative errors are plotted in figure 22, and they demonstrate why the alternate algorithm delivers less error for segment curve characteristics up to at least cubic order ($k = 3$) in radius.

REFERENCES

Houck, Jacob A.; and Bowles, Roland L.: Effects of Rotor Model Degradation on the Accuracy of Rotorcraft Real-Time Simulation. NASA TN D-8378, 1976.

Houck, Jacob A.; Moore, Frederick L.; Howlett, James J.; Pollack, Kenneth S.; and Browne, Mary M.: Rotor Systems Research Aircraft Simulation Mathematical Model. NASA TM-78629, 1977.

Mackie, D. Brian; and Alderete, Thomas S.: A Real-Time, Dual Processor Simulation of the Rotor System Research Aircraft. NASA TN D-8328, 1977.

Selby, Samuel M., ed.: Handbook of Tables for Mathematics. The Chemical Rubber Co., Cleveland, Ohio, 4th ed., 1970, p. 466.

TABLE 1.- COMPUTED rpm WITH VEHICLE VELOCITY

Vehicle velocity, knots	rpm, rad/sec
0-180	22.1416
190	21.9424
200	21.3972
210	20.8520
220	20.3069
230	19.7617
240	19.2165
250	18.6714
260	18.1262
270	17.5811
280	17.0359
290	16.4907
300	15.9456

TABLE 2.- UNIFORM-SEGMENT EVALUATION RADII

Evaluation point, n	Evaluation radii for number of evaluation points, N			
	3	5	7	10
1	0.1667	0.1	0.0714	0.05
2	.5000	.3	.2143	.15
3	.8333	.5	.3571	.25
4		.7	.5000	.35
5		.9	.6429	.45
6			.7857	.55
7			.9286	.65
8				.75
9				.85
10				.95

TABLE 3.- UNIFORM-SEGMENT ALGORITHM RELATIVE ERRORS

Number of evaluation points, N	Relative error in blade moment if the force profile is:		
	Constant	Linear	Quadratic
1	0	-0.2500	-0.5000
2	0	-.0625	-.1250
3	0	-.0278	-.0556
4	0	-.0156	-.0312
5	0	-.0100	-.0200
6	0	-.0069	-.0138
7	0	-.0051	-.0102
8	0	-.0039	-.0078
9	0	-.0031	-.0062
10	0	-.0025	-.0050

TABLE 4.- EQUAL-ANNULI EVALUATION RADII

Evaluation point, n	Evaluation radii for number of evaluation points, N			
	3	5	7	10
1	0.4082	0.3162	0.2673	0.2236
2	.7071	.5477	.4629	.3873
3	.9129	.7071	.5976	.5000
4		.8367	.7071	.5916
5		.9478	.8018	.6708
6			.8864	.7416
7			.9636	.8062
8				.8660
9				.9220
10				.9747

TABLE 5.- EQUAL-ANNULI ALGORITHM RELATIVE ERRORS

Number of evaluation points, N	Relative error in blade moment if the force profile is:		
	Constant	Linear	Quadratic
1	0.4142	0.5000	0.4142
2	.2144	.1893	.1145
3	.1446	.1061	.0537
4	.1091	.0702	.0313
5	.0876	.0508	.0206
6	.0732	.0390	.0146
7	.0628	.0311	.0109
8	.0550	.0256	.0085
9	.0490	.0216	.0068
10	.0441	.0185	.0056

TABLE 6.- EQUAL-ANNULI MIDPOINT EVALUATION RADII

Evaluation point, n	Evaluation radii for number of evaluation points, N			
	3	5	7	10
1	0.2887	0.2236	0.1890	0.1581
2	.6969	.5398	.4562	.3817
3	.9082	.7035	.5946	.4975
4		.8345	.7053	.5901
5		.9472	.8005	.6698
6			.8855	.7409
7			.9629	.8056
8				.8655
9				.9216
10				.9743

TABLE 7.- EQUAL-ANNULI MIDPOINT ALGORITHM RELATIVE ERRORS

Number of evaluation points, N	Relative error in blade moment if the force profile is:		
	Constant	Linear	Quadratic
1	0	-0.2500	-0.5000
2	0	-.0947	-.1464
3	0	-.0531	-.0707
4	0	-.0351	-.0420
5	0	-.0254	-.0280
6	0	-.0195	-.0201
7	0	-.0156	-.0151
8	0	-.0128	-.0119
9	0	-.0108	-.0095
10	0	-.0092	-.0079

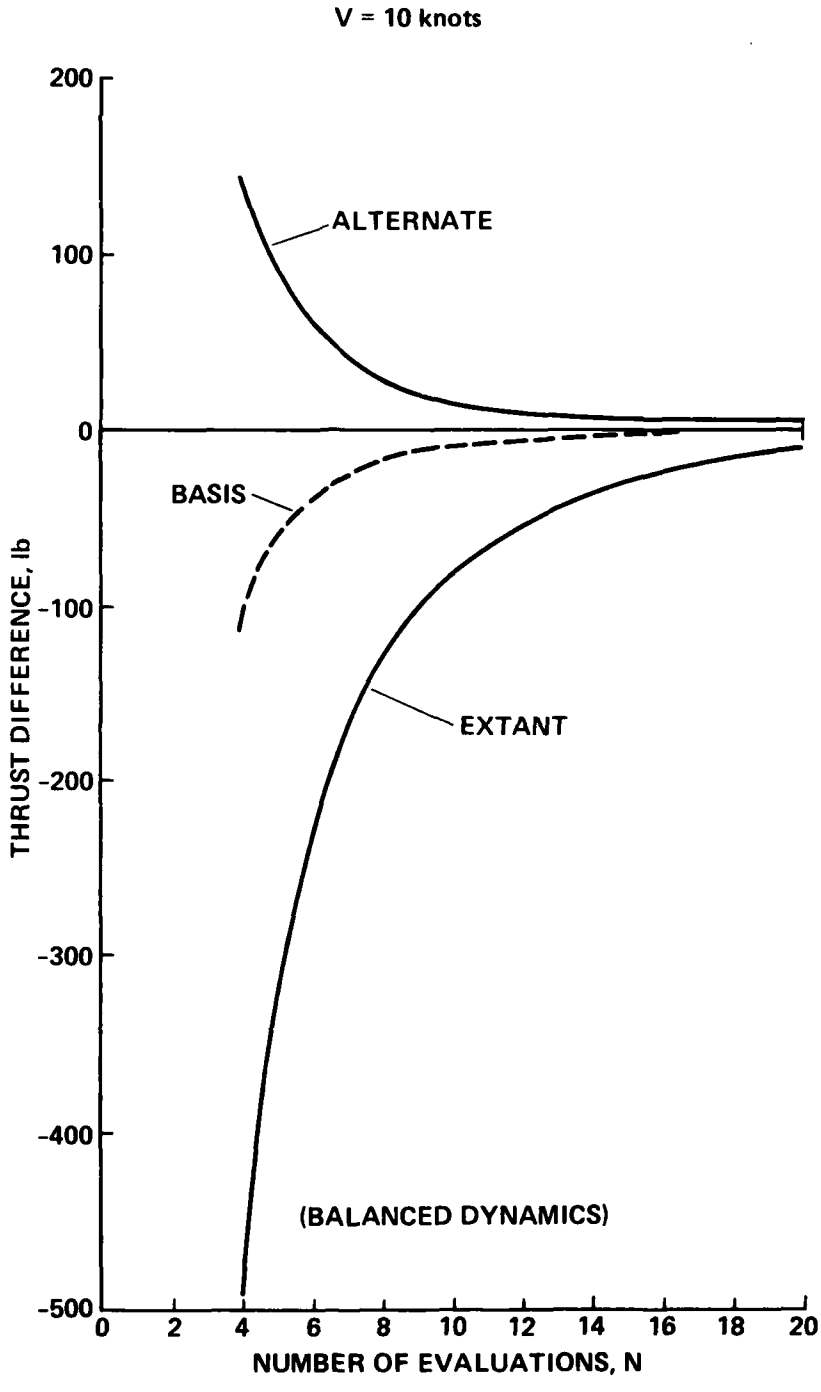

Figure 1.- Thrust differences, v = 10 knots.

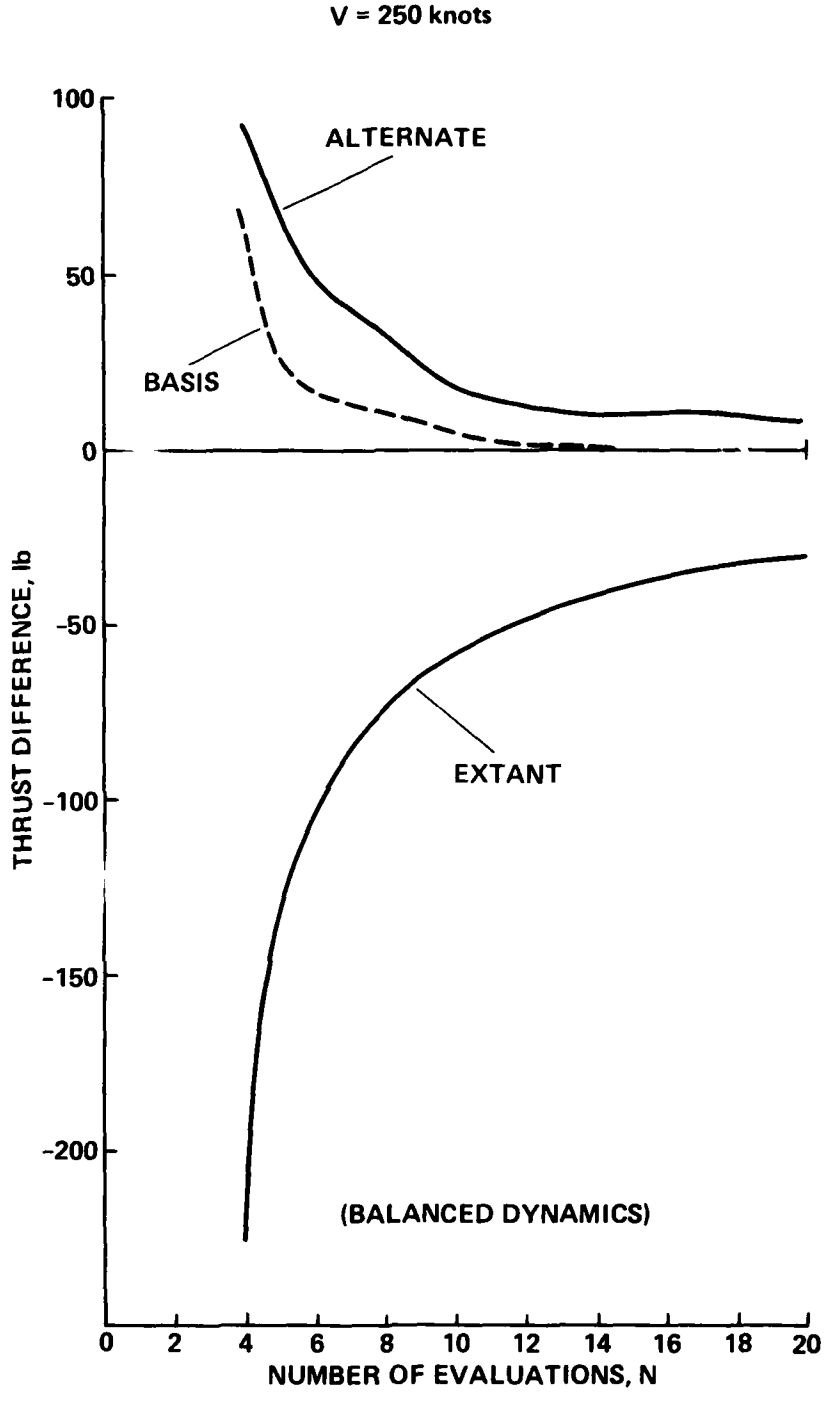

Figure 2.- Thrust differences, v = 250 knots.

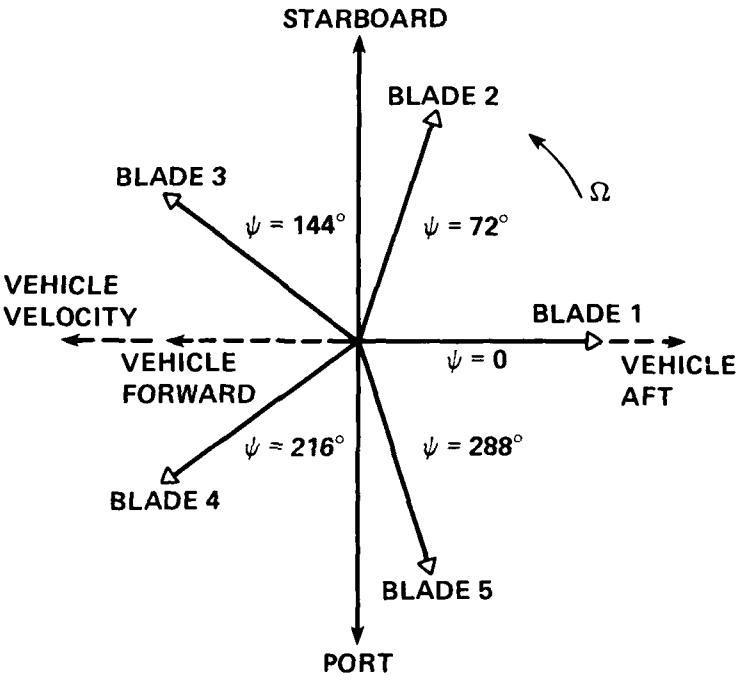

Figure 3.- Standard blade orientation.

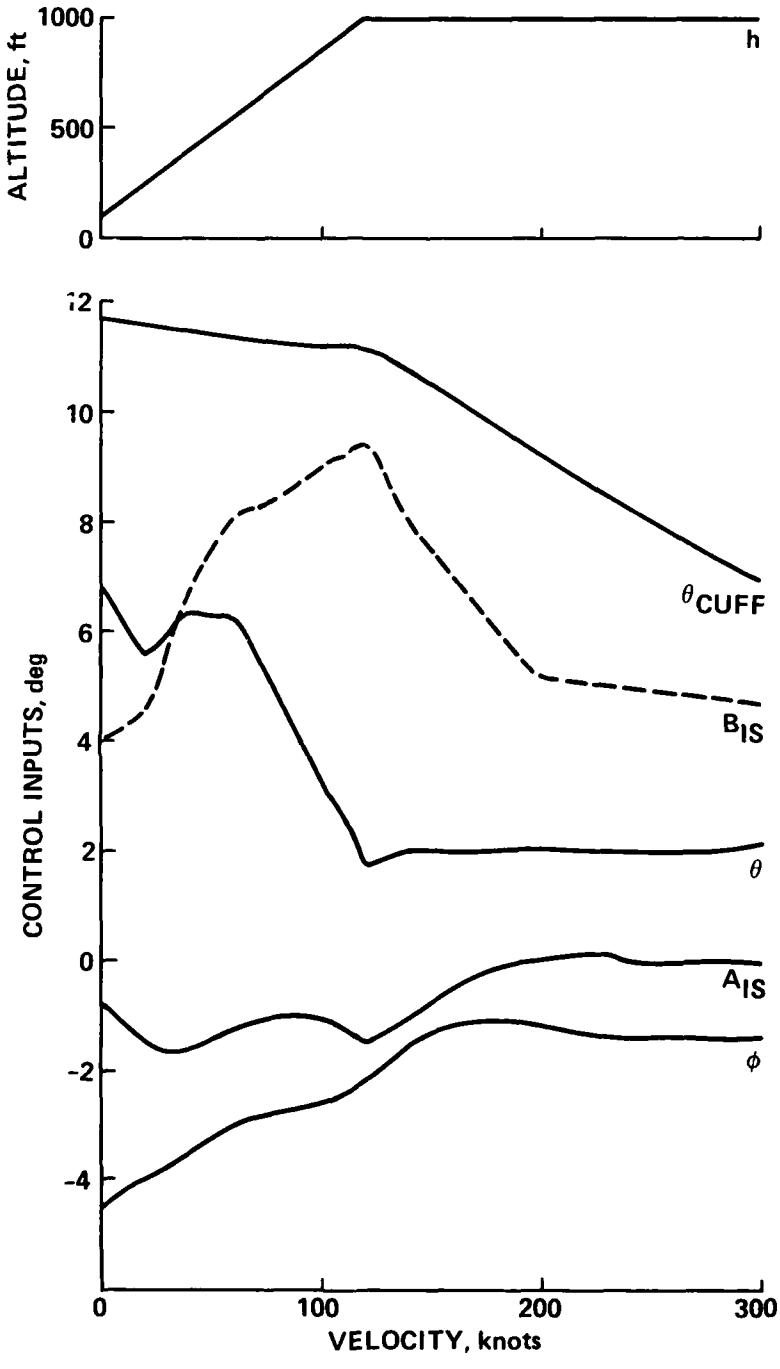

Figure 4.- Control profile.

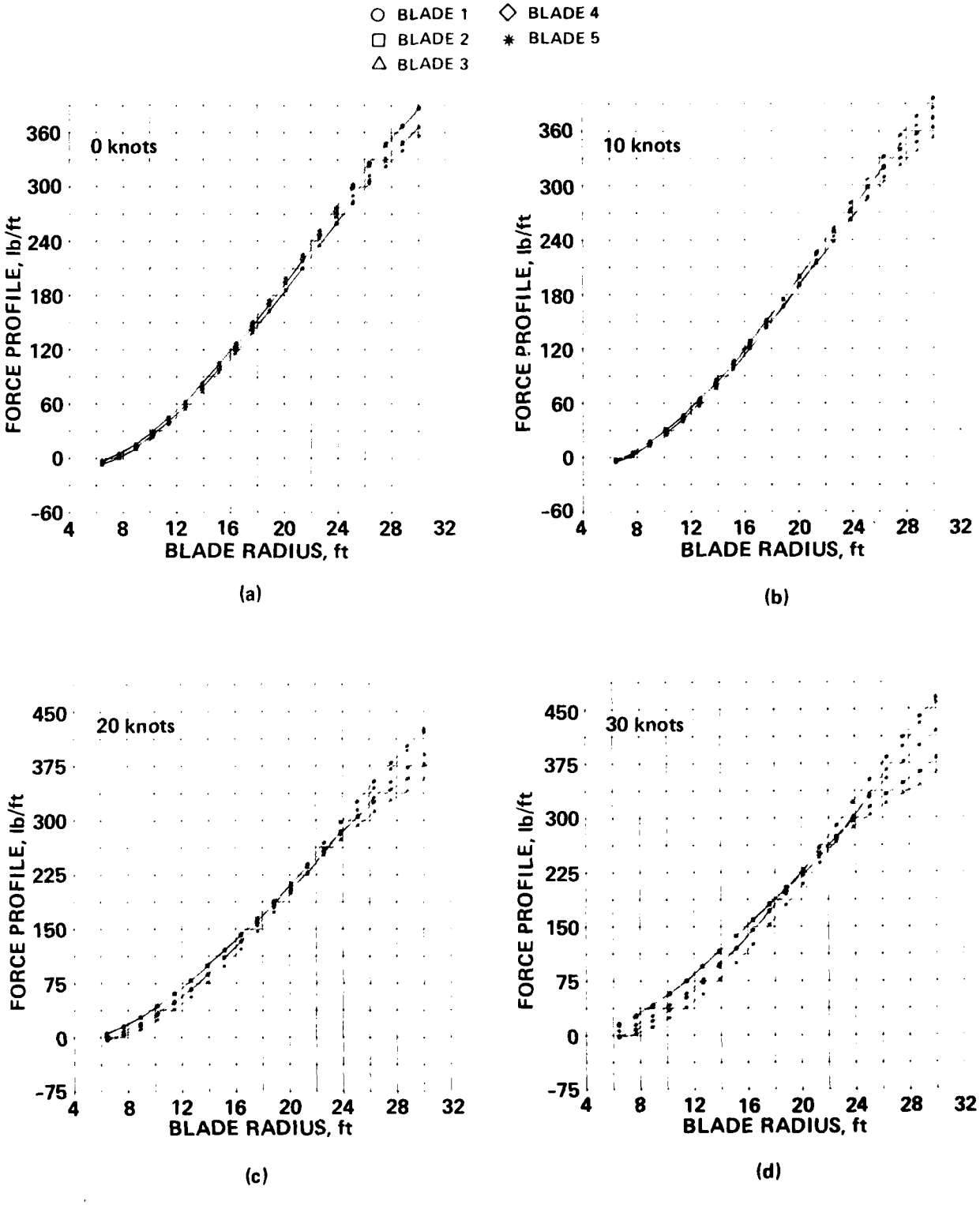

Figure 5.- Lift-force profiles.

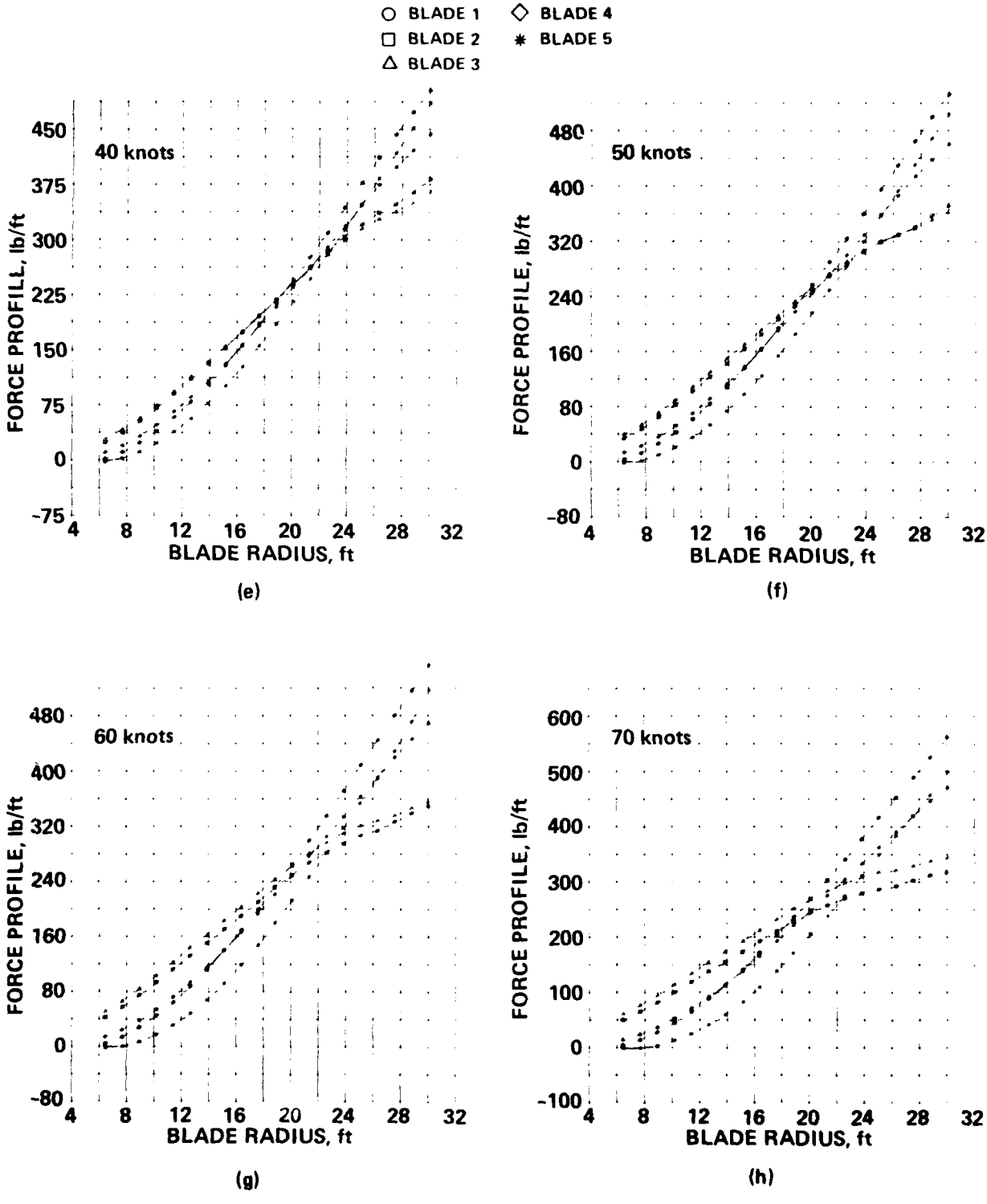

Figure 5.- Continued.

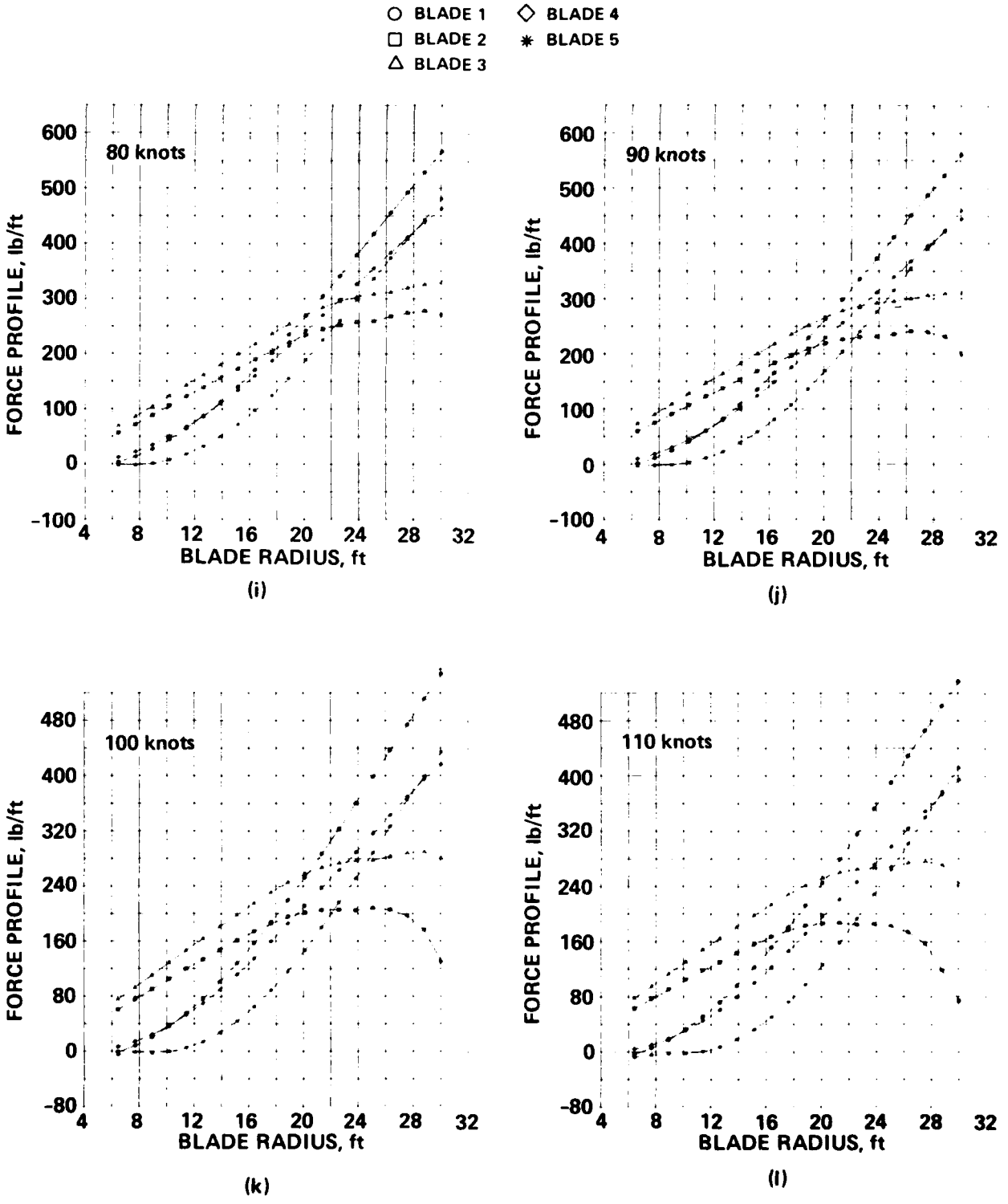

Figure 5.- Continued.

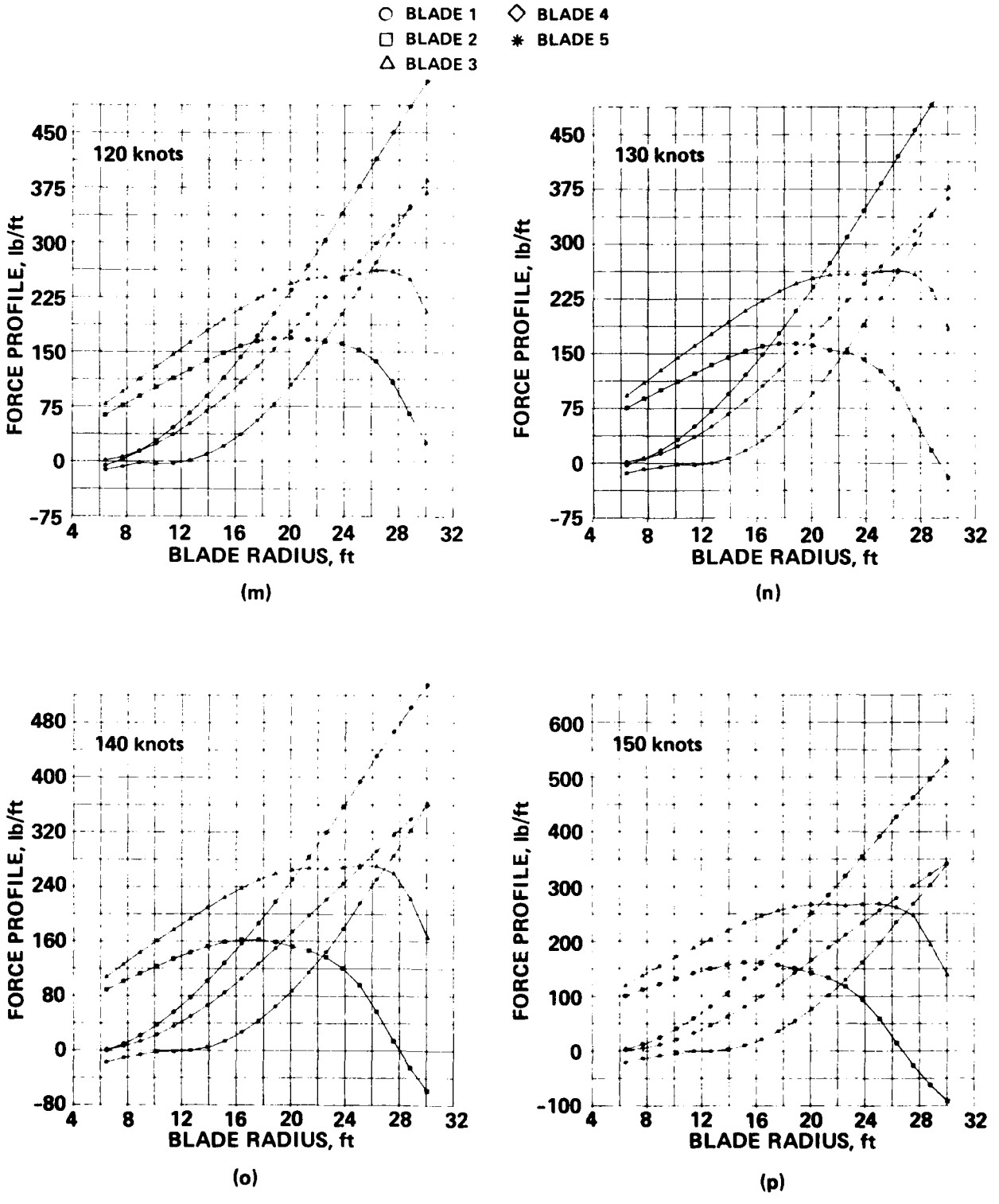

Figure 5.- Continued.

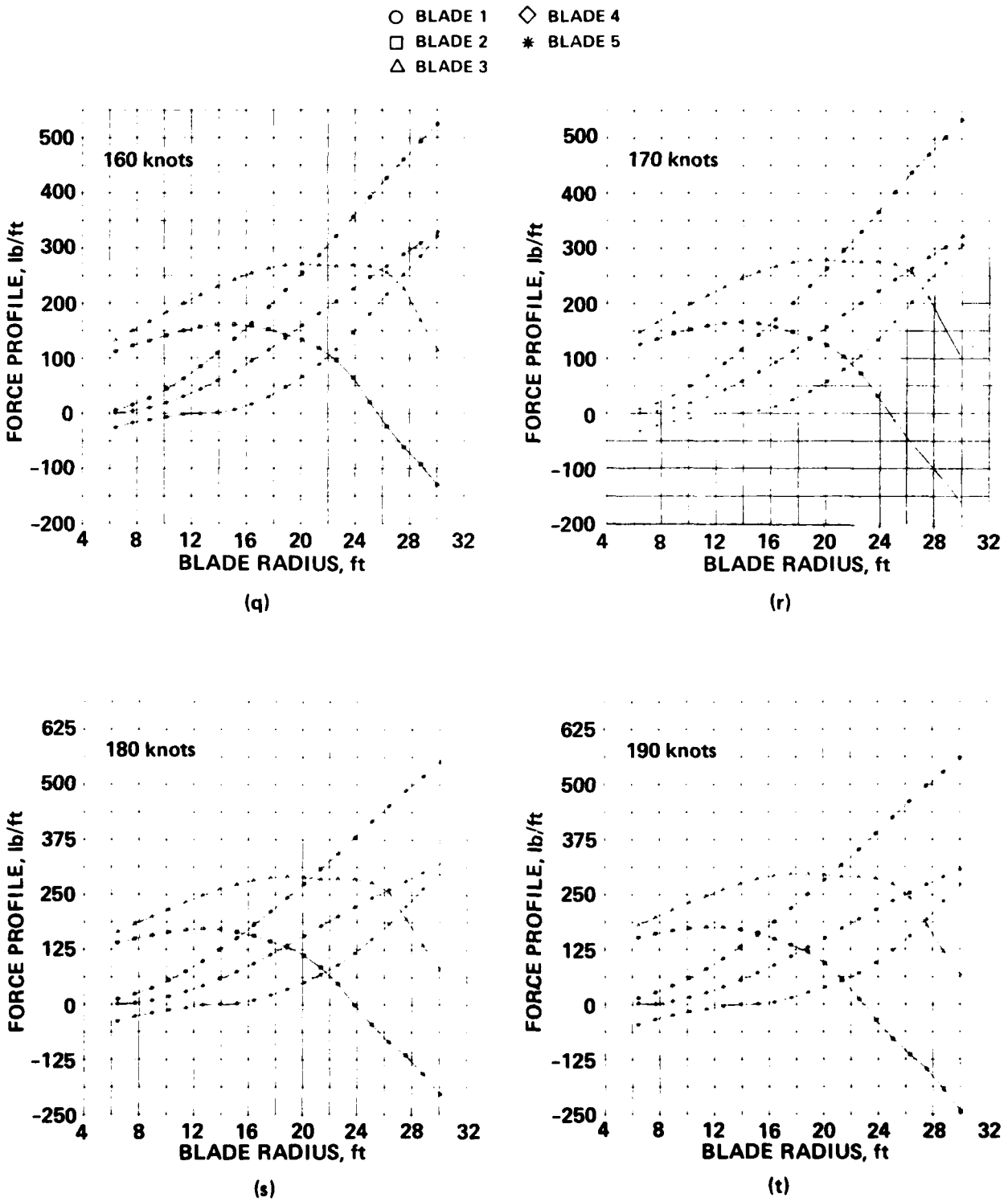

Figure 5.- Continued.

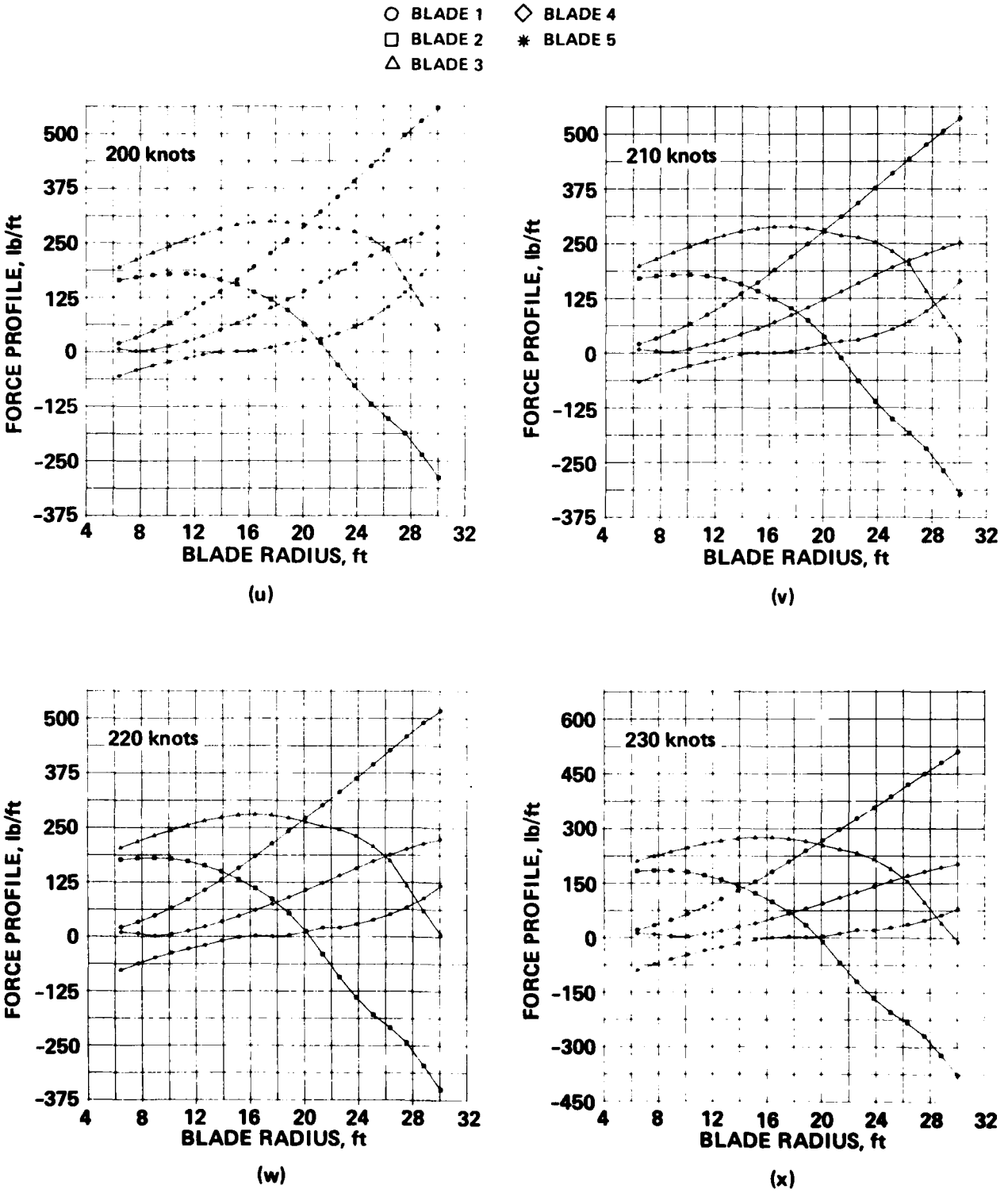

Figure 5.- Continued.

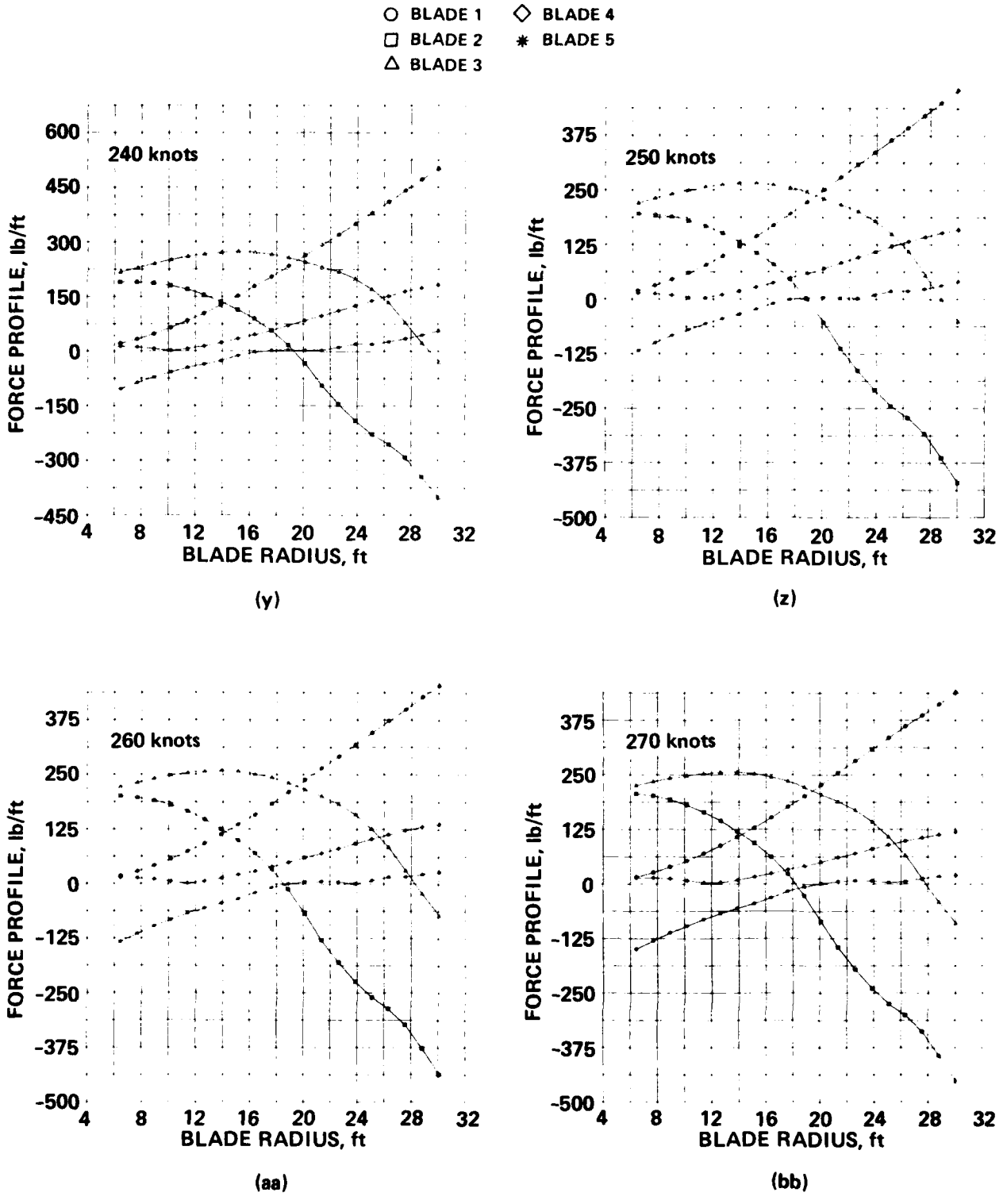

Figure 5.- Continued.

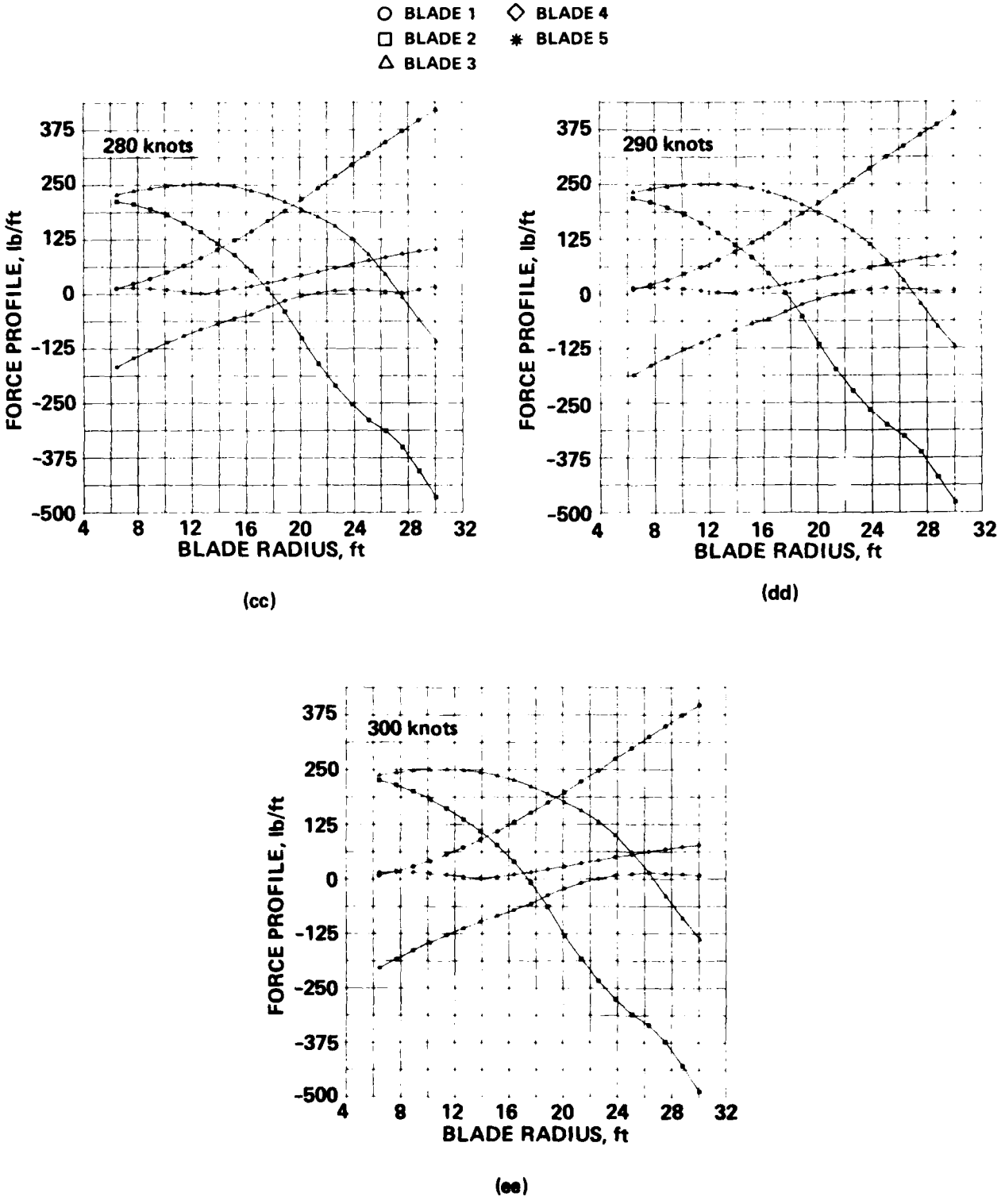

Figure 5.- Concluded.

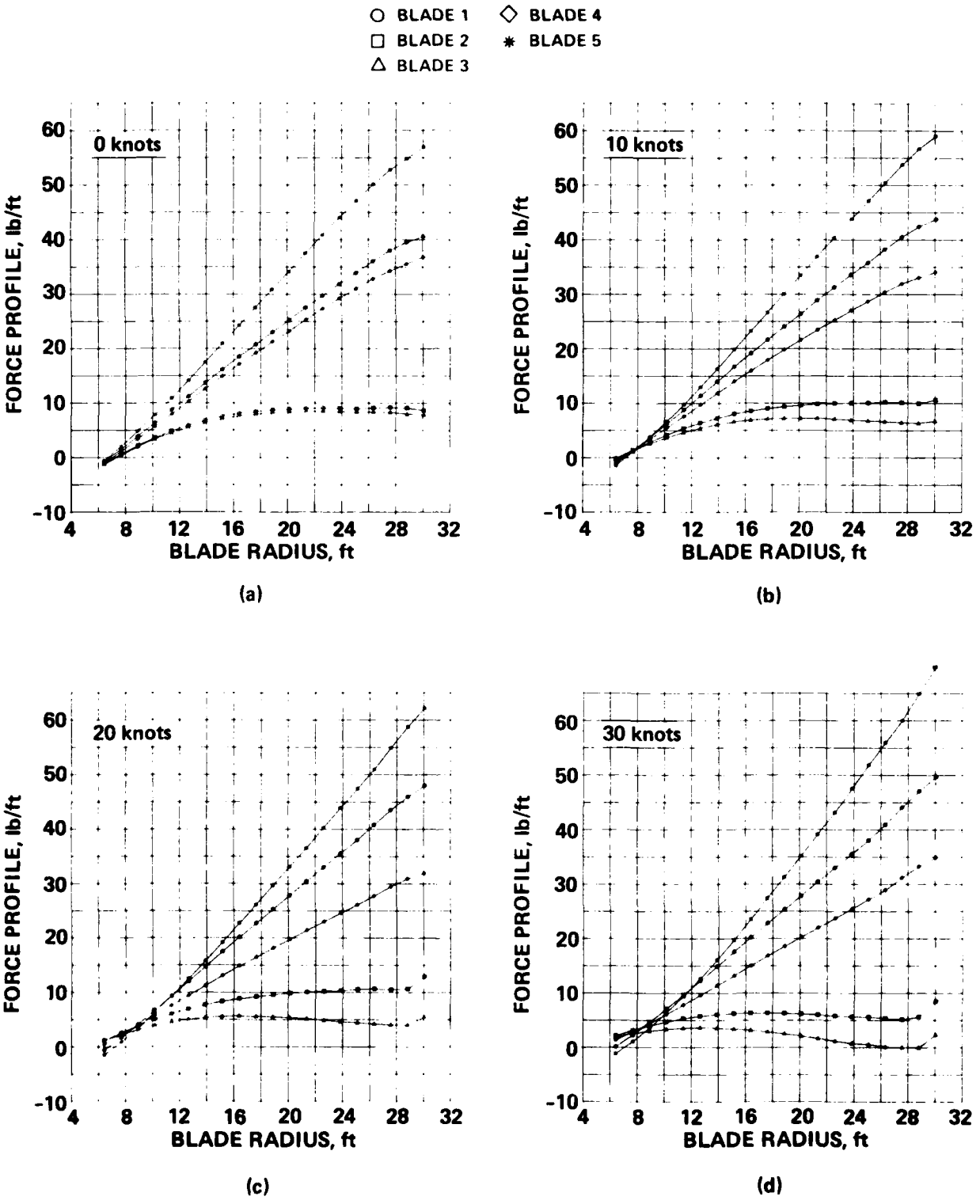

Figure 6.- Drag-force profiles.

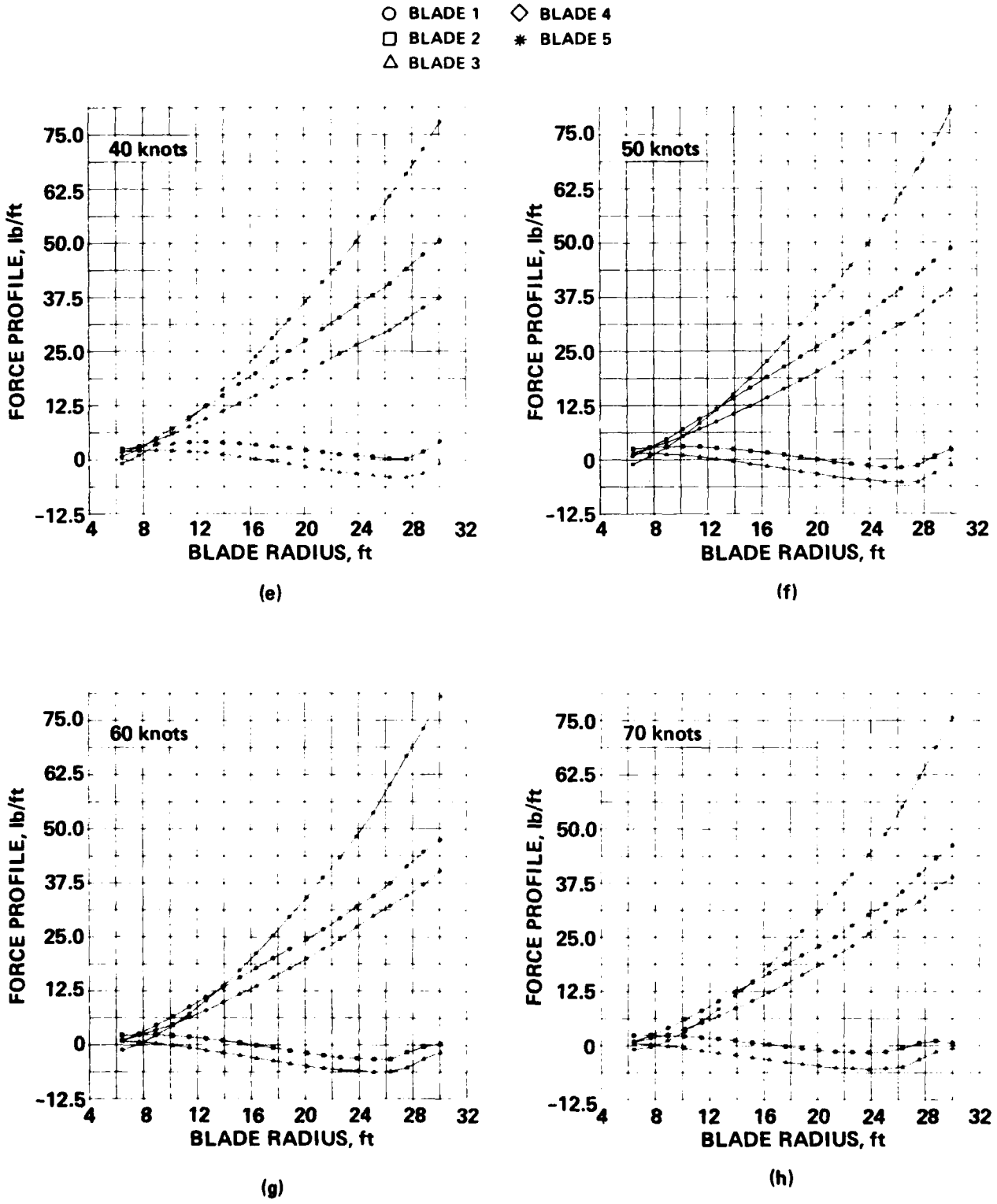

Figure 6.- Continued.

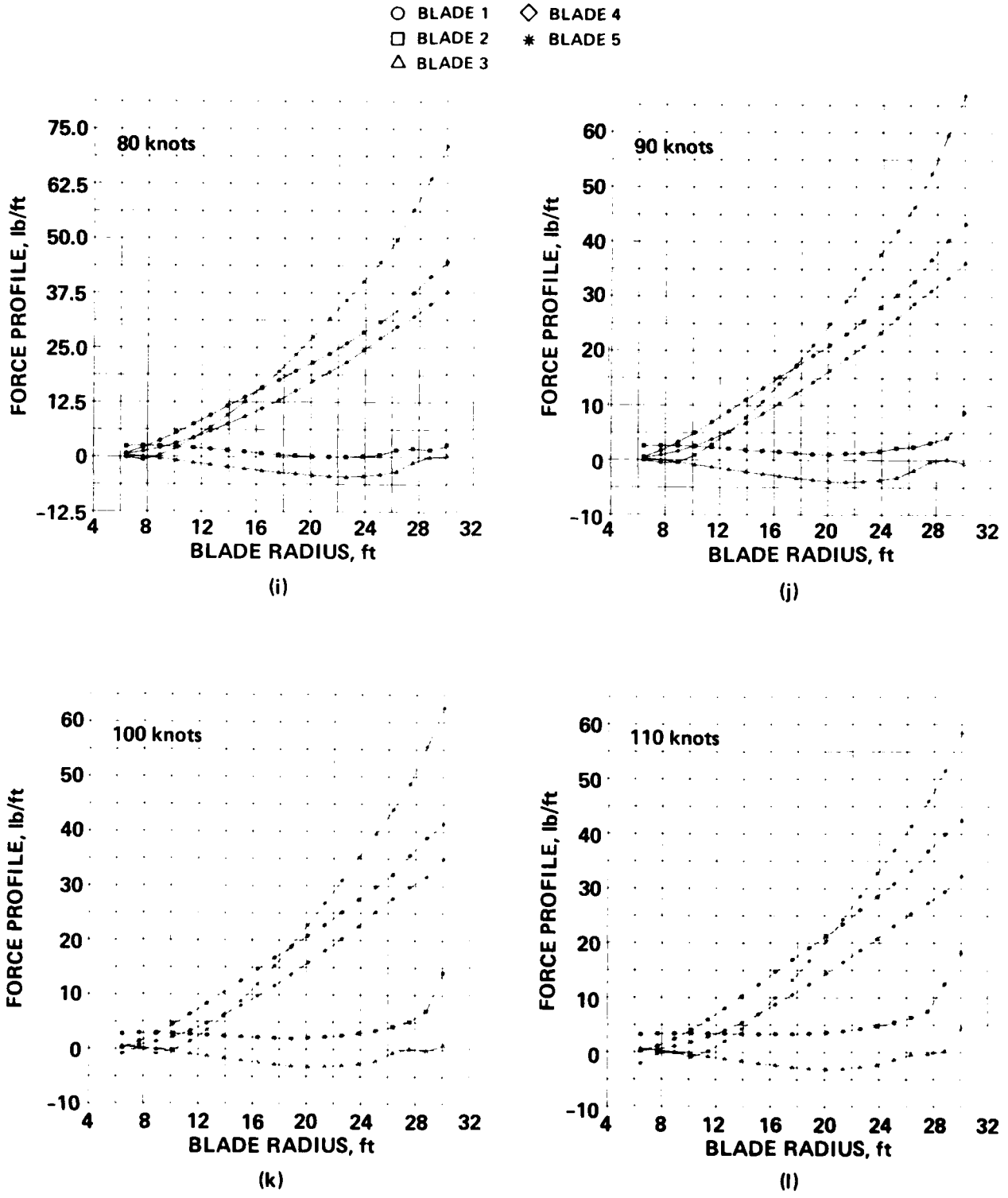

Figure 6.- Continued.

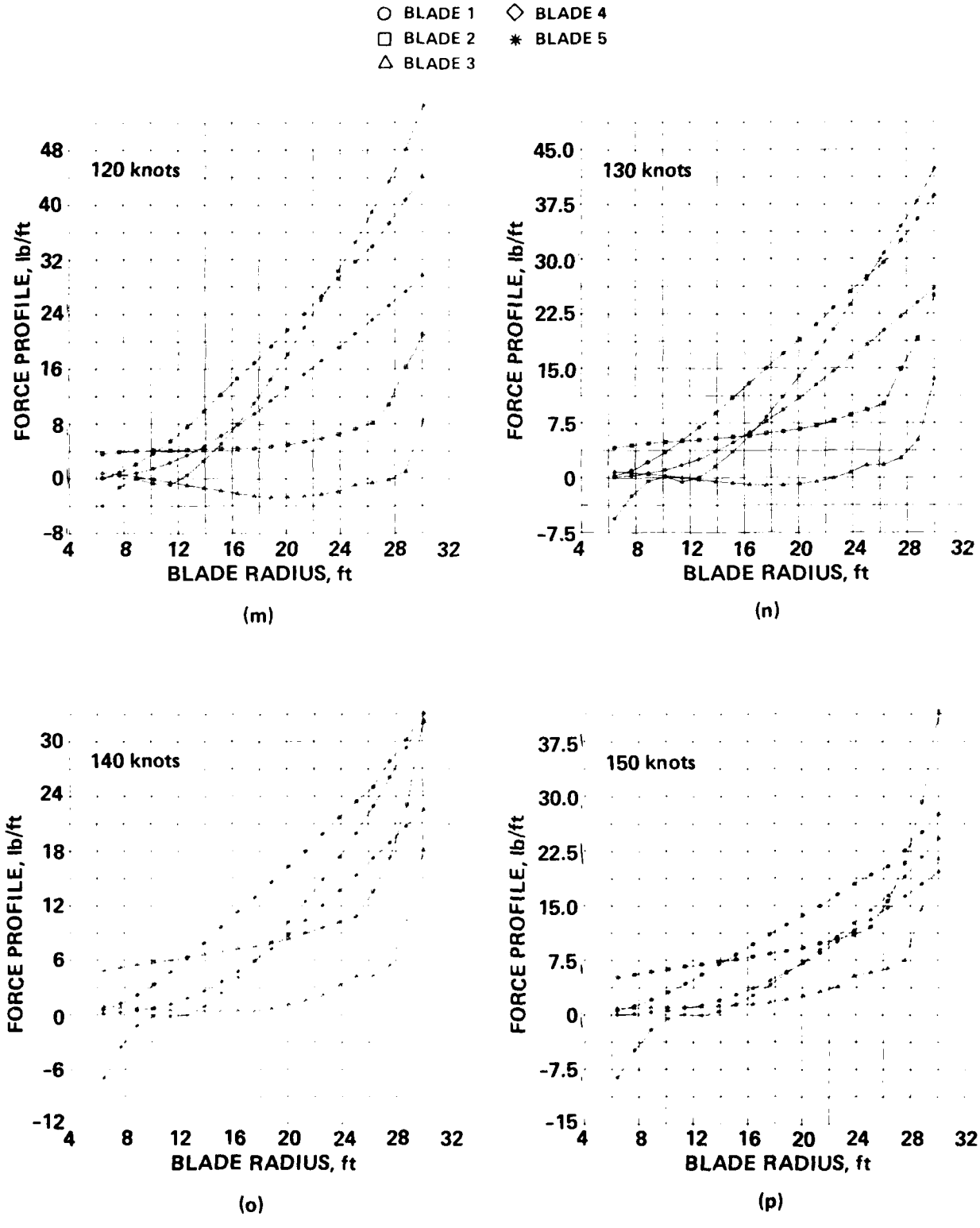

Figure 6.- Continued.

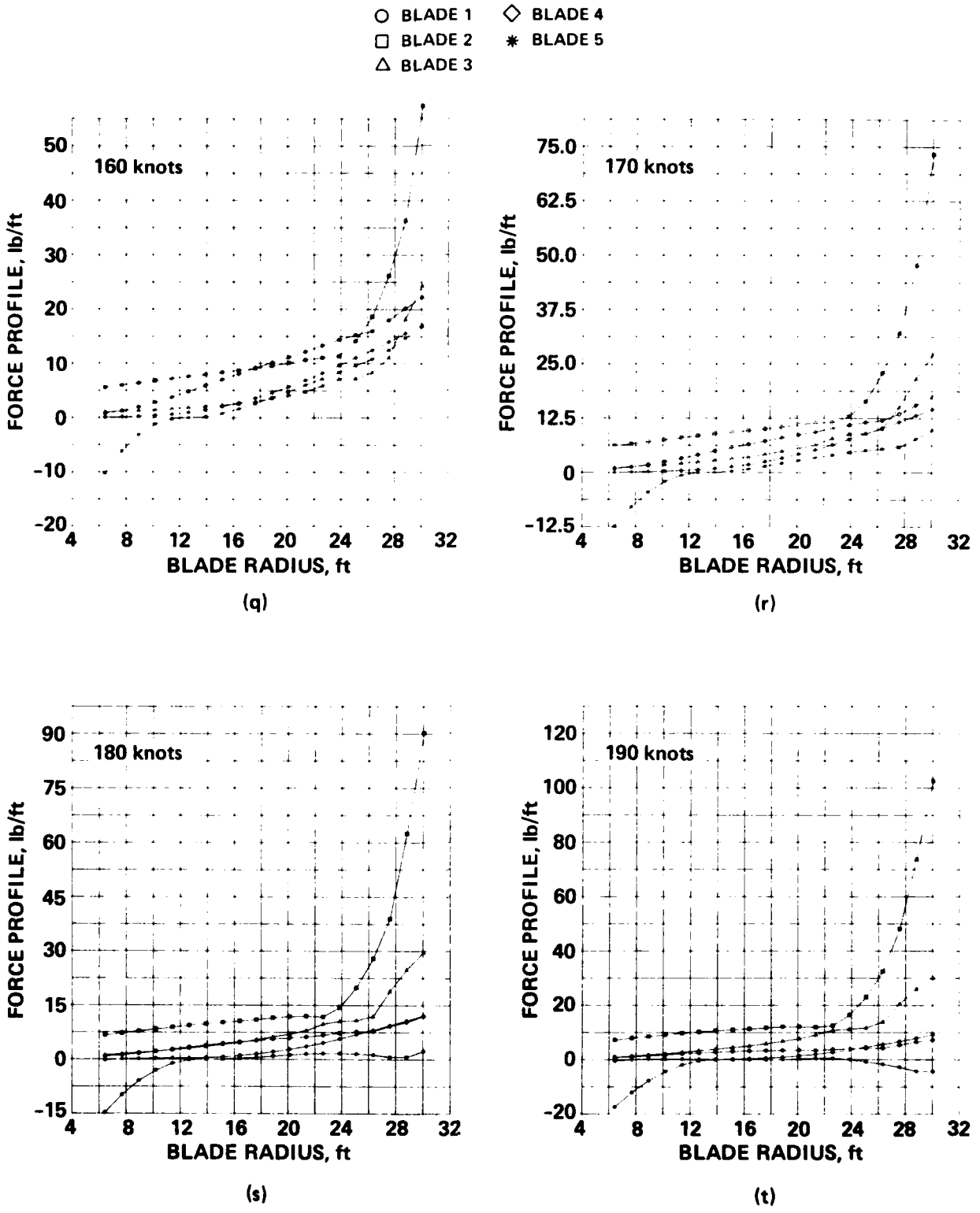

Figure 6.- Continued.

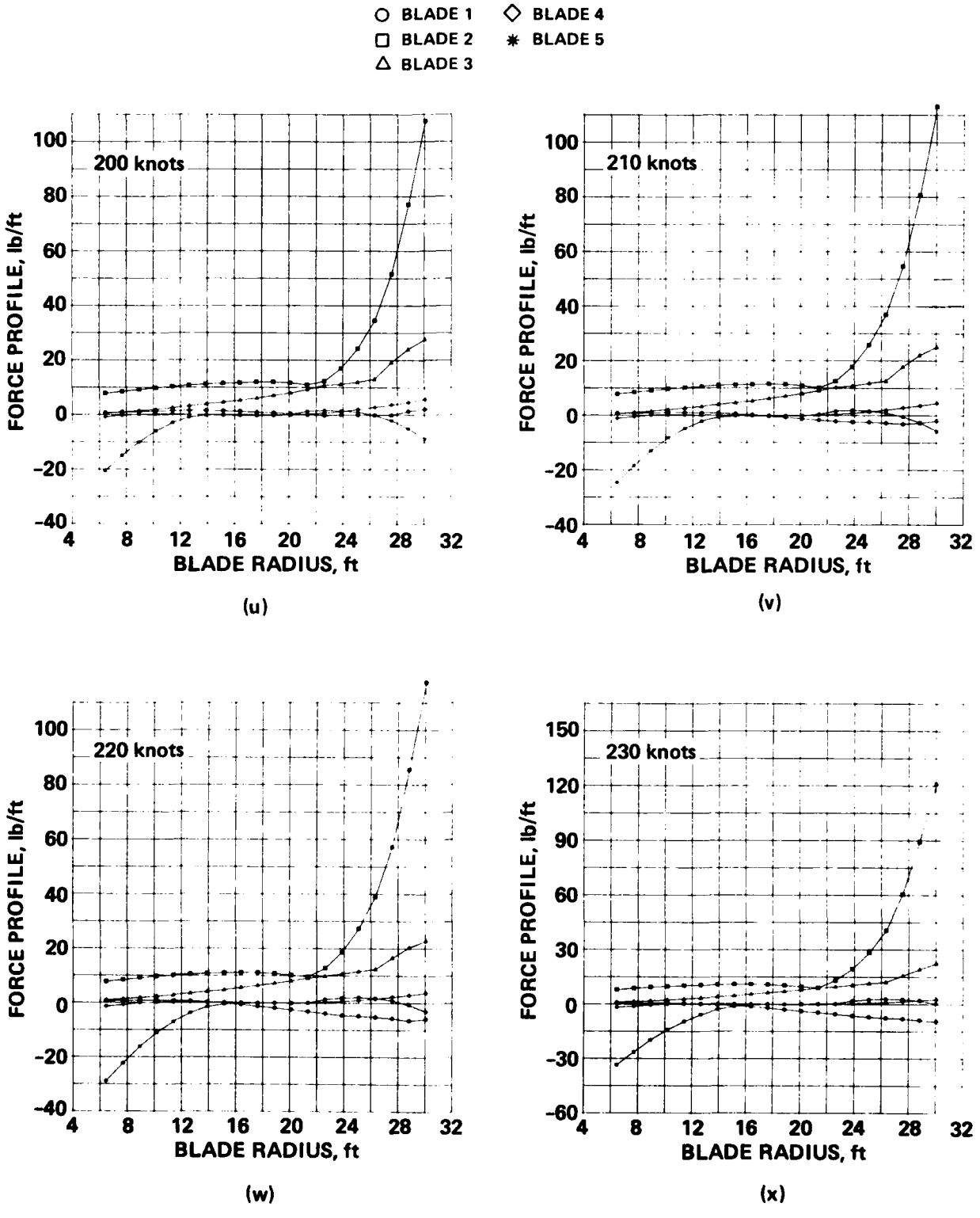

Figure 6.- Continued.

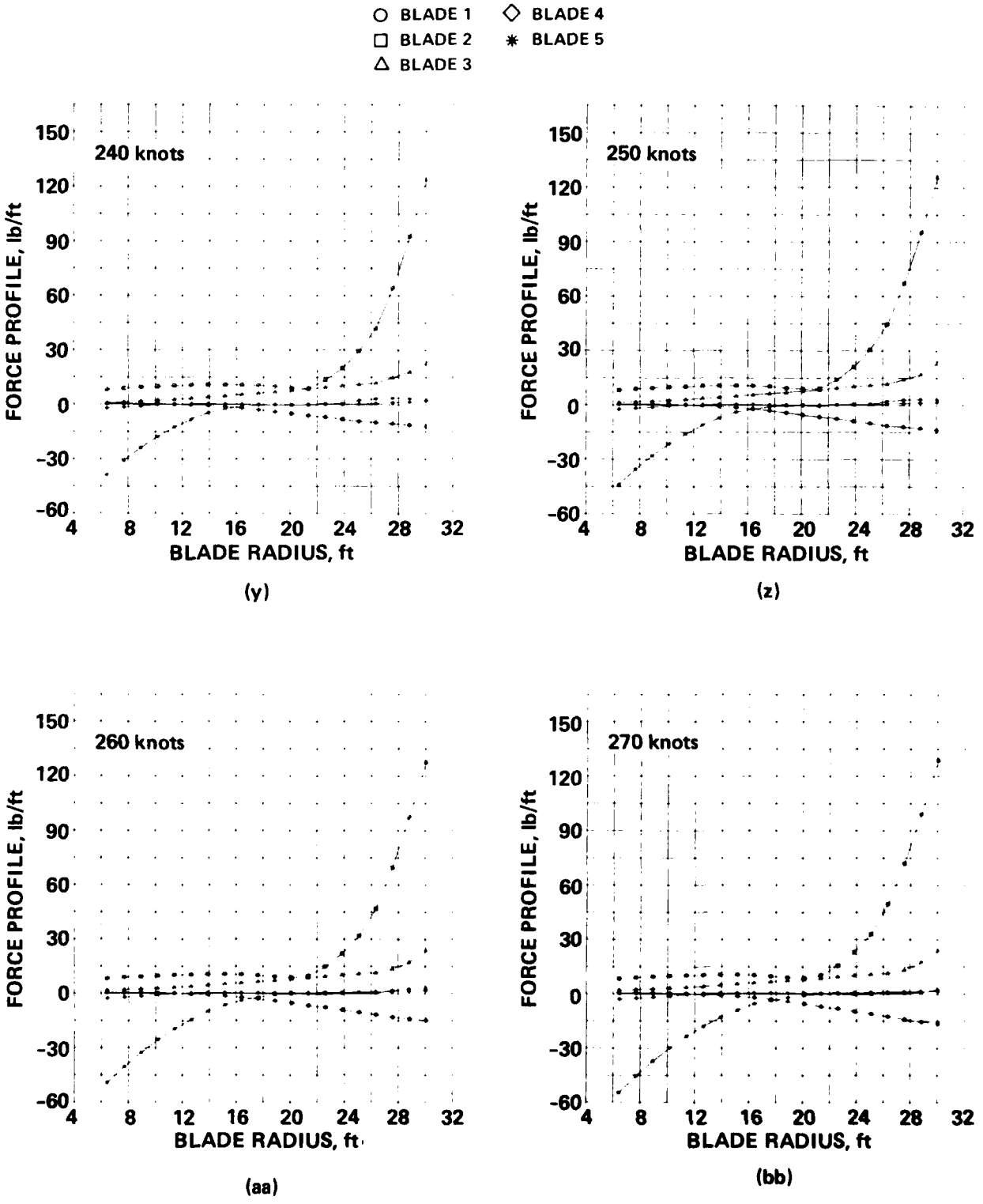

Figure 6.- Continued.

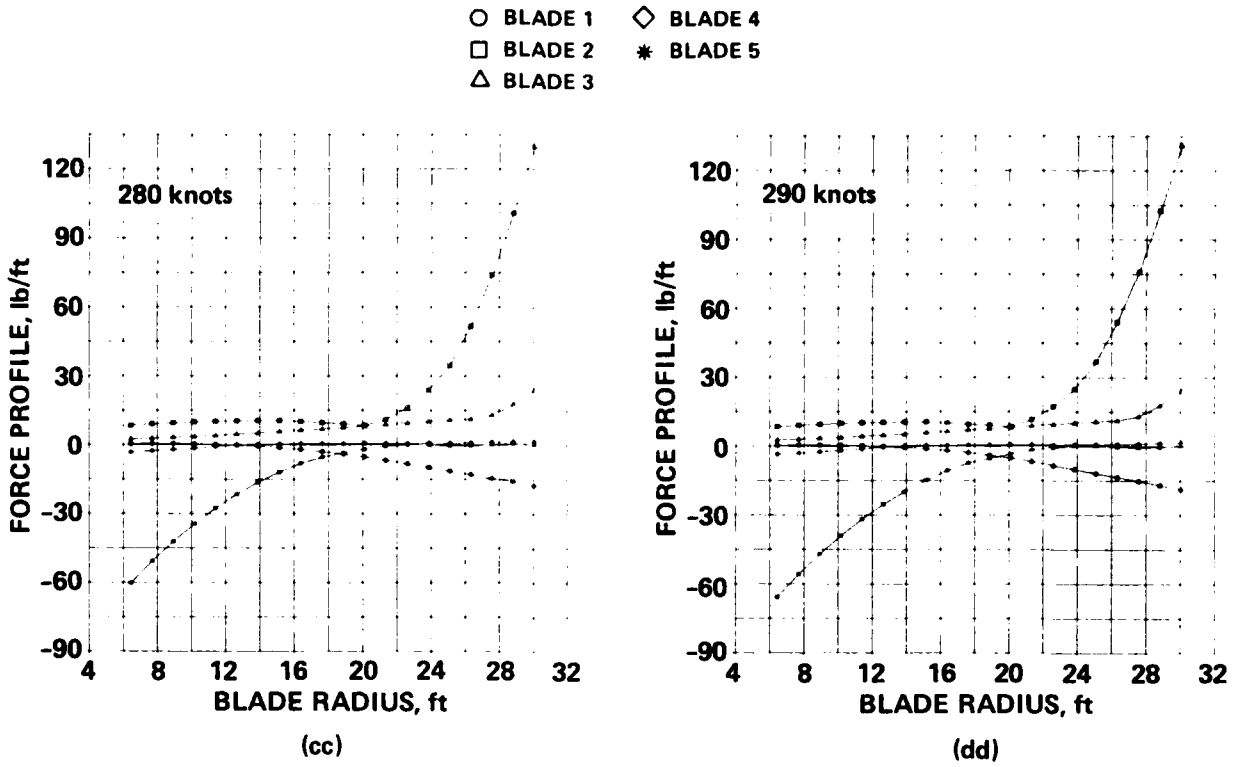

(cc) (dd)

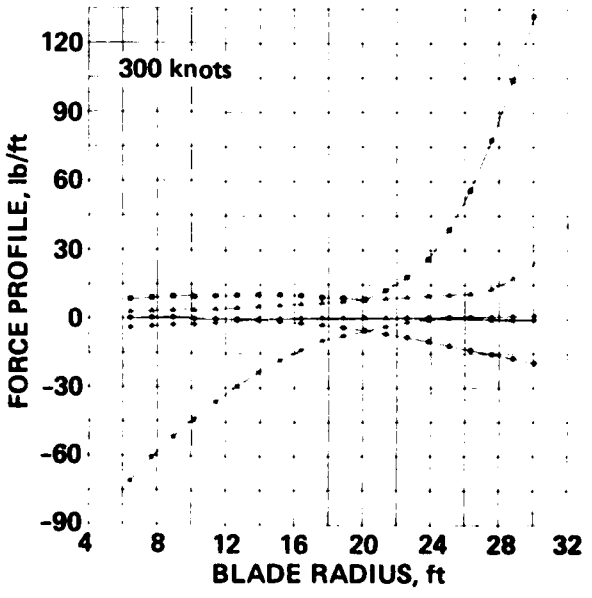

(ee)

Figure 6.- Concluded.

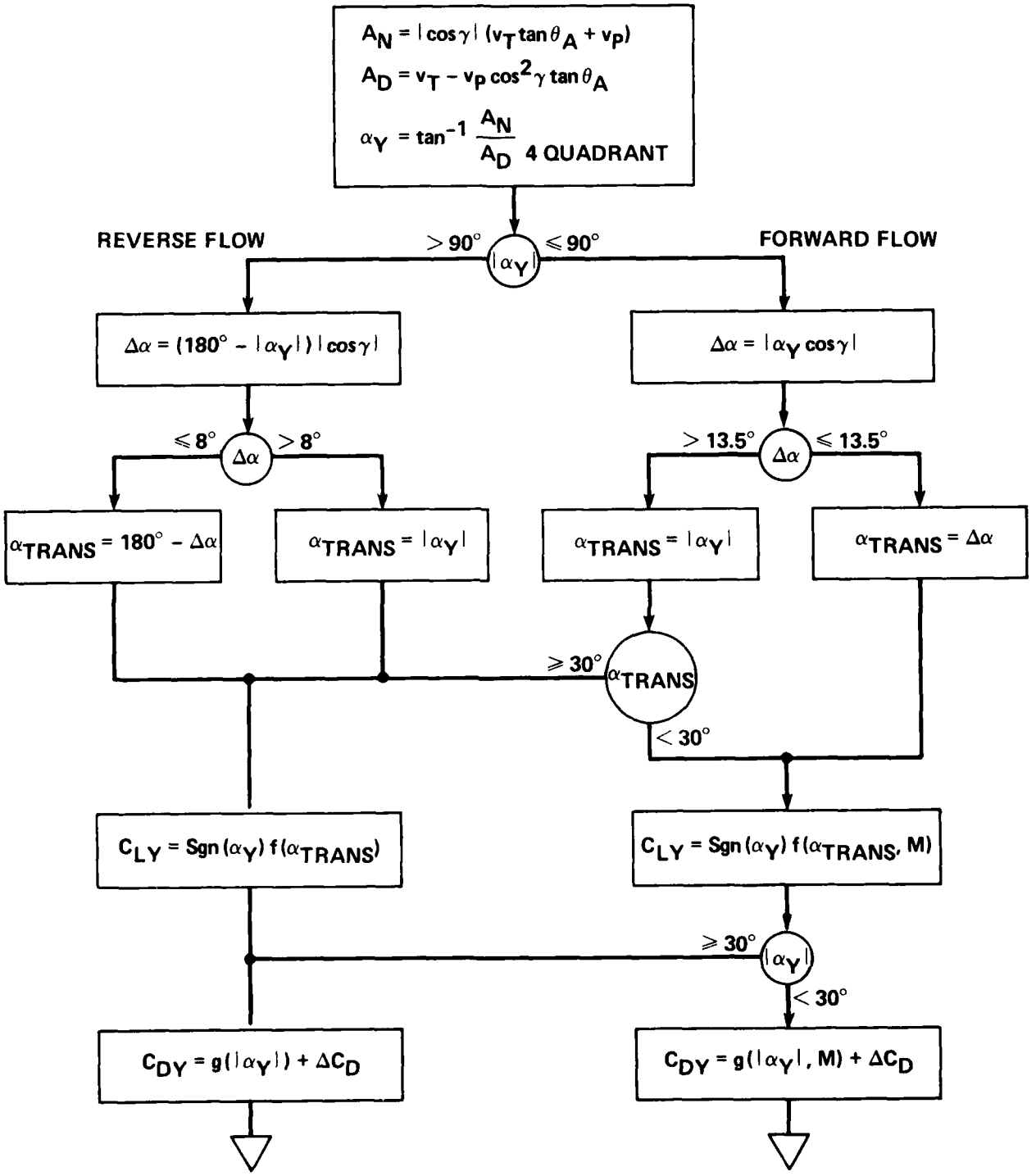

Figure 7.- Aerodynamic coefficient logic.

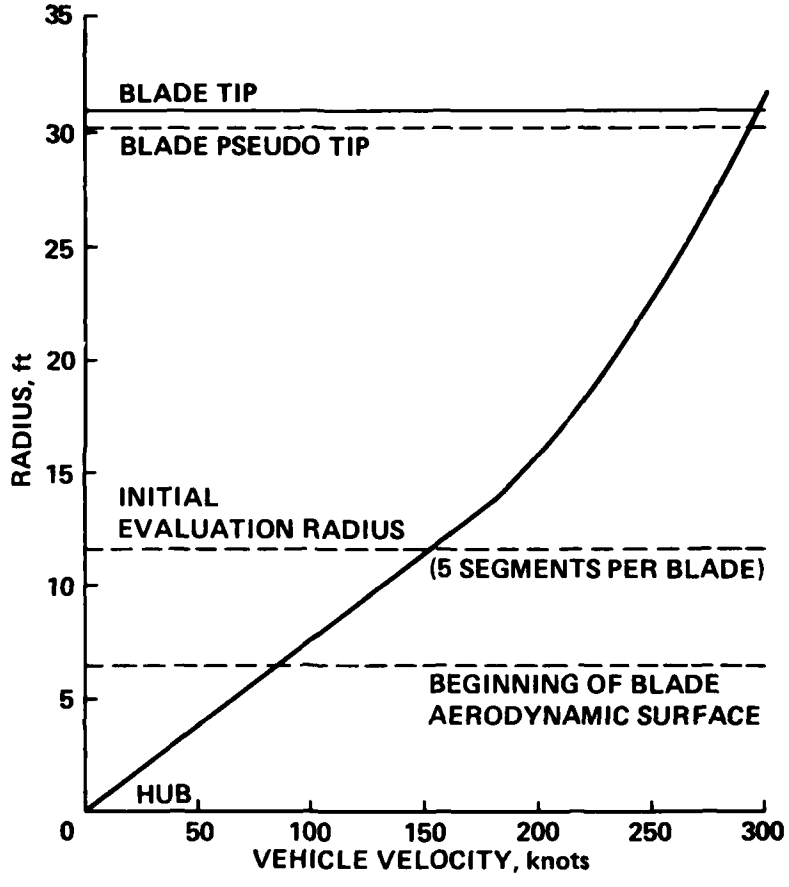

Figure 8.- Simplified stall onset radii, azimuth = 270°.

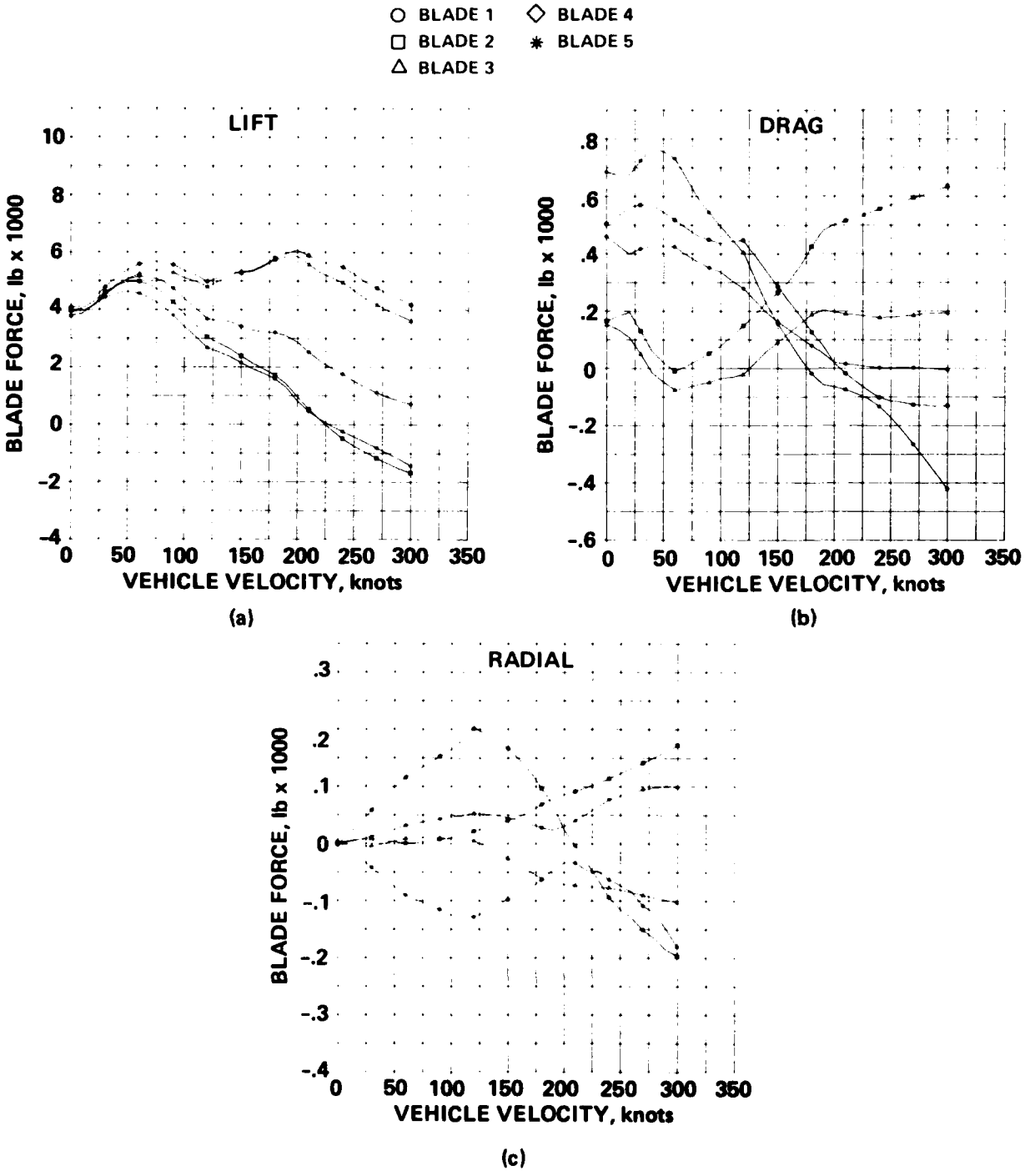

Figure 9.- Total blade aerodynamic forces and moments excluding tip loss.

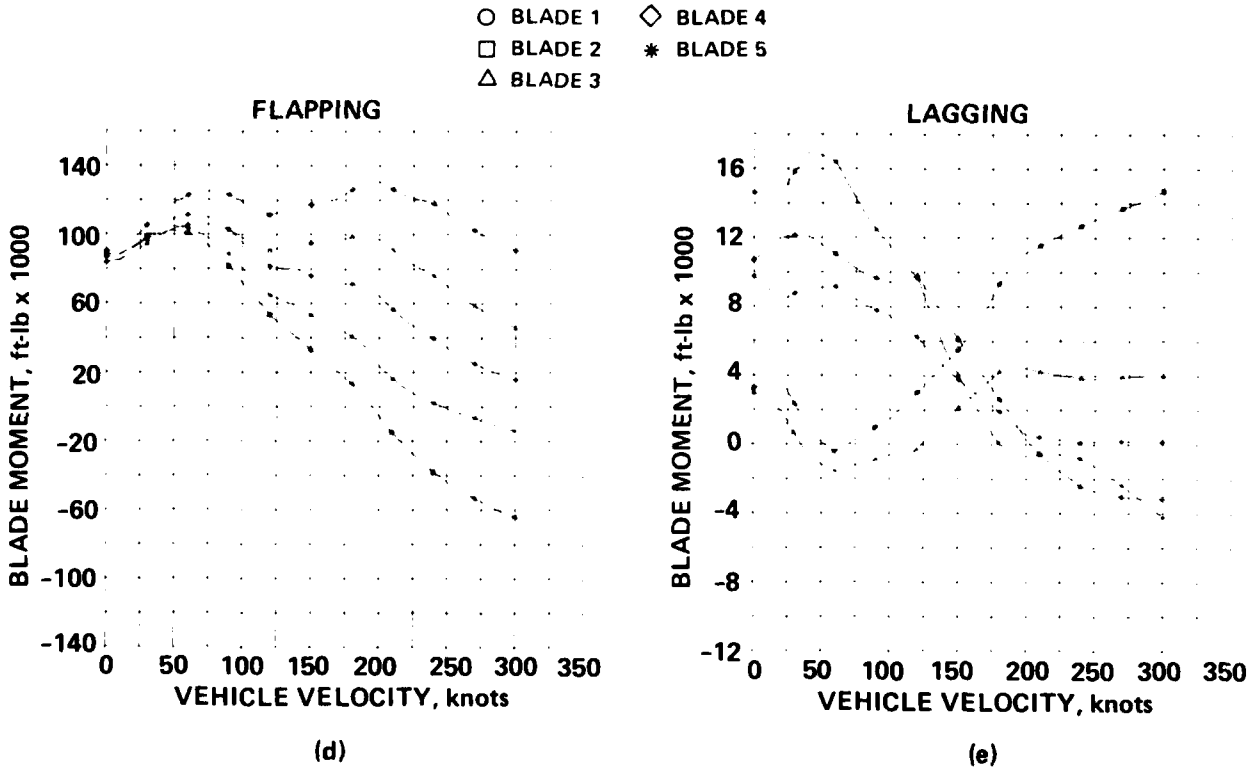

Figure 9.- Concluded.

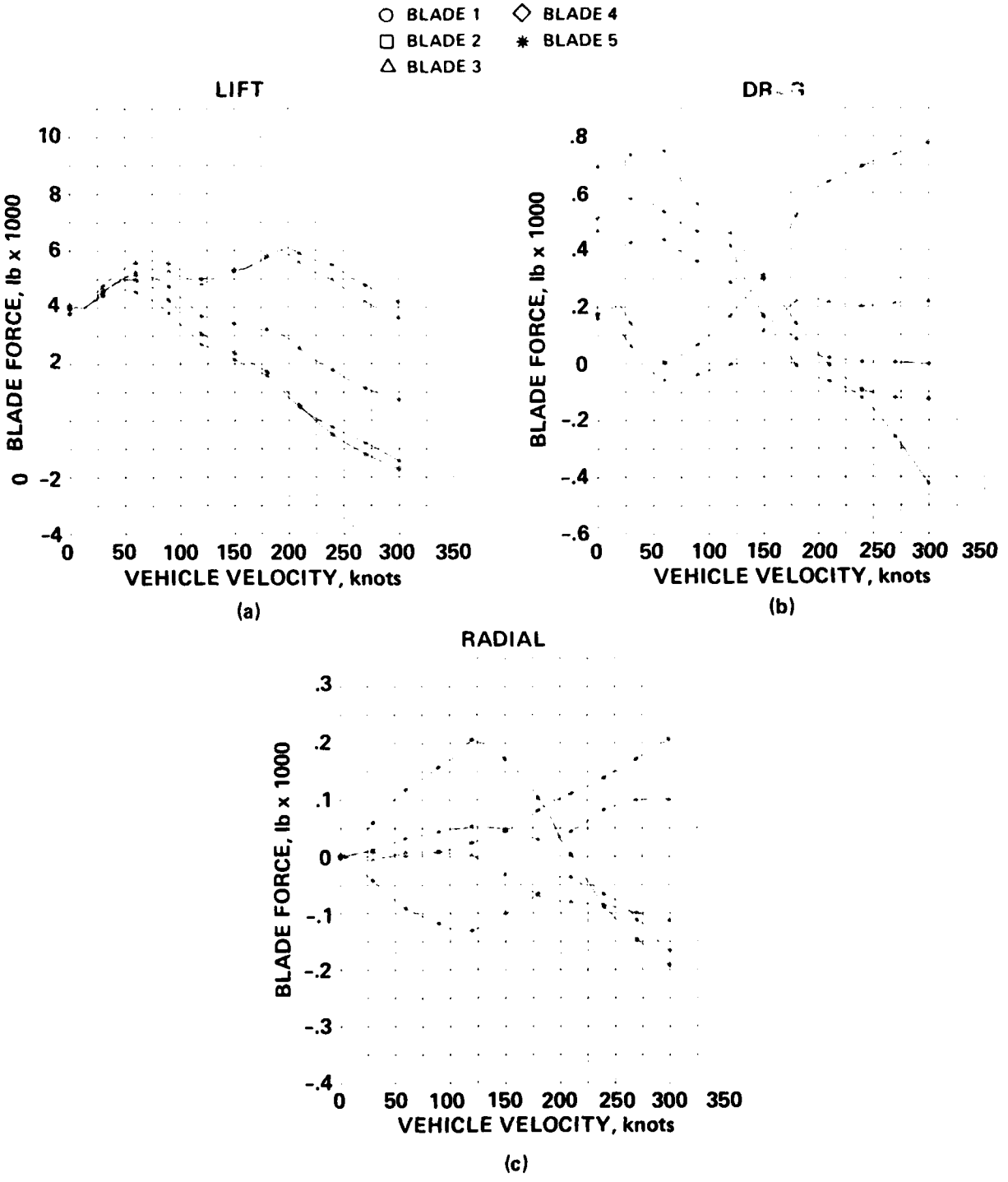

Figure 10.- Total blade aerodynamic forces and moments including tip loss.

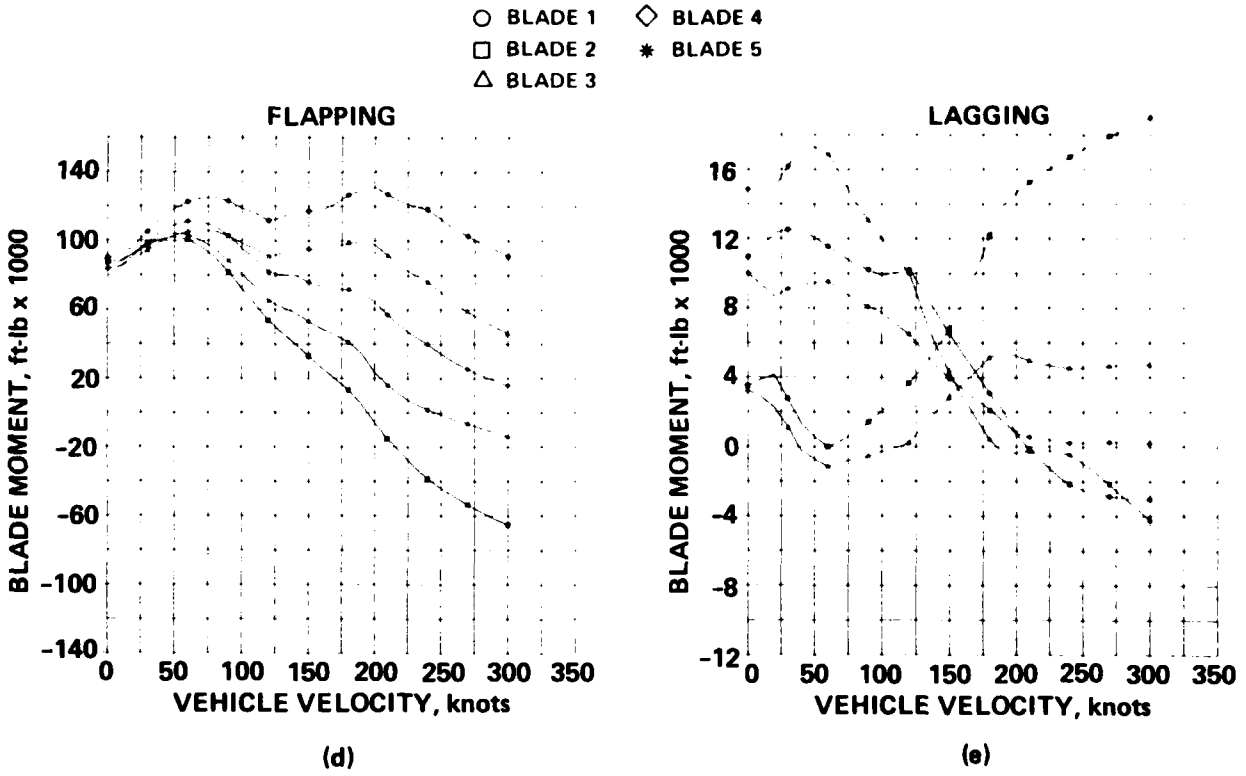

Figure 10.- Concluded.

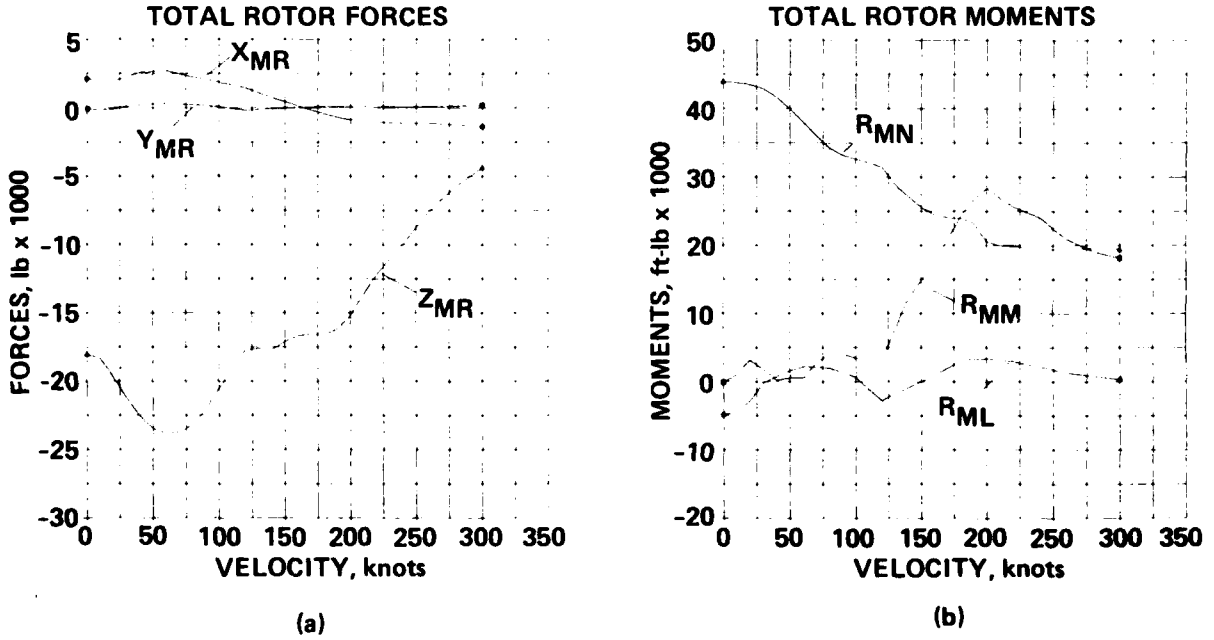

Figure 11.- Basis, total rotor outputs, body axis system.

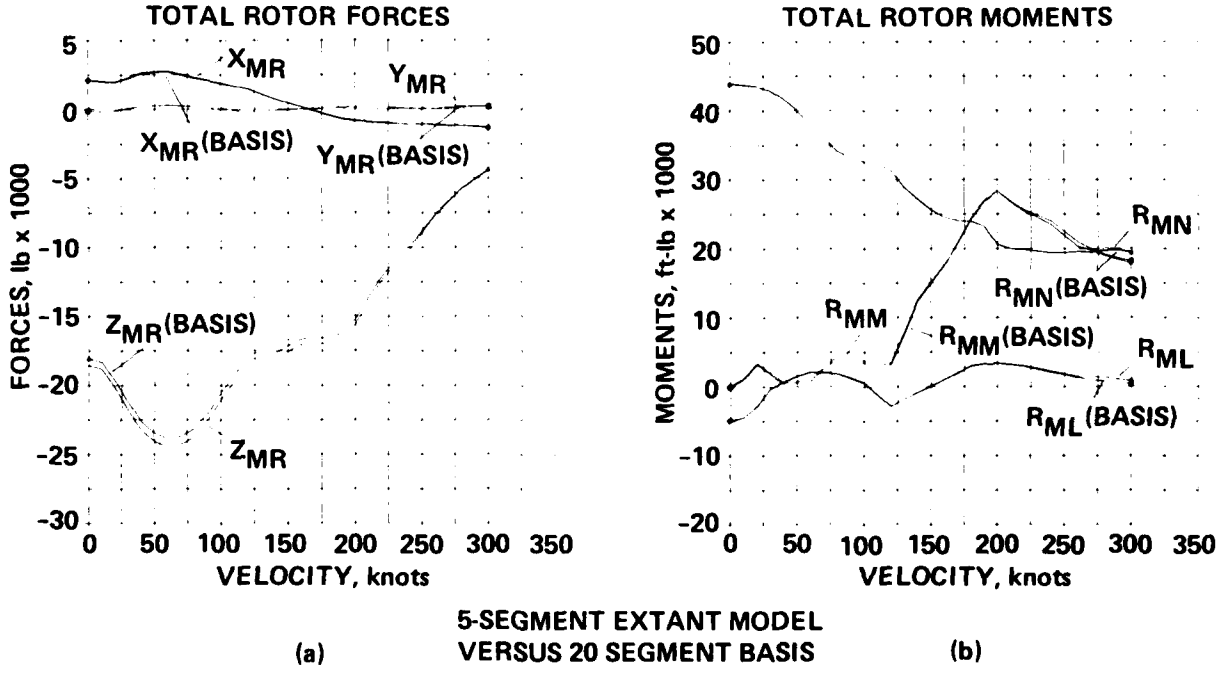

Figure 12.- Total rotor outputs of extant model, constrained condition.

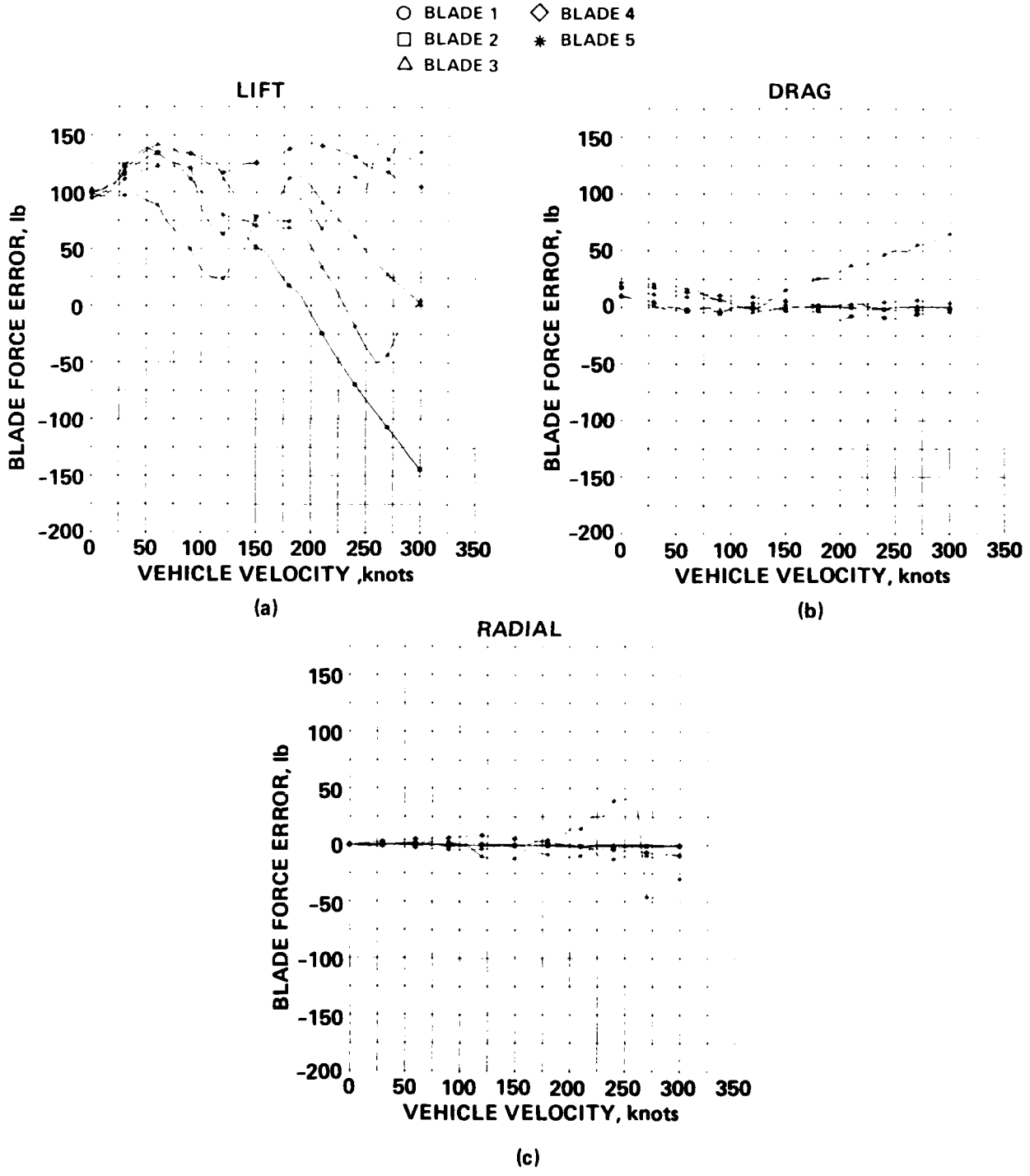

Figure 13.- Aerodynamic errors of extant model, constrained condition, five segments.

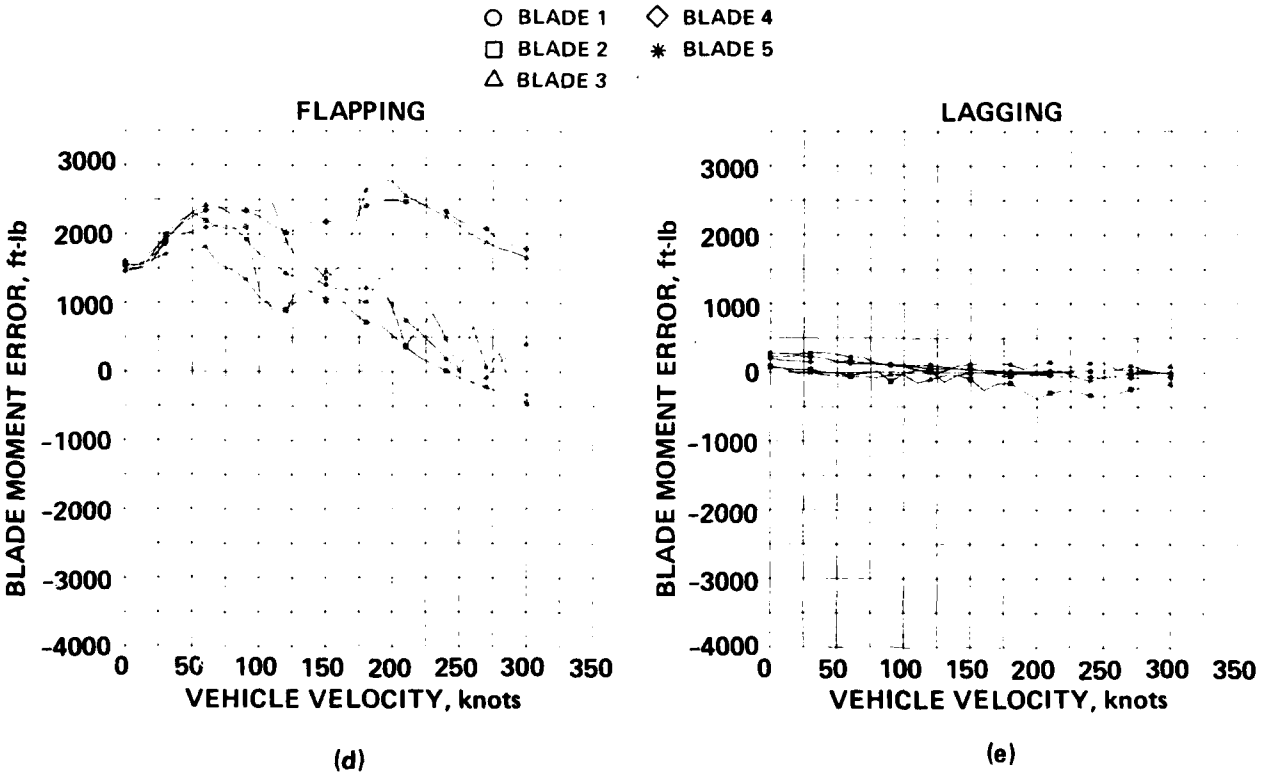

Figure 13.- Concluded.

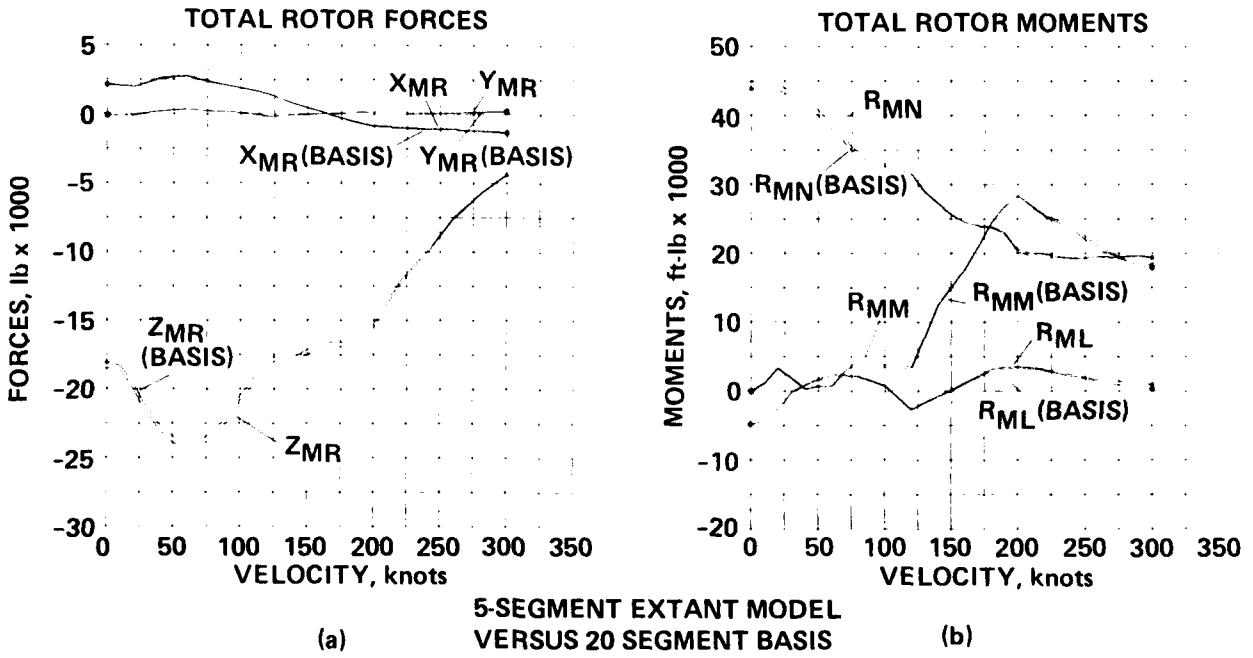

Figure 14.- Total rotor outputs of extant model, balanced condition.

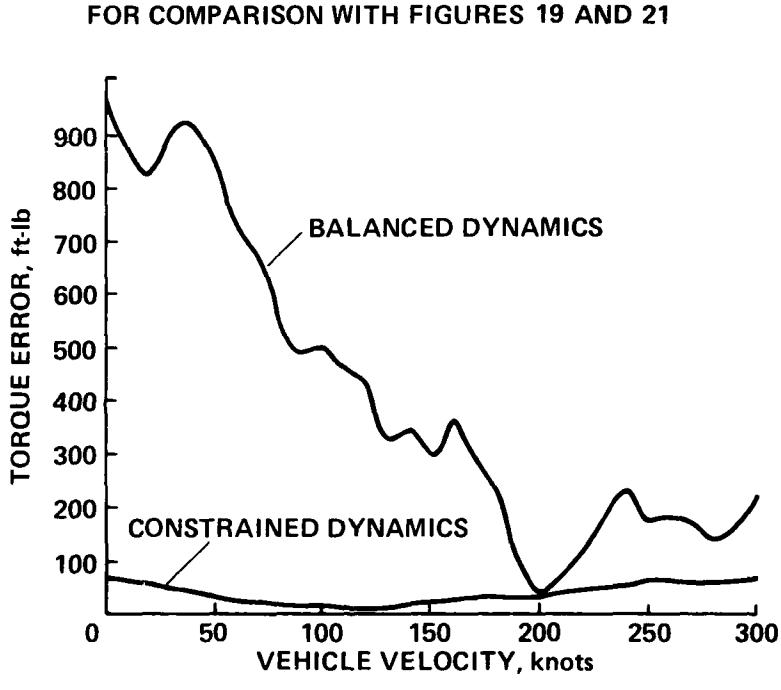

Figure 15.- Torque comparison of extant model with five segments.

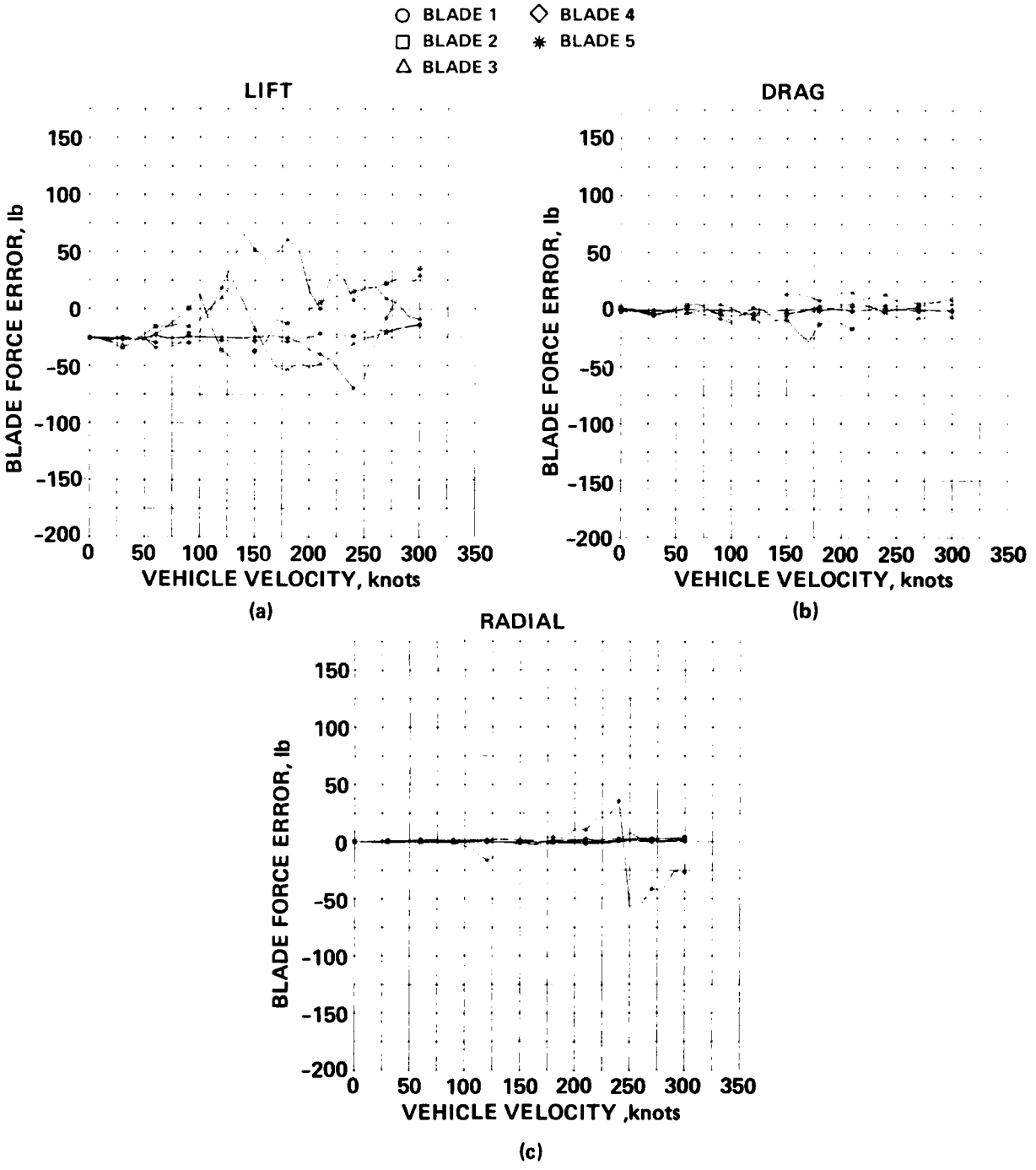

Figure 16.- Aerodynamic errors of alternate model, constrained condition, five segments.

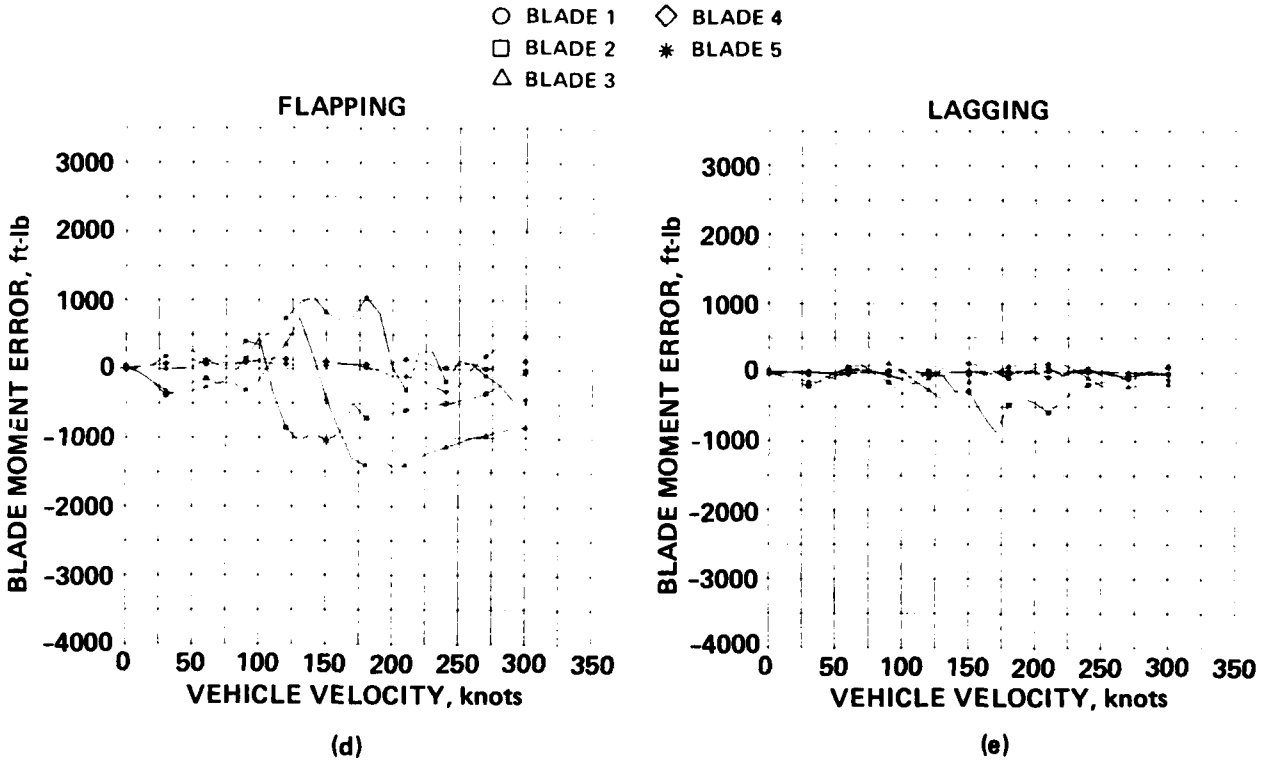

Figure 16.- Concluded.

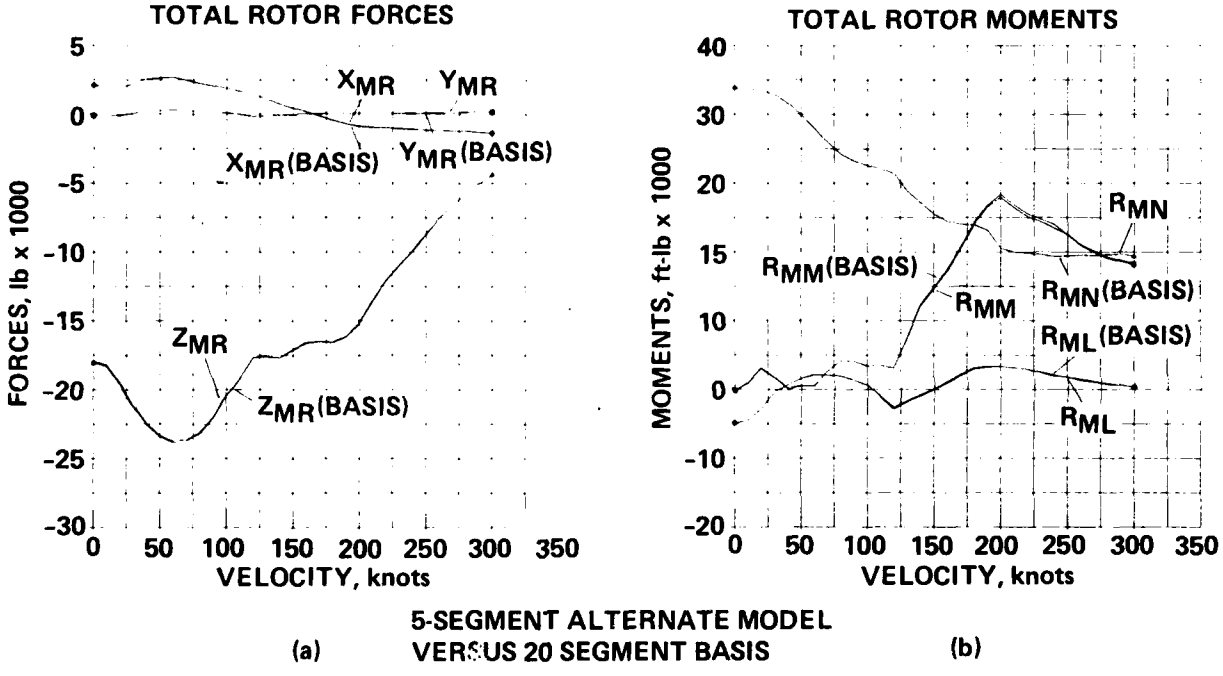

Figure 17.- Total rotor outputs of alternate model, constrained condition.

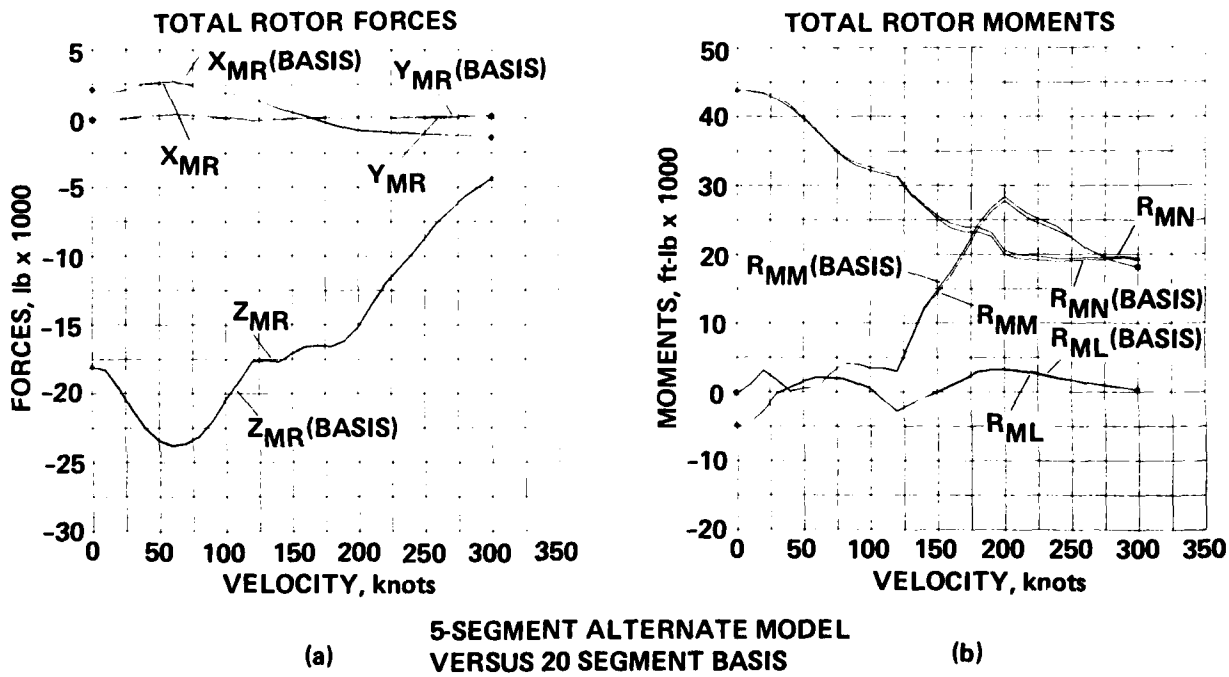

Figure 18.- Total rotor outputs of alternate model, balanced condition.

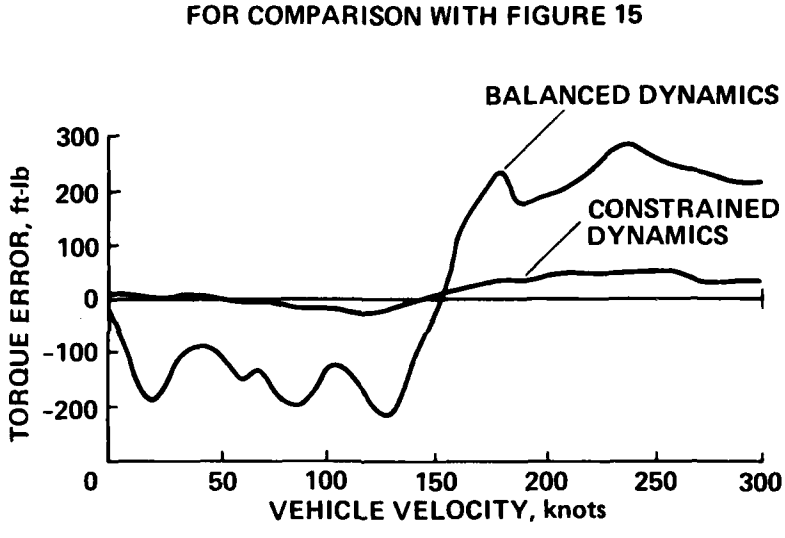

Figure 19.- Torque comparison of alternate model with five evaluations.

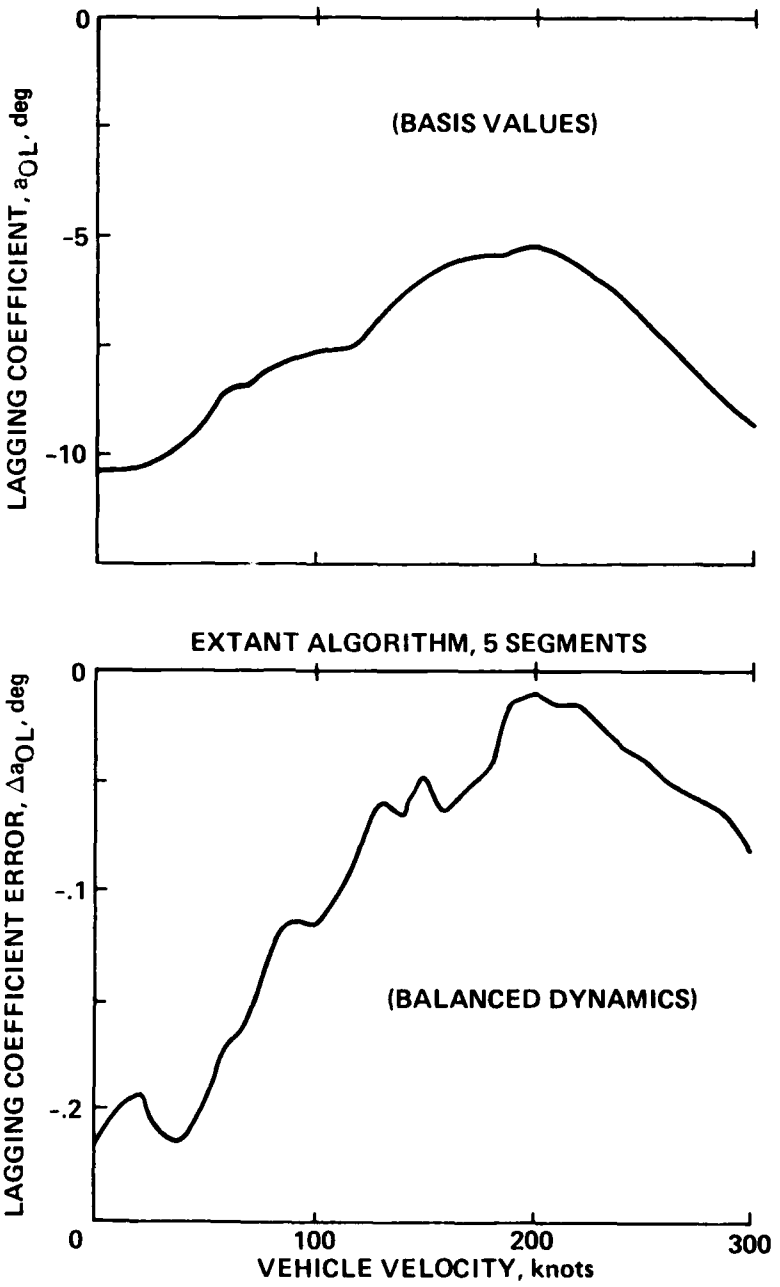

Figure 20.- Lagging coefficient variation.

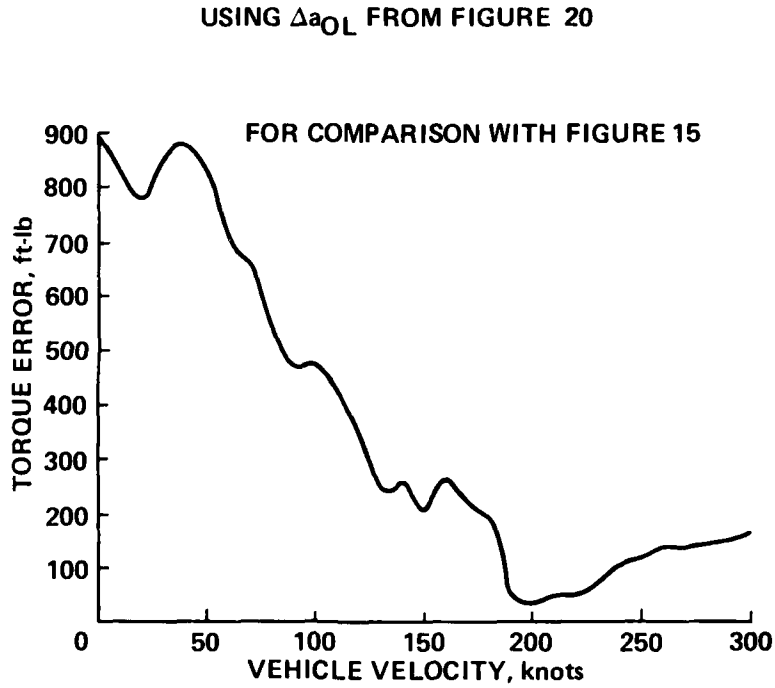

Figure 21.- Computed torque error.

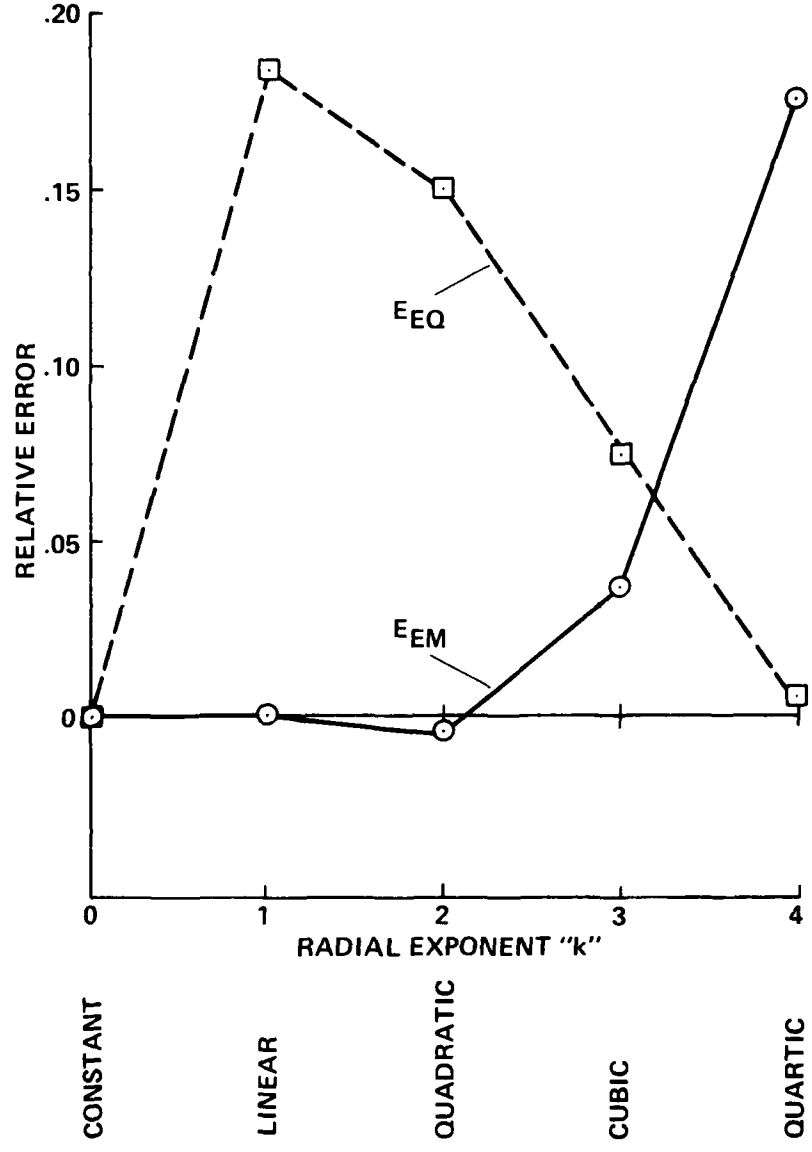

Figure 22.- Algorithmic relative errors for polynomial-force profile.

1. Report No. NASA TP-2026 AVRADCOM TR 81-A-14	2. Government Accession No.	3. Recipient's Catalog No
4. Title and Subtitle ESTABLISHMENT OF A ROTOR MODEL BASIS		5. Report Date June 1982 6. Performing Organization Code
7. Author(s) R. E. McFarland		8. Performing Organization Report No. A-8605
9. Performing Organization Name and Address Aeromechanics Laboratory AVRADCOM Research and Technology Laboratories NASA Ames Research Center Moffett Field, CA 94035		10. Work Unit No. T-5232 11. Contract or Grant No.
12. Sponsoring Agency Name and Address National Aeronautics and Space Administration, Washington, D.C. 20546 and U.S. Army Aviation Research and Development Command, St. Louis, MO 63166		13. Type of Report and Period Covered Technical Paper 14. Sponsoring Agency Code 992-21-01

15. Supplementary Notes

Point of contact: R. E. McFarland, Ames Research Center, Mail Stop 243-9, Moffett Field, CA 94035, (415) 965-5165 or FTS 448-5165.

16. Abstract

Radial-dimension computations in the RSRA's blade-element model are modified for both the acquisition of extensive baseline data and for real-time simulation use. The baseline data, which are for the evaluation of model changes, use very small increments and are of high quality. The modifications to the real-time simulation model are for accuracy improvement, especially when a minimal number of blade segments is required for real-time synchronization. An accurate technique for handling tip loss in discrete blade models is developed. The mathematical consistency and convergence properties of summation algorithms for blade forces and moments are examined and generalized integration coefficients are applied to equal-annuli midpoint spacing. Rotor conditions identified as "constrained" and "balanced" are used and the propagation of error is analyzed.

17. Key Words (Suggested by Author(s)) Rotor mathematical model Real-time simulation Tip loss Segmentation Constrained and balanced conditions	18. Distribution Statement Unclassified - Unlimited Subject Category - 05		
19. Security Classif. (of this report) Unclassified	20. Security Classif. (of this page) Unclassified	21. No. of Pages 92	22. Price* A05

*For sale by the National Technical Information Service, Springfield, Virginia 22161

NASA-Langley, 1982


DATE
ILME
8